

DISSERTATION

submitted to the
Combined Faculties for the Natural Sciences and for Mathematics

of the
Ruperto-Carola-University of Heidelberg, Germany

for the degree of
Doctor of Natural Sciences

presented by

M.Sc. Eilif Benjamin Muller
born in Revelstoke, British Columbia, Canada

Date of oral examination: 06.02.2007

Markov Process Models
for Neural Ensembles
with Spike-Frequency Adaptation

Referees: Prof. Dr. K. Meier
Prof. Dr. A. Destexhe

Markovprozess Modelle für neuronale Ensembles mit Spike-Frequenzadaptation

Diese Arbeit stellt ein Modell basierend auf einem Markovprozess für ein Ensemble von spike-frequenz-adaptierendem Neuronen vor. Gängige Methoden wie “mean-adaptation”-Näherungen und die Theorie der inhomogenen Erneuerungsprozesse werden durch allgemeine Besetzungsdichtemethoden zu einem einheitlichen, theoretischen Rahmen vereinigt und erweitert. Diese Erweiterung erlaubt, unter anderem, die Beschreibung von Korrelationen zwischen aufeinanderfolgenden Interspike-Intervallen. Methoden sowohl zur effizienten Erzeugung inhomogener Realisationen des vorgestellten Markovprozesses, als auch zur numerischen Lösung der Ensemblegleichungen und zur numerischen Bestimmung der Interspike-Intervallkorrelationen erster Ordnung werden präsentiert. Darüber hinaus wird gezeigt, dass durch eine adiabatische Näherung die fünfdimensionale Mastergleichung für ein leitfähigkeitbasiertes Integrate-and-Fire Neuron mit Spike-Frequenzadaptation und einem relativen Refraktärzeitmechanismus zu einer zweidimensionalen Verallgemeinerung des vorgestellten Markovprozesses reduziert werden kann. Für statische und dynamische Stimuli werden die durch Monte-Carlo-Simulationen bestimmten negativen seriellen Interspike-Intervallkorrelationen bzw. die zeitliche Dynamik der Aktivität des fünfdimensionalen Systems von dem vereinfachten zweidimensionalen Markovprozess mit hoher Genauigkeit reproduziert. Die Methoden werden angewandt, um die möglichen Funktionen von Spike-Frequenzadaptation zu erforschen. Verwicklungen für die Kodierung früh im Primatensivisionssystem, wo die funktionelle Kopplung zwischen fixierten Augenbewegungen und Spike-Frequenzadaptation schon bekannt ist, werden diskutiert.

Markov Process Models for Neural Ensembles with Spike-Frequency Adaptation

A Markov process model for spike-frequency adapting neural ensembles is proposed which synthesizes existing mean-adaptation approaches for spike-frequency adaptation and inhomogeneous renewal theory with population density methods resulting in a unified and tractable framework which accounts for correlations between subsequent interspike intervals. A method for efficiently generating inhomogeneous realizations of the proposed Markov process is given, methods for solving the population equation are presented, and an expression for the first-order interspike interval correlation is derived. Further, it is shown that the full five-dimensional master equation for a conductance-based integrate-and-fire neuron with spike-frequency adaptation and a relative refractory mechanism can be reduced to a two-dimensional generalization of the proposed Markov process by an adiabatic elimination of fast variables. For static and dynamic stimulation, negative serial interspike interval correlations and transient population responses respectively of Monte-Carlo simulations of the full five-dimensional system can be accurately described by the proposed two-dimensional Markov process. The techniques are applied to investigate possible functional roles of spike-frequency adaptation. Implications are discussed for coding early in the primate visual system, where fixational eye movements and adaptation mechanisms are known to be functionally coupled.

*Do you ever question your life
Do you ever wonder why
Do you ever see in your dreams...
All the castles in the sky
Oh tell me why...
Do we build castles in the sky
Oh tell me why...
All the castles way up high.*

Martine Theeuwen



M.C. Escher, "Castle in the air".

All M.C. Escher works (c) 2006 The M.C. Escher Company - The Netherlands.

All rights reserved. Used by permission. www.mcescher.com.

An imagination is, to attempt to put it to words, a fleeting image in the mind's eye idealizing and anticipating, often influenced by desires and predispositions, how the world behaves under our influence. How to realize what one imagines?

For simple objects and desires, such as the want of consuming the apple resting on the buro, the facilities of the mind find little challenge and hoards of subordinate subconscious zombies alot themselves in a wink so that the mind can be entertained by more exciting dreams.

For contemplating the clock-work of the facilities of the mind, the mind yet lacks the support of an appropriate language. Imaginations run wild as a child in a candy store of diverse selection, that in browsing for his fancy here, forgets what was over there. We construct theories of its function which are castles in the sky. Supported by a tortoise swimming in the sea, we jesture towards the dream as if to raise the water and bring us closer to the truth. Still, legend has it, a wise old lady once reported it's turtles all the way down. The young man inquires, "but dear grandmother, I see a sea of turtles. How should I choose?" She pauses, and her gaze seeks tranquility at the horizon as if she is multiplying large numbers in her head. "Choose however you like."

*So it is a struggle in the dark
except for a few occasional glimmers of light
until the approach of one or more attempts is so close
that it cannot be denied.*

Kenneth S. Cole, Membranes, Ions and Impulses

Contents

Abstract	iii
1 Foundations	3
1.1 Introduction	3
1.2 Spike-Frequency Adaptation	5
1.3 Ordinary Renewal Theory	7
1.4 Inhomogeneous Renewal Theory	8
1.5 Beyond Renewal Theory	11
1.5.1 Computing Renewal Quantities	15
1.5.2 Correlations	16
2 Ensembles of Detailed Neurons	19
2.1 Neuron Model, Adaptation, Input	19
2.2 Ensemble Behavior	21
2.3 Calibration of Markov Process Models	24
2.3.1 Determining the Static Hazard Function for Adapting Markov Models	24
2.3.2 Constructing Inhomogeneous Hazard Functions	26
2.3.3 Renewal Theory Models	26
3 Numerics and Computational Methods	29
3.1 Numerical Solution of Master Equations	29
3.2 Neuron Simulations	30
3.3 Generating Realizations of Adapting Markov Processes	31
3.4 Numerical Solution of the Renewal Master Equation	31
3.5 Generating Realizations of a General Inhomogeneous Renewal Process	31
4 Results	35
4.1 Comparisons of Calibrated Models to Full System	35
4.1.1 Interspike Interval Distributions	35
4.1.2 Interspike Interval Correlations	36
4.1.3 Firing Rate Dynamics	37
4.2 Beyond Mean-Adaptation Approximations	43
4.2.1 Validity of Mean-Adaptation Theories	44

4.3	Correlations due to Temporal Averaging	45
4.3.1	Time-Averaged Joint ISI Distribution	49
4.3.2	Example: Sinusoidal Poisson Process	49
4.4	Inhomogeneous Gamma Renewal Process Models	50
4.4.1	Response to Step Stimuli	54
4.4.2	Filtering Properties of an Inhomogeneous Gamma Renewal Process	54
4.4.3	Compounding Effects in Successive Adapting Populations .	57
4.4.4	Network Response	59
5	Discussion	67
5.1	Comparison with Other Studies of Adaptation	68
5.2	On the Adiabatic Reduction of the Master Equation	70
5.3	Beyond Renewal Theory	71
5.4	Supra-Threshold Stimuli	72
5.5	Synchrony	74
5.6	Implications for Early Visual Coding	75
5.7	Concluding Remarks	76
A	Neuron and Adaptation Model Parameters	79
B	Further Details on the Adiabatic Reduction	81
	References	85
	Acknowledgments	91

Chapter 1

Foundations

For if truth be at all within the reach of human capacity, 'tis certain it must lie very deep and abstruse; and to hope we shall arrive at it without the utmost pains must certainly be esteemed sufficiently vain and presumptuous.

David Hume, A Treatise of Human Nature

1.1 Introduction

Since Ramón y Cajal's proposal at the turn of the 20th century that the central nervous system is made up of billions of separate neurons that communicate via junctions coined synapses, we can ask the question: What is the nature of the communication between neurons? Contemporaries of Cajal, such as Julius Bernstein, were aware of electrical pulses, so-called action potentials, generated by nerve tissues, and could measure their time courses and velocities of propagation (Bernstein, 1902; Schuetze, 1983; Seyfarth, 2006). It was the seminal work of Alan Hodgkin and Andrew Huxley (Hodgkin & Huxley, 1952), using the recently invented voltage-clamp technique (Curtis & Cole, 1939) to investigate overshoots of the neuron membrane potential during an action potential, which resulted in the now standard approach for describing and modeling action potential generation and propagation. While initially the Hodgkin-Huxley equations, as they are now known, were solved using hand operated calculating machines (Huxley, 2002), the same general framework, augmented by a bouquet of additional ionic currents, is the basis for modern large-scale compartmental modeling (Meunier & Segev, 2002). Phenomenological models for neuronal excitability such as the integrate-and-fire (I&F) neuron models due to (Lapicque, 1907) which predate the work of Hodgkin and Huxley (HH) can be formulated in a hybrid way to take on

much of the qualitative and quantitative behavior of HH models while remaining analytically tractable and efficient for simulating large-scale neural networks (Destexhe, 1997). One example of such a hybrid model is the conductance-based integrate-and-fire neuron model considered in the present dissertation work.

Given an adequate description of the behavior of single neuron classes, it is natural to direct one's attention to the behavior of networks of neurons as occurring in the biological specimen, in for example the cortex, if one seeks to understand the nature of the neural code. Given neuron firing rates and interconnectivity in the cortex, each neuron there is under intense bombardment by both excitatory and inhibitory synapses. These mutually opposing showers of excitation and inhibition induce highly irregular fluctuations of the membrane potential reminiscent of a random walk. The resulting dominance of the mean synaptic conductances over the leak results in a markedly shortened effective membrane time constant, a dynamical regime known as the high-conductance state (Destexhe, Rudolph, & Paré, 2003; Shelley, McLaughlin, Shapley, & Wielaard, 2002). In this regime action potentials are emitted when the membrane potential chances across the firing threshold and the resulting interspike intervals (ISIs) appear stochastic and are roughly gamma distributed (Softky & Koch, 1993; Destexhe, Rudolph, Fellous, & Sejnowski, 2001; Dayan & Abbott, 2001, pp. 33).

Originally introduced in (Knight, 1972), and recently the subject of intense study, population density formalisms provide powerful tools to understand neural ensemble and network behavior in the active network state of the cortex, for example, in a quantitative way (Brunel, 2000; Omurtag, Knight, & Sirovich, 2000; Nykamp & Tranchina, 2000, 2001; Fourcaud & Brunel, 2002; Meffin, Burkitt, & Grayden, 2004; Renart, Brunel, & Wang, 2004). Such studies are mostly restricted to exactly solvable white noise input approximations, with notable exceptions (Nykamp & Tranchina, 2001; Fourcaud & Brunel, 2002). In (Fourcaud & Brunel, 2002), the key observation is made that colored input noise due to synaptic filtering results in a probability density of the membrane potential which is non-zero near the threshold, and allows neurons to respond instantaneously to injected currents. Conductance-based neurons with finite synaptic time constants are treated in (Rudolph & Destexhe, 2003; Richardson, 2004; Rudolph & Destexhe, 2005; Richardson & Gerstner, 2005), however only in the sub-threshold regime, limiting their applicability for understanding single cell ensemble firing statistics and networks dynamics. The problem with threshold has yet to be solved exactly, however it is treated in (Moreno-Bote & Parga, 2004a, 2004b; Büsing, 2006).

An alternate and fruitful approach to describe the statistics of neural firing is to apply renewal theory as presented in detail in (Gerstner & Kistler, 2002). The defining characteristic of renewal theory is that the firing probability is modeled as a function the time since last spike, or age, and successive ISIs are statistically independent. As such, these models neglect by definition the observations in (Chacron, Pakdaman, & Longtin, 2003) and (Lindner & Longtin, 2003) that neurons with spike-frequency adaptation (SFA), a mechanism present in the majority of excitatory cells, exhibit negative serial ISI correlations.

While the great majority of excitatory neurons exhibit SFA, there has yet to be a population density treatment accounting for it, given the difficulty in treating the added dimension analytically and numerically. The aim of the present study is to account for the ensemble behavior of spike-frequency adapting neurons in the high-conductance state in a quantitative way. Thus opening the doors to quantitative studies of the function of SFA for the coding dynamics of large networks.

To begin, this chapter will provide the necessary background on SFA and inhomogeneous renewal theory, and go beyond the renewal theory formalism by introducing a dependence between ISIs resulting in a Markov model described by a master equation, the standard continuity equation describing the time evolution of the ensemble probability distribution. A connection to renewal theory is found by a suitable variable transformation, and expressions for the ISI distribution and conditional ISI distribution are derived. Chapter 2 treats the full five dimensional master equation of the canonical conductance-based integrate-and-fire neuron model driven by Poisson spike trains augmented by SFA and a relative refractory mechanism of the form given in (Dayan & Abbott, 2001, pp. 166). By applying an adiabatic elimination of fast relaxing variables (Haken, 1983; Gardiner, 1984), it is argued that this five-dimensional master equation can be approximated by a two-dimensional master equation of the same form as the “beyond renewal theory” Markov model proposed in this chapter. Methods to calibrate the generalized hazard function of the Markov model by fitting to Monte-Carlo simulations of the full system are given. By reasoning as in (Fourcaud & Brunel, 2002; Renart et al., 2004; La Camera, Rauch, Lüscher, Senn, & Fusi, 2004), it is shown how the generalized hazard function applies in the dynamic case by accounting for synaptic filtering. In chapter 3, numerical methods are given for solving the master equations, and generating realizations of the proposed Markov processes. In chapter 4, predictions for ISI correlations and conditional ISI distributions in the static case, and firing rates in the dynamic case due to the proposed Markov model are compared to Monte-Carlo simulations of the full system. The master equation is then employed to analyze the domain of validity of previous mean-adaptation approaches to model the ensemble firing rate of spike-frequency adapting ensembles. Further, the correlations introduced due to gathering statistics in time rather than over trial, as is typical in analysis of biological data, are modeled and analyzed. Finally, inhomogeneous gamma renewal processes are used to investigate the filtering properties due to spike-frequency adaptation, the compounding effects of successive adapting populations, and the balanced network response to adapting transients. Functional implications of spike-frequency adaptation are considered in the discussion.

1.2 Spike-Frequency Adaptation

Spike-frequency adaptation (SFA) refers to the intrinsic property of certain neurons to fire with gradually increasing interspike intervals (ISIs) in response to a

steady injection of supra-threshold current *in-vitro*. SFA is ubiquitous: It has been observed in many neural systems of diverse species (Fuhrmann, Markram, & Tsodyks, 2002). In the mammalian visual system for example, the majority of retinal ganglion cells (RGCs) (O'Brien, Isayama, Richardson, & Berson, 2002), geniculate relay neurons (Smith, Cox, Sherman, & Rinzel, 2001), and neocortical and hippocampal regular spiking pyramidal neurons (McCormick, Connors, Lighthall, & Prince, 1985) exhibit SFA.

The *in-vitro* conditions used to experimentally verify the presence of SFA are far from the operational mode of a typical neuron in a network. For spike-frequency adapting neurons driven by noisy currents representing input from an active network, the characteristic increasing interspike interval transient is difficult to detect by inspection due to highly variable spiking. Regardless, even in the static case (homogeneous noise) the effects of SFA can be observed in the correlations of ISIs (Chacron et al., 2003; Lindner & Longtin, 2003). In the dynamic case, the ensemble firing rate transient induced by SFA can be clearly seen in the so-called peri-stimulus time-histogram gathered over multiple trials of the stimulus protocol.

Phenomenological models for SFA and related relative refractory mechanisms augmenting a standard conductance-based integrate-and-fire neuron model are standard and given in (Dayan & Abbott, 2001, pp. 166) or (Koch, 1999, pp. 339) and recently generalized in (Brette & Gerstner, 2005). In (Benda & Herz, 2003), it is shown that a large class of biophysical mechanisms which induce SFA can be reduced to these conductance-based phenomenological models. Similar but current-based Adaptation mechanisms have been studied in (van Vreeswijk & Hansel, 2001) and the related threshold fatigue model for adaptation, also known as dynamic threshold, in (Chacron et al., 2003; Lindner & Longtin, 2003). See (Ermentrout, Pascal, & Gutkin, 2001) for a bifurcation analysis of I_{ahp} , the after-hyperpolarization current, a calcium-dependent potassium current, and, I_{m} , the muscarinic slow voltage-dependent potassium current, the biophysical mechanisms behind SFA, using a Hodgkin-Huxley type modeling framework.

Mean-adaptation approximations for the firing rate of populations of spike-frequency adapting neurons augmenting the standard Wilson & Cowan neuron population equations (Wilson & Cowan, 1972) were devised in (Latham, Richmond, Nelson, & Nirenberg, 2000; Fuhrmann et al., 2002) and used to study the synchronizing effects of SFA. Universal mean-adaptation methods for modeling the firing rate of adapting neurons subject to supra-threshold noise-free current input are given in (Benda & Herz, 2003). In (La Camera et al., 2004), mean-adaptation methods are investigated to describe the static and dynamic firing rates of a large class of integrate-and-fire neuron models with current-based and dynamic threshold adaptation mechanisms driven by noisy input currents representing input from an active network. The phenomenological firing rate relaxation dynamics of previous Wilson & Cowan studies is replaced in (La Camera et al., 2004) with a firing rate which depends instantaneously on filtered synaptic currents as suggested in (Fourcaud & Brunel, 2002; Renart et al., 2004). While for Wilson & Cowan ap-

proaches the relaxation time constant is a free parameter, the approach due to (La Camera et al., 2004) has no free parameters and excellent agreement is reported in the static and dynamic case for several neuron models.

1.3 Ordinary Renewal Theory

Poisson and gamma renewal processes, both special cases of an *ordinary renewal process*, enjoy widespread use in the literature to model the firing statistics of both cortical neurons and primary sensory neurons. Here the definition of an ordinary renewal process is reviewed and some useful properties presented, following the more detailed discussion available in (Cox, 1962).

Suppose a system which resets after a time, T , has elapsed since the last reset. Suppose that T , deemed the renewal interval, is a continuous random variable identically distributed with probability density function (PDF), $f(\tau)$, defined as

$$f(\tau) := \lim_{\Delta\tau \rightarrow 0^+} \frac{\text{prob}\{\tau < T \leq \tau + \Delta\tau\}}{\Delta\tau}. \quad (1.1)$$

This system one calls, then, an *ordinary renewal process*. One calls the system a *Poisson process* with rate ρ if

$$f(\tau) = \rho \exp(-\rho\tau). \quad (1.2)$$

One calls the system a *gamma renewal process* (GRP) with parameters a and b if

$$f(\tau) = \frac{\tau^{a-1} \exp(-\frac{\tau}{b})}{b^a \Gamma(a)}. \quad (1.3)$$

An ordinary renewal process is also called *homogeneous*, since the PDF is independent of time.

The *hazard function*, $\rho(\tau)$, sometimes called the *renewal density*, is defined for a renewal process as

$$\rho(\tau) = \lim_{\Delta\tau \rightarrow 0^+} \frac{\text{prob}\{> 0 \text{ renewals in } [\tau, \tau + \Delta\tau)\}}{\Delta\tau}, \quad (1.4)$$

where τ denotes the time since the last renewal¹. Since the probability of more than one renewal in $\Delta\tau$ is $O(\Delta\tau^2)$, $\rho(\tau)\Delta\tau$ for $\Delta\tau$ sufficiently small gives the probability that one renewal occurs during the aging of the system from τ to $\tau + \Delta\tau$. Thus, the hazard function has units of 1/time, and gives the temporal density of renewals or the average instantaneous renewal rate of a system of age

¹For the discussion of renewal processes, the notation of (Cox, 1962) is followed except: τ denotes age, t denotes time when later considering the inhomogeneous case, and ρ instead of h denotes the hazard function.

τ . The hazard function can be uniquely determined from the PDF (Cox, 1962). Specifically,

$$\rho(\tau) = \frac{f(\tau)}{\mathcal{F}(\tau)}, \quad (1.5)$$

where

$$\mathcal{F}(\tau) = \int_{s=\tau}^{\infty} f(s)ds \quad (1.6)$$

is known as the survivor function, as it gives the probability of no renewal (survival) for a time τ following the last renewal.

Given the hazard function, the PDF is also uniquely determined since it can be shown that

$$\mathcal{F}(\tau) = \exp\left(-\int_0^{\tau} \rho(s)ds\right), \quad (1.7)$$

and it follows from (1.5) that

$$f(\tau) = \rho(\tau) \exp\left(-\int_0^{\tau} \rho(s)ds\right). \quad (1.8)$$

Thus, it is a general result that for an ordinary renewal process, the hazard function uniquely determines the PDF and vice-versa.

1.4 Inhomogeneous Renewal Theory

To what extent neural firing patterns are random due to sensory noise and various unreliabilities of the neural substrate or rather part of a complex and dynamic code remains an ongoing debate (Softky & Koch, 1993; Rieke, Warland, de Ruyter van Steveninck, & Bialek, 1997; Shadlen & Newsome, 1998; Bialek, 2002). Nevertheless, it is common modeling practice to express time varying macroscopic parameters, such as local activity or stimulus intensity, in the instantaneous rate parameter of an inhomogeneous Poisson process, inherently assuming stochasticity in coding. Indeed, at the sensory periphery, such a rate coding hypothesis seems to be the whole story (Bialek, 2002; Uzzell & Chichilnisky, 2004). Where relative refractory periods or SFA effects are to be modeled, gamma renewal processes are often used, or other related renewal hazard recovery dynamics (Uzzell & Chichilnisky, 2004). Such studies are generally limited to static parameters of the spike train statistics, since the random number generation schemes required to generate an inhomogeneous gamma renewal process are not present in the literature of the neuron modeling community. Occasionally, the standard inverse-integrated-rate function approach for Poisson processes (Devroye, 1986) is applied directly to the gamma renewal process without considering the effect this has on the shape parameter, a , of the gamma distribution in equation 1.3 (Gazères, Borg-Graham, & Frégnac, 1998).

A formalism for treating a general inhomogeneous renewal process is given in detail in (Gerstner & Kistler, 2002) in sections 5.2, 5.3, 6.2.2 and 6.3.2. While the

treatment in section 6.2.2 is developed for Spike Response Model neurons with escape noise, and in section 6.3.2 for populations of neurons satisfying a few basic assumptions, it is not explicitly stated there that the analysis is that of an arbitrary inhomogeneous renewal process, though it is mentioned briefly in (Gerstner, 2001). First, this fact is reiterated by producing the main results of section 6.2.2 and 6.3.2 of (Gerstner & Kistler, 2002) using an inhomogeneous generalization of the notation of (Cox, 1962), a classic reference work on homogeneous renewal theory. Subsequently, In section 3.5, a recipe is presented for efficiently generating spike trains of a general inhomogeneous renewal process.²

The basic assumption of inhomogeneous renewal theory is that the state of the modeled system can be described by a single state variable, τ , the time since last renewal, or age of the system, and time t . The limiting probability density for the neuron to spike, or more generally, for the system to renew after surviving a time interval τ ,

$$\rho(\tau, t) = \lim_{\Delta t \rightarrow 0^+} \frac{\text{prob}\{> 0 \text{ renewals in } [t, t + \Delta t) \mid \tau\}}{\Delta t}, \quad (1.9)$$

also known as the hazard function (Cox, 1962), is a function of time, t , and age, τ .

The ensemble firing rate³ at t , denoted by $\alpha(t)$, is the expectation value,

$$\alpha(t) = \langle \rho(t) \rangle = \int_0^\infty \rho(s, t) f^-(s, t) ds, \quad (1.10)$$

where $f^-(\tau, t)$ denotes the inhomogeneous probability density function (PDF) of times since last renewal, also called the backward recurrence-time in (Cox, 1962), or the refractory density in (Gerstner & Kistler, 2002). Following conventional notation, the argument t is the time parameter, and is not to be mistaken for a distribution variable. Thus normalization is only over the distribution variable τ , i.e.

$$\int_0^\infty f^-(\tau, t) d\tau = 1. \quad (1.11)$$

This notational convention for including a time parameter in the PDF will be used throughout the text. The PDF, $f^-(\tau, t)$, can be determined by reasoning that the probability that the system has an age in the interval $(\tau, \tau + \Delta\tau)$ is equal to the probability that there is a renewal in the time interval $(t - \tau, t - \tau + \Delta\tau)$ and that the system subsequently survives until t . This yields

$$f^-(\tau, t) = \alpha(t - \tau) \mathcal{F}(\tau, t - \tau), \quad (1.12)$$

²In what follows, the pitfall of other studies which erroneously assume an intensity-rescaling transformation of a stationary gamma renewal process with parameter a (see equation 1.3) yields an inhomogeneous gamma renewal process with parameter a (Barbieri, Quirk, Frank, Wilson, & Brown, 2001; Gazères et al., 1998), is avoided by working exclusively with the inhomogeneous hazard function.

³The ensemble firing rate is referred to as the population activity, $A(t)$, in (Gerstner & Kistler, 2002).

where $\mathcal{F}(\Delta t, t)$ is the inhomogeneous survival function, representing the probability that the system will survive for a time Δt after spiking at t . Generalizing equation 1.2.10 in (Cox, 1962) for the inhomogeneous case, one has

$$\mathcal{F}(\Delta t, t) = \exp\left(-\int_0^{\Delta t} \rho(s, t+s)ds\right). \quad (1.13)$$

Plugging equation 1.12 into 1.10 results in the equivalent of equations 6.44 and 6.45 of (Gerstner & Kistler, 2002).

A differential formulation of equation 1.10-1.13 is possible. First note that age increases with increasing t and thus

$$\frac{d\tau}{dt} = 1.$$

This suggests a transform of the age variable $\tau \rightarrow \tau' = t - \tau$, as in equation 6.46 of (Gerstner & Kistler, 2002). This new age variable, τ' , is stationary with the evolution of t . Define the stationary backward recurrence-time PDF as

$$f_s^-(\tau', t) := f^-(t - \tau', t).$$

Thus

$$\begin{aligned} \frac{d}{d\tau} f_s^-(\tau', t) &= \frac{\partial}{\partial t} f_s^-(\tau', t) \\ &= \frac{\partial}{\partial t} \left(\alpha(\tau') \mathcal{F}(t - \tau', \tau') \right), \end{aligned}$$

and differentiation of equation 1.13 yields $\frac{d}{dt} \mathcal{F}(t - \tau', \tau') = \mathcal{F}(t - \tau', \tau') \rho(t - \tau', t)$, whereby one has

$$\begin{aligned} \frac{d}{dt} f_s^-(\tau', t) &= -\alpha(\tau') \mathcal{F}(t - \tau', \tau') \rho(t - \tau', t) \\ \frac{d}{dt} f_s^-(\tau', t) &= -f_s^-(\tau', t) \rho(t - \tau', t). \end{aligned} \quad (1.14)$$

This relation determines $\frac{d}{dt} f_s^-(\tau', t)$ for $\tau' \in (-\infty, t)$. Additionally, normalization of $f_s^-(\tau, t)$ must be preserved, namely

$$\int_{-\infty}^{\infty} \frac{\partial}{\partial t} f_s^-(\tau, t) d\tau = 0. \quad (1.15)$$

Splitting the integral into three regions of interest one has

$$\begin{aligned} \lim_{\Delta t \rightarrow 0^+} \left[\int_{-\infty}^{t-\Delta t} \frac{\partial}{\partial t} f_s^-(s, t) ds \right. \\ \left. + \int_{t-\Delta t}^{t+\Delta t} \frac{\partial}{\partial t} f_s^-(s, t) ds \right. \\ \left. + \int_{t+\Delta t}^{\infty} \frac{\partial}{\partial t} f_s^-(s, t) ds \right] = 0. \end{aligned}$$

Since $f_s^-(\tau' > t, t) = 0$, the third integral is zero. One has then

$$\lim_{\Delta t \rightarrow 0^+} \int_{t-\Delta t}^{t+\Delta t} \frac{\partial}{\partial t} f_s^-(s, t) ds = - \int_{-\infty}^t \frac{\partial}{\partial t} f_s^-(s, t) ds.$$

Since the contribution from equation 1.14 in the integral on the left hand side is vanishing, it is necessary to add an additional term to $\frac{d}{dt} f_s^-(\tau, t)$ which is zero for all $\tau \neq t$ but which has a finite integral when integrating around t . This can be achieved by addition of a δ -function term, namely

$$\frac{d}{dt} f_s^-(\tau, t) \rightarrow \frac{d}{dt} f_s^-(\tau, t) - \delta(\tau - t) \int_{-\infty}^t \frac{\partial}{\partial t} f_s^-(s, t) ds.$$

Notice the factor behind the δ -function is $\alpha(t)$. Thus one has the final form,

$$\begin{aligned} \frac{d}{dt} f_s^-(\tau', t) = & \begin{cases} -f_s^-(\tau', t) \rho(t - \tau', t), & \tau' < t \\ 0, & \tau' \geq t \end{cases} \\ & + \alpha(t) \delta(\tau' - t), \end{aligned} \quad (1.16)$$

defined for $\tau' \in (-\infty, \infty)$. Equation 1.16 expressed in terms of $f^-(\tau, t)$ results in the master equation (Risken, 1996)

$$\frac{\partial}{\partial t} f^-(\tau, t) = -\frac{\partial}{\partial \tau} f^-(\tau, t) - f^-(\tau, t) \rho(\tau, t) + \alpha(t) \delta(\tau), \quad (1.17)$$

defined for $\tau \in [0, \infty)$. Thus, the renewal process is a special case of the more general Markov process.

Given $\alpha(t)$, the number of renewals that occur on the interval $(t, t+dt)$ summed over m trials (or m realizations of a renewal process) is Poisson distributed with a mean, $\mu = \alpha(t) \cdot m \cdot dt$ and standard deviation, $\sigma = \sqrt{\mu}$. The ensemble firing rate estimated to a resolution Δt by binning spike times wrt t of sufficiently many trials is known as the peri-stimulus time histogram (PSTH).

1.5 Beyond Renewal Theory

The defining characteristic of renewal theory is that the firing probability is modeled as a function the time since last spike, or age, and successive ISIs are statistically independent. As such, these models neglect by definition the observations in (Chacron et al., 2003) and (Lindner & Longtin, 2003) that neurons with spike-frequency adaptation (SFA), a mechanism present in the majority of excitatory cells, exhibit negative serial ISI correlations.

As stated in (Gerstner & Kistler, 2002, pp. 246), “A generalization of the [renewal] population equation to neuron models with [spike-frequency] adaptation is not straightforward since the [renewal] formalism assumes that only the last

spike suffices. ... A full treatment of adaptation would involve a density description in the high-dimensional space of the microscopic neuronal variables [as in] (Knight, 2000).”

In section 2.2 a full treatment of the density description mentioned above is provided. However, before proceeding it is instructive to consider what a model might look like which allows for a statistical dependence (correlation) between subsequent ISIs.

Consider the standard phenomenological model for SFA proposed in (Dayan & Abbott, 2001) where a given neuron model is augmented with a conductance $g_s(t)$ which makes the jump $g_s(t + dt) = g_s(t) + q_s$ when the neuron spikes at time t and is otherwise governed by

$$\frac{dg_s(t)}{dt} = -\frac{1}{\tau_s}g_s(t). \quad (1.18)$$

Now consider a neuron that has g_s as a state variable and a probability density to fire of the form

$$h_g(g_s, t) = \lim_{\Delta t \rightarrow 0^+} \frac{\text{prob}\{\gt 0 \text{ spikes in } [t, t + \Delta t] \mid g_s\}}{\Delta t}, \quad (1.19)$$

where g_s evolves in time by equation 1.18. This process is analogous to a renewal process, but now with a single state variable, g_s , which is not reset at each occurrence of a spike, but which slowly forgets with a timescale of τ_s due to equation 1.18. For a model of this form, it is possible for correlations to arise between subsequent ISIs. Both the renewal hazard function, $\rho(\tau, t)$, and the $h_g(g_s, t)$ defined here are referred to as hazard functions as they both represent a probability density of the system to spike, given the state variable τ or g_s .

It is straight-forward to show that the ensemble of such neurons is a Markov process governed by a master equation of the form

$$\begin{aligned} \frac{\partial}{\partial t}P(g_s, t) &= \frac{\partial}{\partial g_s} \left[\frac{g_s}{\tau_s} P(g_s, t) \right] \\ &\quad + h_g(g_s - q_s, t)P(g_s - q_s, t) \\ &\quad - h_g(g_s, t)P(g_s, t), \end{aligned} \quad (1.20)$$

where $P(g_s, t)$ is the distribution of state variables g_s with $P(g_s < 0, t) \equiv 0$. The distribution $P(g_s, t)$ is analogous to the distribution of ages, $f^-(\tau, t)$, of renewal theory, and equation 1.20 is analogous to the renewal theory equation 1.17. The model defined by equation 1.20 is referred to as the 1-D Markov (1DM) model throughout the text. See Table 3.1 for an overview of the models considered in the text.

Understanding the connection of the 1DM model to its renewal theory cousin

is facilitated by transforming g_s to a pseudo age variable t_s by⁴

$$t_s = \eta(g_s) := -\tau_s \log(g_s/q_s). \quad (1.21)$$

The hazard function $h_g(g_s, t)$ becomes $h(t_s, t) = h_g(\eta^{-1}(t_s), t)$, a hazard function as in equation 1.9 of the pseudo age variable t_s , but defined also for $t_s < 0$. The distribution of states $P(g_s, t)$ becomes $P(t_s, t)$, where they are related by

$$P(t_s, t) = P(g_s = \eta^{-1}(t_s), t) \frac{d}{dt_s} \eta^{-1}(t_s). \quad (1.22)$$

The reset condition is not $t_s \mapsto 0$ as for a renewal process, but

$$\begin{aligned} t_s \mapsto \eta(g_s + q_s) &= -\tau_s \log\left(\frac{g_s}{q_s} + 1\right) \\ &= -\tau_s \log\left(\exp\left(\frac{-t_s}{\tau_s}\right) + 1\right). \end{aligned} \quad (1.23)$$

The variable t_s is then a general state variable which no longer represents the time since last spike, as in renewal theory. Defining the reset mapping

$$\psi(t_s) := -\tau_s \log\left(\exp\left(\frac{-t_s}{\tau_s}\right) + 1\right), \quad (1.24)$$

with its inverse given by

$$\psi^{-1}(t_s) = -\tau_s \log\left(\exp\left(\frac{-t_s}{\tau_s}\right) - 1\right), \quad (1.25)$$

whereby $\psi(\psi^{-1}(t)) = t$ and $\psi^{-1}(\psi(t)) = t$ as required by the definition of the inverse, the reset condition becomes $t_s \mapsto \psi(t_s)$. Since $\psi : \mathbb{R} \rightarrow \mathbb{R}^-$, it follows that all trajectories are reinserted at negative pseudo ages, and it can be seen from the form of ψ that “younger” trajectories are reinserted at more negative pseudo ages. This dependence of the reinserted state on the state just prior to spiking yields a Markov process (Risken, 1996) which cannot be described by the subset of Markov processes encompassed by renewal theory.

The master equation in terms of t_s takes the form

$$\begin{aligned} \frac{\partial}{\partial t} P(t_s, t) &= -\frac{\partial}{\partial t_s} P(t_s, t) \\ &+ \begin{cases} -h(t_s, t)P(t_s, t), & t_s \geq 0 \\ h(\psi^{-1}(t_s), t)P(\psi^{-1}(t_s), t) - h(t_s, t)P(t_s, t) & t_s < 0. \end{cases} \end{aligned} \quad (1.26)$$

⁴The convention of using positional arguments for functions and labeled arguments for derivatives will be followed throughout the text. Probability distributions are excepted from this rule, as they are not functions but densities. The notation “:=” denotes definition of a function and it’s positional arguments.

revealing the advantage of the variable transformation $g_s \rightarrow t_s$: The deterministic drift term in equation 1.20 for the exponential decay of g_s is transformed to a constant drift term in t_s analogous to age in renewal theory. As a result, much can be calculated by analogy to renewal theory, and one is freed from the difficulty of treating the non-constant drift towards zero in equation 1.20 numerically. It will be seen in later sections that $h(t_s, t)$ is, in practice, approximately of the form

$$h(t_s, t) = a_h(t) \exp(-b_h(t)q_s \exp(-t_s/\tau_s)) \quad (1.27)$$

for the neuron model and SFA mechanism considered here, where $a_h(t)$ and $b_h(t)$ are determined by the stimulus. The subscript h distinguishes a_h and b_h from the parameters a and b of the gamma renewal process.

For the static case where $h(t_s, t) \equiv h(t_s)$, $P(t_s)$ can be found from equation 1.26 by setting $\partial/\partial t P(t_s, t) = 0$. The resulting equation for $t_s \geq 0$,

$$\frac{\partial}{\partial t_s} P(t_s) = -h(t_s)P(t_s), \quad (1.28)$$

is exactly as for a renewal process. The solution is the homogeneous survival function

$$P(t_s) = k\mathcal{W}(t_s, 0), \quad (1.29)$$

where

$$k = \left[\int_{-\infty}^{\infty} \mathcal{W}(t_s, 0) dt_s \right]^{-1} \quad (1.30)$$

is a constant of normalization, and the generalized survival function,

$$\mathcal{W}(\Delta t, t_s^0) = \exp\left(-\int_0^{\Delta t} h(t_s^0 + s) ds\right), \quad (1.31)$$

and analogously the inhomogeneous generalized survival function

$$\mathcal{W}(\Delta t, t_s^0, t) = \exp\left(-\int_0^{\Delta t} h(t_s^0 + s, t + s) ds\right), \quad (1.32)$$

represent the probability that a system with initial state $t_s^0 \in \mathbb{R}$ will survive for a time Δt , and a time Δt after t , respectively and are analogous to the survival function of renewal theory, except for the explicit dependence on the initial state, t_s^0 . The distribution $P(t_s)$ for $t_s < 0$ was solved numerically by discretizing and integrating back from $t_s = 0$. An iterative analytical approach is given in (Büsing, 2006).

The distribution of pseudo ages just prior to spiking at t , $P^*(t_s, t)$, is related to $P(t_s, t)$ by

$$P^*(t_s, t) = \frac{h(t_s, t)P(t_s, t)}{\alpha(t)}, \quad (1.33)$$

where

$$\alpha(t) = \int_{-\infty}^{\infty} h(t_s, t)P(t_s, t) dt_s \quad (1.34)$$

is the normalizing constant and also the firing rate of the ensemble.

The distribution of pseudo ages just after spiking at t , $P^\dagger(t_s, t)$, is related to $P^*(t_s, t)$ by transforming variables by the reset mapping (equation 1.24) for a probability distribution:

$$P^\dagger(t_s, t) = P^*(\psi^{-1}(t_s), t) \frac{d}{dt_s} \psi^{-1}(t_s). \quad (1.35)$$

1.5.1 Computing Renewal Quantities

The various quantities of renewal theory such as the ISI distribution, hazard function, and survival function are of interest, and are straight-forward to calculate.

First, the renewal survival function, $\mathcal{F}(\tau, t)$, the probability that a system which spiked at t will survive the time interval τ is given by

$$\mathcal{F}(\tau, t) = \int_{-\infty}^{\infty} \mathcal{W}(\tau, t_s, t) P^\dagger(t_s, t) dt_s. \quad (1.36)$$

The ISI distribution, $f(\tau, t)$, the probability that a neuron which spiked at t will survive for an interval τ and subsequently spike at $t + \tau$ is

$$f(\tau, t) = \int_{-\infty}^{\infty} h(t_s + \tau, t + \tau) \mathcal{W}(\tau, t_s, t) P^\dagger(t_s, t) dt_s. \quad (1.37)$$

Equivalently in terms of $P^*(t_s, t)$,

$$f(\tau, t) = \int_{-\infty}^{\infty} h(\psi(t_s) + \tau, t + \tau) \mathcal{W}(\tau, \psi(t_s), t) P^*(t_s, t) dt_s. \quad (1.38)$$

The hazard function of the system in a renewal sense, $\rho(\tau, t)$, where τ is a true age, is by definition the firing rate of the sub-population which previously spiked at time $t - \tau$. Thus,

$$\rho(\tau, t) = \int_{-\infty}^{\infty} h(t_s, t) P(t_s, t | \text{spike at } t - \tau) dt_s, \quad (1.39)$$

where the state distribution of the system given a spike at $t - \tau$, $P(t_s, t | \text{spike at } t - \tau)$, can be determined by reasoning that it is the distribution of states just after spiking with arguments $t_s - \tau$ and $t - \tau$, $P^\dagger(t_s - \tau, t - \tau)$, which subsequently survive the interval τ ,

$$P(t_s, t | \text{spike at } t - \tau) = k_1 P^\dagger(t_s - \tau, t - \tau) \mathcal{W}(\tau, t_s - \tau, t - \tau), \quad (1.40)$$

where k_1 is the normalization factor

$$k_1 = \left[\int_{-\infty}^{\infty} P^\dagger(t_s - \tau, t - \tau) \mathcal{W}(\tau, t_s - \tau, t - \tau) dt_s \right]^{-1}, \quad (1.41)$$

and by inspection of equation 1.36,

$$k_1 = \mathcal{F}(\tau, t - \tau), \quad (1.42)$$

such that

$$\rho(\tau, t) = \frac{1}{\mathcal{F}(\tau, t - \tau)} \int_{-\infty}^{\infty} h(t_s, t) P^\dagger(t_s - \tau, t - \tau) \mathcal{W}(\tau, t_s - \tau, t - \tau) dt_s. \quad (1.43)$$

Clearly, the numerator is just $f(\tau, t - \tau)$, resulting in

$$\rho(\tau, t) = \frac{f(\tau, t - \tau)}{\mathcal{F}(\tau, t - \tau)}. \quad (1.44)$$

This verifies that the standard renewal theory relation given by equation 1.5, generalized for the homogeneous case, still holds. It is interesting to note that, in the inhomogeneous case, there is an alternate definition for the ISI distribution which is equally sensible, namely, define $\hat{f}(\tau, t)$ as the probability that a neuron which spiked at $t - \tau$ will survive the interval τ and subsequently spike at t . This is the ISI distribution which treats the spike at t as the final spike of the ISI, rather than the initial spike as in equation 1.38. If one prefers this alternate definition of the ISI distribution, as in (Gerstner & Kistler, 2002), then one has

$$\hat{f}(\tau, t) = \int_{-\infty}^{\infty} h(t_s + \tau, t) \mathcal{W}(\tau, t_s, t - \tau) P^\dagger(t_s, t - \tau) dt_s, \quad (1.45)$$

implying that $\hat{f}(\tau, t) = f(\tau, t - \tau)$ and equation 1.44 becomes

$$\rho(\tau, t) = \frac{\hat{f}(\tau, t)}{\mathcal{F}(\tau, t - \tau)}. \quad (1.46)$$

1.5.2 Correlations

In this section, an expression for the joint serial ISI distribution, $f(\tau_{i+1}, \tau_i, t)$, will be derived for the proposed adapting Markov process, and shown to exhibit ISI correlations.

Recall the definition of the absence of correlations between two random variables: τ_i and τ_{i+1} are uncorrelated (independent) if and only if

$$f(\tau_{i+1}, \tau_i) = f(\tau_{i+1})f(\tau_i), \quad (1.47)$$

where $f(\tau_{i+1}, \tau_i)$ is the joint probability distribution of two back to back ISIs in the homogeneous case.

For the inhomogeneous case, a separation of this joint distribution $f(\tau_{i+1}, \tau_i, t)$ by Bayes' theorem,

$$f(\tau_{i+1}, \tau_i, t) = f(\tau_{i+1}, t | \tau_i) f(\tau_i, t - \tau_i), \quad (1.48)$$

reveals a subtlety: The time argument of $f(\tau_i, t)$, the marginal distribution of τ_i , must be retarded by τ_i . This is due to the fact that for τ_i to precede τ_{i+1} at t , it must occur at $t - \tau_i$. Given that $f(\tau, t)$ is known, it is left to determine an expression for $f(\tau_{i+1}, t|\tau_i)$. This can be achieved using equation 1.38 by replacing $P^*(t_s, t)$ with the conditional distribution of states just after spiking given a spike at $t - \tau_i$, which is denoted by $P^*(t_s, t|\tau_i)$.

The distribution $P^*(t_s, t|\tau_i)$, the conditional distribution of states *just prior to spiking*, given a spike at $t - \tau_i$, takes the form

$$P^*(t_s, t|\tau_i) = k_2 h(t_s, t) P(t_s, t | \text{spike at } t - \tau_i), \quad (1.49)$$

where k_2 is a normalization factor, and an expression for $P(t_s, t | \text{spike at } t - \tau_i)$ was given in equation 1.40. By inspection, it can be seen that $k_2^{-1} = \rho(\tau_i, t)$.

Plugging this expression for $P^*(t_s, t|\tau_i)$ into equation 1.38 yields

$$\begin{aligned} f(\tau_{i+1}, \tau_i, t) = \\ f(\tau_{i+1}, t|\tau_i) f(\tau_i, t - \tau_i) = \int_{-\infty}^{\infty} h(\psi(t_s) + \tau_{i+1}, t + \tau_{i+1}) \mathcal{W}(\tau_{i+1}, \psi(t_s), t) \\ \times h(t_s, t) \mathcal{W}(\tau_i, t_s - \tau_i, t - \tau_i) P^\dagger(t_s - \tau_i, t - \tau_i) dt_s, \end{aligned} \quad (1.50)$$

an inhomogeneous expression for the joint ISI distribution of two successive ISIs.

It is instructive to verify that for the case of a renewal process, equation 1.50 predicts no correlations. For a renewal process, $\psi(t_s) = 0$ and $P^\dagger(t_s, t) = \delta(t_s)$, such that equation 1.50 becomes

$$\begin{aligned} f(\tau_{i+1}, \tau_i, t) = \\ h(\tau_{i+1}, t + \tau_{i+1}) \mathcal{W}(\tau_{i+1}, 0, t) \cdot h(\tau_i, t) \mathcal{W}(\tau_i, 0, t - \tau_i). \end{aligned} \quad (1.51)$$

In addition, the ISI distribution given by equation 1.37 reduces to

$$f(\tau, t) = h(\tau, t + \tau) \mathcal{W}(\tau, 0, t), \quad (1.52)$$

the inhomogeneous equivalent to equation 1.5 of ordinary renewal theory. Thus, it can be seen by inspection that equation 1.51 is of the form

$$f(\tau_{i+1}, \tau_i, t) = f(\tau_{i+1}, t) f(\tau_i, t - \tau_i), \quad (1.53)$$

implying as expected that successive ISIs are uncorrelated for a renewal process.

While the calculations in this chapter are perhaps difficult when seen for the first time, they become almost trivial once one is familiar with the various quantities, \mathcal{W} , P^\dagger , etc., and how they fit together to calculate a quantity of interest. Thus, while it has not yet occurred to the author, it is not unreasonable to expect that one could find an abstract algebra to express the calculations in a more concise way. Such an algebra would facilitate, among other things, a generalization of the calculations to higher order serial correlations, and make such calculations interesting to a wider audience.

Chapter 2

Ensembles of Detailed Neurons

It appears then that a sufficiently complex stochastic process will give a satisfactory representation of a discrete source.

Claude E. Shannon, The Mathematical Theory of Communication

In this chapter, the canonical conductance-based integrate-and-fire neuron model driven by Poisson spike trains, augmented by mechanisms for spike-frequency adaptation and a relative refractory period will be considered. It will be shown that the full five-dimensional master equation for this system can be reduced to a two-dimensional generalization of the one-dimensional Markov model (1DM) of the previous chapter by an adiabatic elimination of fast variables. Fitting methods are given for calibrating the reduced two-dimensional model and renewal theory models to this full system.

2.1 Neuron Model, Adaptation, Input

Following (Rudolph & Destexhe, 2003; Richardson, 2004; Richardson & Gerstner, 2005; Rudolph & Destexhe, 2005), considered here are the equations for the membrane potential, $v(t)$, and excitatory and inhibitory synaptic conductances, $g_e(t)$ and $g_i(t)$, of the conductance-based integrate-and-fire neuron driven by Poisson input:

$$c_m \frac{dv(t)}{dt} = g_l(E_l - v(t)) + g_e(t)(E_e - v(t)) + g_i(t)(E_i - v(t)) \quad (2.1)$$

$$\frac{dg_e(t)}{dt} = -\frac{1}{\tau_e} g_e(t) + q_e \mathcal{S}_e(t) \quad (2.2)$$

$$\frac{dg_i(t)}{dt} = -\frac{1}{\tau_i} g_i(t) + q_i \mathcal{S}_i(t), \quad (2.3)$$

where c_m represents the membrane capacitance, g_l the leak conductance, E_x the various reversal potentials, q_x the quantal conductance increases, and τ_x the synaptic time constants. The exact parameters used are given in appendix A. The excitatory and inhibitory input spike trains, $\mathcal{S}_x(t)$ with $x \in \{e, i\}$ respectively, are given by

$$\mathcal{S}_x(t) = \sum_k \delta(t - s_{x,k}), \quad (2.4)$$

where $s_{x,k}$ are the spike-times of a realization of an inhomogeneous Poisson process (Papoulis & Pillai, 1991). Thus, $\mathcal{S}_x(t)$ satisfies the constraints

$$\langle \mathcal{S}_x(t) \rangle = \nu_x(t) \quad (2.5)$$

$$\langle \mathcal{S}_x(t) \mathcal{S}_x(t') \rangle = \nu_x(t) \nu_x(t') + \nu_x(t') \delta(t - t'). \quad (2.6)$$

Here $\nu_x(t)$ represents the time varying rate of the inhomogeneous Poisson process and $\langle \rangle$ represents the expectation value over the ensemble of realizations. In what follows, all Poisson processes are assumed inhomogeneous unless otherwise stated.

To put the neuron in a state of high-conductance, it is bombarded by $N_e = 1000$ and $N_i = 250$ excitatory and inhibitory Poisson processes all with rate functions $\lambda_e(t)$ and $\lambda_i(t)$ respectively so that

$$\nu_x(t) = N_x \lambda_x(t). \quad (2.7)$$

A simple thresholding mechanism approximates the action potential dynamics of real neurons: If $v(t)$ exceeds the threshold, v_{th} , $v(t)$ is reset to v_{reset} . Thus, analogous to the input spike train, the output spike train takes the form

$$\mathcal{A}(t) = \sum_k \delta(t - s_k), \quad (2.8)$$

where s_k are the times of membrane potential threshold crossings enumerated by k .

SFA and a relative refractory period can be modeled both with the addition of a current to equation 2.1 of the form proposed in (Dayan & Abbott, 2001),

$$g_y(t)(E_y - v(t)), \quad (2.9)$$

where E_y is a reversal potential. The conductance $g_y(t)$ is governed by

$$\frac{dg_y(t)}{dt} = -\frac{1}{\tau_y} g_y(t) + q_y \mathcal{A}(t), \quad (2.10)$$

where τ_y and q_y are the time constant and quantal conductance increase of the mechanism. The subscripts $y = s$ and $y = r$ label SFA and the relative refractory mechanism, respectively. Defining

$$\beta_v(v, g_e, g_i, g_s, g_r) := g_l(E_l - v) + \sum_{\mu=e,i,s,r} g_\mu(E_\mu - v), \quad (2.11)$$

and for $\mu = e, i, s, r$,

$$\beta_\mu(g_\mu) := -\frac{1}{\tau_\mu}g_\mu, \quad (2.12)$$

the five-dimensional system of coupled differential equations describing the conductance-based spike-frequency adapting relative refractory integrate-and-fire neuron driven by Poisson input is:

$$c_m \frac{dv(t)}{dt} = \beta_v(v(t), \dots, g_r(t)) - (V_{\text{th}} - V_{\text{reset}}) \mathcal{A}(t) \quad (2.13)$$

$$\frac{dg_x(t)}{dt} = \beta_x(g_x(t), t) + q_x \mathcal{S}_x(t) \quad (2.14)$$

$$\frac{dg_y(t)}{dt} = \beta_y(g_y(t), t) + q_y \mathcal{A}(t), \quad (2.15)$$

where $x \in \{e, i\}$ and $y \in \{s, r\}$. Equations 2.13-2.15 are referred to as the full five-dimensional (5DF) model throughout the text (see the model overview in Table 3.1). The parameters used are given in Table A.1.

2.2 Ensemble Behavior

It is natural to look for an ensemble description of equations 2.13-2.15, given that the input is described in terms of an ensemble.

Equations 2.13-2.15 are a set of concurrent first order differential equations, i.e. the right hand sides at time t are functions of the instantaneous values of the state variables, $(v(t), g_e(t), g_i(t), g_s(t), g_r(t))$, implying no delays or memory effects are to be modeled. The system is, therefore, a *Markov process* and given an initial distribution $P(v, g_e, g_i, g_s, g_r, t_0)$ for some t_0 , the evolution of $P(v, g_e, g_i, g_s, g_r, t)$ can be described by a suitable master equation (Risken, 1996). For the system in question here, the master equation takes the form

$$\begin{aligned} \frac{\partial}{\partial t} P(v, g_e, g_i, g_s, g_r, t) &= -\text{div } J(v, g_e, g_i, g_s, g_r, t) \\ &+ \delta(v - v_{\text{reset}}) J_v(v_{\text{th}}, g_e, g_i, g_s - q_s, g_r - q_r, t), \end{aligned} \quad (2.16)$$

where the probability current density, J , is a vector with components

$$J_v(v, g_e, g_i, g_s, g_r, t) = \beta_v(v, g_e, g_i, g_s, g_r, t) P(v, g_e, g_i, g_s, g_r, t) \quad (2.17)$$

$$J_\mu := \beta_\mu(g_\mu, t) P(v, g_e, g_i, g_s, g_r, t), \quad (2.18)$$

with $\mu \in \{s, r\}$. For J_e and J_i see appendix B. The δ term in equation 2.16 implements the reinsertion of probability flux that crosses the threshold, and is equivalent to an appropriately chosen boundary condition. Furthermore, it is defined that $P(v, g_e, g_i, g_s, g_r, t) = 0$ if one or more of the conductances g_e, \dots, g_r is negative.

There exists a wealth of literature treating master equations of conductance and current-based integrate-and-fire neuron models in the absence of adaptation and relative refractory mechanisms (Knight, 1972; Gerstner, 1995; Brunel, 2000; Omurtag et al., 2000; Nykamp & Tranchina, 2000; Knight, Omurtag, & Sirovich, 2000; Gerstner, 2000; Fourcaud & Brunel, 2002; Rudolph & Destexhe, 2003; Richardson, 2004; Rudolph & Destexhe, 2005; Richardson & Gerstner, 2005). The usual approach is to make the so-called diffusion approximation, yielding generally a Fokker-Planck equation for the membrane potential, and perhaps one or two other dimensions treating synaptic conductances.

A novel approach is given here, applicable for neurons in the high-conductance state, whereby the variables v, g_e, g_i are eliminated by a technique known as an adiabatic elimination of fast variables (Haken, 1983; Gardiner, 1984), and the system is reduced to a master equation for the two-dimensional marginal probability distribution, $P(g_s, g_r, t)$, of the slow variables, g_s and g_r . As it will be seen, the membrane potential, v , and the synaptic conductances, g_e and g_i , are thus encapsulated in the hazard function, $h_g(g_s, g_r, t)$. The static input case, λ_e, λ_i , is treated here. The reasoning is generalized for dynamic external input $\lambda_e(t), \lambda_i(t)$ in section 2.3.

Followed here is the intuitive treatment of adiabatic elimination given in (Haken, 1983). To begin, $P(v, \dots, g_r)$ is integrated over the fast variables v, g_e, g_i yielding the marginal distribution for the slow variables g_s, g_r ,

$$P(g_s, g_r, t) = \int_0^\infty \int_0^\infty \int_{-\infty}^{v_{th}} P(v, g_e, g_i, g_s, g_r, t) dv dg_e dg_i. \quad (2.19)$$

Integrating equation 2.16 over v, g_e, g_i yields

$$\begin{aligned} \frac{\partial}{\partial t} P(g_s, g_r, t) = & - \sum_{\mu=s,r} \frac{\partial}{\partial g_\mu} (\beta_\mu(g_\mu) P(g_s, g_r, t)) \\ & - \int_0^\infty \int_0^\infty \beta_v(v_{th}, g_e, g_i, g_s, g_r) P(v_{th}, g_e, g_i, g_s, g_r, t) dg_e dg_i \\ & + \int_0^\infty \int_0^\infty \beta_v(v_{th}, g_e, g_i, g_s - q_s, g_r - q_r) P(v_{th}, g_e, g_i, g_s - q_s, g_r - q_r, t) dg_e dg_i. \end{aligned} \quad (2.20)$$

For the details of the calculation, see appendix B. Now the marginal distribution for the slow variables is separated from the full distribution under the integral in equation 2.20 such that

$$P(v, g_e, g_i, g_s, g_r, t) = P(v, g_e, g_i, t | g_s, g_r, t) P(g_s, g_r, t), \quad (2.21)$$

and *the adiabatic approximation* as in (Haken, 1983) is made, i.e. that

$$P(v, g_e, g_i, t | g_s, g_r, t) \approx P^{(g_s, g_r)}(v, g_e, g_i, t) P(g_s, g_r, t), \quad (2.22)$$

where $P^{(g_s, g_r)}(v, g_e, g_i, t)$ is the solution to the three-dimensional master equation for the canonical conductance-based integrate-and-fire neuron with a constant bias current, $I(g_s, g_r) = g_s(E_s - v) + g_r(E_r - v)$, with neither SFA nor the relative refractory mechanism. This is equivalent to the assumption that v, g_e, g_i are immediately at equilibrium given the slow variables, or in other words, the system responds adiabatically to the dynamics of the slow variables g_s, g_r . The adiabatic assumption ensures the two-dimensional process of the slow state variables, $(g_s(t), g_r(t))$, is a Markov process.

Now defining the hazard function

$$h_g(g_s, g_r, t) := \int_0^\infty \int_0^\infty \beta_v(v_{th}, g_e, g_i, g_s, g_r) P^{(g_s, g_r)}(v, g_e, g_i, t) dg_e dg_i, \quad (2.23)$$

the master equation 2.20 becomes

$$\begin{aligned} \frac{\partial}{\partial t} P(g_s, g_r, t) &= - \sum_{\mu=s,r} \frac{\partial}{\partial g_\mu} (\beta_\mu(g_\mu) P(g_s, g_r, t)) \\ &\quad - h_g(g_s, g_r, t) P(g_s, g_r, t) \\ &\quad + h_g(g_s - q_s, g_r - q_r, t) P(g_s - q_s, g_r - q_r, t). \end{aligned} \quad (2.24)$$

The model defined by equation 2.24 is referred to as the 2-D Markov (2DM) model throughout the text (see the model overview in Table 3.1).

The assumption that g_s is slow compared to v, g_e, g_i is easily justified as the timescale of g_s is on the order of 100 ms, while the timescale of v is on the order of 2 ms in the high-conductance state. The timescale of the mean and standard deviation of g_e and g_i are on the order of $\tau_e = 1.5$ ms and $\tau_i = 10$ ms respectively, while the fluctuations of g_e and g_i are the source of stochasticity of the system and on still a shorter timescale, due to their instantaneous jumps.

The timescale of g_r is significantly faster than g_s , though its treatment as a slow variable also justifiable, be it in a somewhat indirect manner. As has been argued in (Fourcaud & Brunel, 2002; Renart et al., 2004), for neurons with synaptic time constants comparable to or larger than the effective membrane time constant and driven by sufficient input noise, as is the case here, the firing rate follows the input current almost instantaneously. It is this property which allows the dynamic firing rate to be treated as a function of the time-dependent means and variances of the synaptic conductances in (La Camera et al., 2004), a method also followed here in section 2.3. This suggests such modulations do not push the system far from equilibrium, and the system returns to equilibrium on a timescale faster than that of the synaptic means (τ_e, τ_i) . Since over the domain of the g_r trajectory for which the integrals on the rhs in equation 2.20 are non-zero, g_r has a timescale comparable to the mean of the synapses, the argument applies equally to g_r . However, since g_r is spike-triggered, g_r remains in the master equation, while the synaptic variables, g_e and g_i , determine $h_g(g_s, g_r, t)$ and can be treated outside of the master equation formalism.

Methods to undertake a rigorous analysis of the error in the adiabatic approximation are beyond the scope of this work. What follows are a variety of numerical comparisons to demonstrate the accuracy and domain of applicability of the proposed approximation.

2.3 Calibration of Markov Process Models

In this section, methods for determining appropriate homogeneous and inhomogeneous hazard functions for the 1DM, 2DM, and renewal models are provided. Since no analytical expression for equation 2.23, or the renewal hazard function of the 5DF model are yet known, fits of the homogeneous hazard functions determined by 5DF Monte-Carlo simulations in the static case are used. The inhomogeneous functions are then constructed from the homogeneous ones by discretizing time and taking one homogeneous hazard function for the duration of a single time bin.

2.3.1 Determining the Static Hazard Function for Adapting Markov Models

Given a finite subset of the possible realizations of the Poisson input spike trains, the 5DF model equations 2.13-2.15 can be integrated for each input realization. Any statistical quantity of interest can then be approximated by averaging or histogramming over this finite set of trajectories. This approach is known as the Monte-Carlo method. By increasing the number of trials in this finite set of realizations, the statistical quantities determined by the Monte-Carlo method converge to the true quantities. Therefore, Monte-Carlo simulations are used for determining the unknown hazard functions as well as later benchmarking the reduced master equations.

By Monte-Carlo simulations of the 5DF model under static stimulation, the quantities $P^*(g_s + g_r)$, $P(g_s + g_r)$, and $\alpha(t)$ can be obtained. Then analogous to equation 1.33, $h_g(g_s, g_r)$ can be determined by

$$h_g(g_s, g_r) = h_g(g_s + g_r) = \frac{\alpha P^*(g_s + g_r)}{P(g_s + g_r)}, \quad (2.25)$$

where the sum of the conductances, $g_s + g_r$, can be treated, rather than each independently because their reversal potentials have been chosen to be equal (see appendix A). It was found that $h_g(g_s, g_r)$ can be fit well by a function of the form:

$$h_g(g_s, g_r) = a_h \exp(-b_h \cdot (g_s + g_r)), \quad (2.26)$$

where a_h and b_h are fit parameters. Some typical fits for various excitatory Poisson input rates are shown in Figure 2.1. For the 1DM model, the same fit parameters were used but with $g_r = 0$. Transforming to (t_s, t_r) by the inverse of equation 1.21 results in

$$h(t_s, t_r) = a_h \exp\left(-b_h \cdot (q_s \exp(-t_s/\tau_s) + q_r \exp(-t_r/\tau_r))\right). \quad (2.27)$$

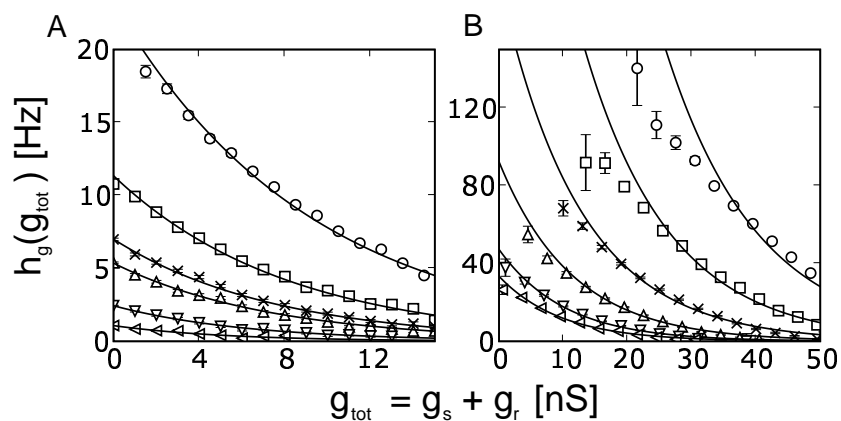


Figure 2.1: $h_g(g_s, g_r) = h_g(g_s + g_r)$ as a function of $g_{\text{tot}} = g_s + g_r$, as determined from 5DF Monte-Carlo (data points, 1000 trials per λ_e , 10 s per trial, $dt = 0.01$ ms) by equation 2.25, was found to be approximately exponential for a range of excitatory stimulation rates, λ_e , with the inhibitory stimulation rate fixed at $\lambda_i = 11.4$ Hz. For the definition of the 5DF model, see Table 3.1. The exponential fits (lines) are good for low rates (\triangleleft : $\lambda_e = 5.26$ Hz, ∇ : $\lambda_e = 5.56$ Hz, \triangle : $\lambda_e = 5.88$ Hz, \times : $\lambda_e = 6.01$ Hz, \square : $\lambda_e = 6.25$ Hz, \circ : $\lambda_e = 6.67$ Hz) in (A), but poorer for g_s near zero for high rates (\triangleleft : $\lambda_e = 6.90$ Hz, ∇ : $\lambda_e = 7.14$ Hz, \triangle : $\lambda_e = 7.69$ Hz, \times : $\lambda_e = 8.33$ Hz, \square : $\lambda_e = 9.09$ Hz, \circ : $\lambda_e = 10.0$ Hz) in (B).

2.3.2 Constructing Inhomogeneous Hazard Functions

Now given the hazard functions determined under static input statistics, the inhomogeneous hazard function given time-varying Poisson input rates $\lambda_e(t), \lambda_i(t)$ can be constructed by accounting for synaptic filtering.

The homogeneous hazard functions given static stimulation rates λ_e, λ_i determined by the recipes in section 2.3.1 are the hazard functions given synaptic conductance distributions parameterized by $\langle g_{e,i} \rangle$, neglecting higher order moments. It can be shown that

$$\frac{d}{dt} \langle g_x(t) \rangle = -\frac{1}{\tau_x} \left(\langle g_x(t) \rangle - q_x \tau_x N_x \lambda_x(t) \right), \quad (2.28)$$

with $x \in \{e, i\}$, a low-pass filter equation of the quantity $q_x \tau_x N_x \lambda_x(t)$ with a cutoff frequency of $2\pi/\tau$ (Gardiner, 1985; Brunel, 2000; La Camera et al., 2004).

As argued in (Fourcaud & Brunel, 2002; Renart et al., 2004), the firing rate of neurons with non-zero synaptic time-constants driven by sufficient noise follow their input currents instantaneously. Then the hazard function $h_g(g_s, g_r, t)$ here is also determined instantaneously by the mean synaptic conductances. Therefore, inhomogeneous parameters $a_h(t)$ and $b_h(t)$ in equation 2.27 can be determined by interpolating the parameters determined from static $\langle g_e \rangle$ and $\langle g_i \rangle$ with the instantaneous dynamic $\langle g_e(t) \rangle$ and $\langle g_i(t) \rangle$ determined by integrating equation 2.28 for some given arbitrary time-varying input parameterized by $\lambda_e(t), \lambda_i(t)$. The resulting inhomogeneous hazard function is then

$$h_g(g_s, g_r, t) = a_h(t) \exp(-b_h(t) \cdot (g_s + g_r)). \quad (2.29)$$

A similar approach was taken in (La Camera et al., 2004), except that the dynamics of the standard deviation of the synaptic conductance is not accounted for by the fitting approach used here. This could be remedied given an analytically solvable neuron model as was used in (La Camera et al., 2004).

In the present study, only time varying excitation is investigated. Treating inhibition in addition would require additional fits and two-dimensional interpolation of the resulting parameters, and would allow the master equations to be used to study balanced randomly connected networks of inhibiting and adapting excitatory neurons, extending (Brunel, 2000; Latham et al., 2000).

2.3.3 Renewal Theory Models

In homogeneous renewal theory, only the time since the last spike (age) enters into the hazard function (Gerstner & Kistler, 2002) to introduce statistical dependence between spike times. While such theories cannot account for ISI correlations due to SFA, they can account for much of the gradual increase in excitability, which follows a spike due to SFA, by an appropriately chosen hazard function. Perhaps surprisingly, such models are sufficient to exhibit “adapting” transients to step stimuli in the inhomogeneous case. Like the 2DM model, one seeks to calibrate

such renewal models to the 5DF system, and assess their suitability for modeling the ensemble firing rate under dynamic stimuli. Sufficient for such a comparison is a recipe for specifying the hazard function as a function of the static stimulus. The dynamic case can then be constructed by using the effective synaptic filtered stimulus to determine the inhomogeneous hazard function at each instant in time, as for the adapting Markov models in the previous section.

For the static case, one can determine the hazard function as a function of the stimulus by interpolating the ISI distribution due to 5DF Monte-Carlo and applying equation 1.5. The renewal model will thus reproduce the ISI distribution of 5DF Monte-Carlo under static stimulation. This process is numerically unstable for large τ , and for the dynamic case too costly. Another approach is to determine the renewal hazard function by the two-dimensional generalization of equation 1.43, as the adiabatic elimination shows the resulting hazard function should accurately describe the full system. There is one caveat: Since the resulting renewal hazard function must be uniquely determined by the stimulus, $P(t_s, t_r, t)$ in equation 1.43¹ must be replaced by $P_\infty(t_s, t_r, t)$, the instantaneous equilibrium distribution, or asymptotic state distribution for large time resulting from a $h(t_s, t_r, t)$ fixed at the instantaneous value at time t . The renewal hazard function determined by this recipe, combined with the renewal master equation 1.17 define what will subsequently be referred to as the effective renewal (ER) model (see the model overview in Table 3.1). The parameters of the GRP hazard function are uniquely determined by the criteria that the hazard function must be equal to the ER renewal hazard function at large τ , and have the same average firing rate. Given the GRP hazard parameters, the GRP hazard function was computed as discussed in section 3.5. Typical hazard functions are shown in Figure 2.2. Indeed, the renewal hazard functions determined by the two-dimensional generalization of equation 1.43 are consistent with those of 5DF Monte-Carlo determined by equation 1.5.

Simulation of the ER model implies that the master equation for $P(t_s, t_r, t)$ must be allowed to converge to $P_\infty(t_s, t_r, t)$ for each time step where the stimulation changes. This is costly, and makes the ER models much less efficient to simulate than the 1DM and 2DM models, but allows a direct comparison of renewal models with the 1DM and 2DM models, and 5DF Monte-Carlo. When the renewal hazard function is known *a priori*, such as for GRPs or when the hazard functions can be fit by simple functions, the renewal theory ensemble equations are comparatively more efficient to simulate than the 1DM and 2DM models.

¹ $P^\dagger(t_s, t_r, t)$ is required and comes from equations 1.33 and 1.35 applied to $P(t_s, t_r, t)$.

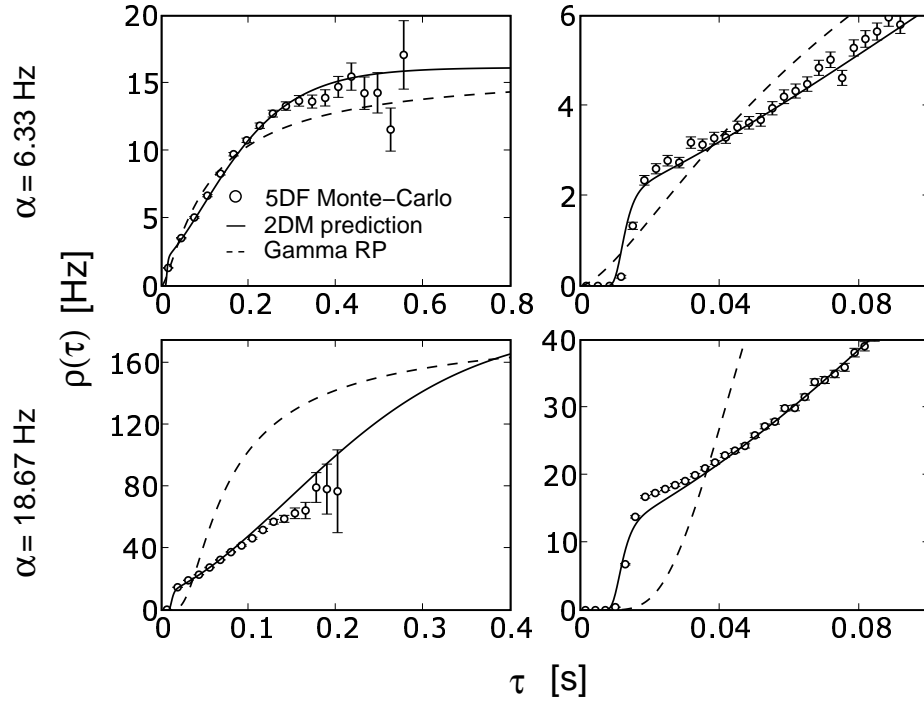


Figure 2.2: The renewal hazard function, $\rho(\tau)$, for an ensemble firing rate of $\alpha = 6.33$ Hz (top row), and $\alpha = 18.67$ Hz (bottom row). The renewal hazard function for 5DF Monte-Carlo (circles) was computed by equation 1.5 with a spike train of 10^4 s. The renewal hazard function due to the 2DM model (solid line) was determined by the two-dimensional generalization of equation 1.43. The renewal hazard function for a gamma renewal process (dashed line) equal to the 2DM renewal hazard function at large τ , and with the same average firing rate was computed as discussed in section 3.5. The small τ region is shown blown-up in the right column. For the definition of the 2DM and 5DF models, see Table 3.1.

Chapter 3

Numerics and Computational Methods

Any computing problem can be solved by adding another level of abstraction—except the problem of having too many layers of abstraction.

Hacker proverb

In this section the numerical techniques applied to solve the various master equations, generate inhomogeneous realizations of the 1DM, 2DM and renewal processes, and solve the 5DF neuron model equations are described.

3.1 Numerical Solution of Master Equations

The 1DM and 2DM master equations were solved numerically by discretizing $P(t_s, t)$ and $P(t_s, t_r, t)$ respectively, applying the exponential Euler method for the death term, and reinserting the lost probability by walking the negative time domain and fetching the probability sources of each bin determined by the inverse reset mapping given by equation 1.25. The one-dimensional case is presented here, and the generalization to two dimensions is straight-forward.

The distribution $P(t_s, t)$ is discretized on equally spaced grids t_s^i and t^j with grid spacings $\Delta t_s := t_s^{i+1} - t_s^i$ and $\Delta t := t^{j+1} - t^j$ respectively, with $\Delta t_s = \Delta t$, such that $P(t_s, t) \rightarrow P^{i,j}$. The discretized form of the master equation 1.26 then takes the form

$$P^{i+1,j+1} = P^{i,j} \exp(-\Delta t \cdot h(t_s^i, t^j)) + P_r^{i,j}, \quad (3.1)$$

where the first term is the exponential Euler computation of loss of probability due to the death term. On the lhs, the first super-script of P , $i + 1$, leads i by

one to implement the constant drift of t_s , $dt_s/dt = 1$. The reinserted probability, $P_r^{i,j}$, is computed for $t_s^i + \Delta t_s < 0$ by

$$\begin{aligned}
 P_r^{i,j} &:= \sum_{m=i_{\text{rif}}(t_s^i)}^{i_{\text{rif}}(t_s^{i+1})-1} P_d^{m,j} \\
 &+ \frac{\psi^{-1}(t_s^{i+1}) - i_{\text{rif}}(t_s^{i+1})}{\Delta t_s} P_d^{i+1,j} \\
 &- \frac{\psi^{-1}(t_s^i) - i_{\text{rif}}(t_s^i)}{\Delta t_s} P_d^{i,j},
 \end{aligned} \tag{3.2}$$

where $P_d^{i,j}$ is the loss of probability computed by

$$P_d^{i,j} := \Delta t \cdot P^{i,j} \cdot h(t_s^i, t^j), \tag{3.3}$$

and i_{rif} refers to the ‘‘reinserted-from’’ index which satisfies

$$t_s^{i_{\text{rif}}(t_s^i)} \leq \psi^{-1}(t_s^i) < t_s^{i_{\text{rif}}(t_s^i)} + \Delta t_s. \tag{3.4}$$

The first term in equation 3.2 is just a sum of all $P_d^{i,j}$ except the fractional last bin which send probability to the interval $t \in [t_s^i, t_s^i + \Delta t_s)$. The second two terms subtract the fractional first and add the fractional last bins of $P_d^{i,j}$ which are reinserted to the interval, and thus implement a sort of anti-aliasing of the reinsertion mapping.

3.2 Neuron Simulations

Monte-Carlo simulations of the full-system (5DF Monte-Carlo) were performed by solving equations 2.13-2.15 using the NEST simulation kernel (Diesmann & Gewaltig, 2002) with a time step of 0.01 ms. Parallelization of the simulation and analysis, for execution on the in-house Linux cluster, was implemented on a per Monte-Carlo trial basis using Python, numpy (Jones, Oliphant, Peterson, et al., 2001–), and a custom master-slave interpreter framework written on top of MPI4PY (Dalcin, Paz, & Storti, 2005). The requisite Python binding for the NEST simulation kernel, PyNEST, is also a custom implementation which enjoys attention from a wider user base (Cannon et al., 2006), as it allows flexible configuration of the simulations without a significant performance reduction (Broker, Chinellato, & Geus, 2005), MATLAB-like analysis on-line, and exposes the simulator core to a modern dynamic programming language with an extensive module library, an enabler for, for example, the parallelization of the simulation *and analysis*.

3.3 Generating Realizations of Adapting Markov Processes

Generating realizations of the proposed 1DM or 2DM processes is straight-forward: The thinning method for a general hazard function described in (Devroye, 1986) can be applied. The quantity $h_{max} = \max_{t_s, t} (h(t_s, t))$ for the 1DM case, or $h_{max} = \max_{t_s, t_r, t} (h(t_s, t_r, t))$ for the 2DM case must be known. The variables t and t_s (1DM), or t, t_s , and t_r (2DM) are required and can have initial values of zero. Sequential intervals are generated using a homogeneous Poisson process with hazard rate $\rho = h_{max}$. Given one such interval, Δt_i , it is added to t and t_s (1DM), or t, t_s , and t_r (2DM). Next, a spike is generated at time t with probability $h(t_s, t)/h_{max}$ (1DM) or $h(t_s, t_r, t)/h_{max}$ (2DM), and if a spike is generated, $t_s \mapsto \psi_s(t_s)$, and $t_r \mapsto \psi_r(t_r)$, where ψ_s and ψ_r refer to the reinsertion mappings as in equation 1.24 with the respective parameters for the two mechanisms.

3.4 Numerical Solution of the Renewal Master Equation

As the renewal master equation 1.17 is just a special case of the 1DM master equation, it can be solved with the same numerical techniques as described in section 3.1. The content of the δ term in equation 1.17 is that all probability lost due to the death term (the second term on the rhs) is accumulated and reinserted to the $\tau = 0$ bin. Thus, one is spared the complication of treating state dependent reinsertion of probability, as was necessary for the 1DM and 2DM master equations.

3.5 Generating Realizations of a General Inhomogeneous Renewal Process

Realizations for a inhomogeneous renewal process with a given hazard function can be also generated by the thinning method as discussed in (Devroye, 1986). The maximum of the hazard function, $\rho_{max} = \max_{\tau, t} (\rho(\tau, t))$, must be known. Sequential event intervals are generated using a homogeneous Poisson process with a rate of ρ_{max} . The resulting spike train is then sequentially thinned, given the event time t and time since last event τ , by the rule:

1. Generate a uniform random number, T , on $[0, 1)$.
2. if $\rho(\tau, t)/\rho_{max} > T$ keep the event in the spike train otherwise remove it.

The remaining event times are consistent with the prescribed hazard function.

For the case of random number generation for a GRP, evaluation of $\rho(\tau, t)$ using equation 1.5 is numerically unstable for large τ , and costly. An implementation of the algorithm (Shea, 1988) for calculating the cumulative hazard function

of a gamma renewal process is available in `pgamma.c` of the Mathlib of the R statistics environment (Ihaka & Gentleman, 1996) under the GNU Public License. Alternatively, the logarithm of the function `gsl_sf_gamma_inc_Q` provided by the GNU Scientific Library can be used. The hazard function can then be calculated by a simple discrete difference calculation of the derivative. Time dependence can be introduced by giving a time dependence to the parameters of the gamma distribution.

A

Model	Description	Keywords
1DM	one-dimensional Markov process	beyond renewal theory, spike-frequency adaptation, master equation, ensemble
5DF	spike-frequency adapting relative refractory conductance-based integrate-and-fire neuron driven by Poisson input	full five-dimensional system, Monte-Carlo, reference, benchmark
2DM	two-dimensional Markov process	adiabatic elimination of 5DF, spike-frequency adaptation, relative refractory period, master equation, ensemble
ER	effective renewal theory model	inhomogeneous, master equation

B

Model	Defined in (section)	Equations	Calibration to 5DF recipe in (section)	Numerics in (section)
1DM	1.5	1.20, 1.26	2.3.1, 2.3.2	3.1 (master equation), 3.3 (realizations)
5DF	2.1, A	2.13-2.15	N/A	3.2
2DM	2.2	2.24	2.3.1, 2.3.2	3.1 (master equation), 3.3 (realizations)
ER	1.4	1.17	2.3.3, 2.3.2	3.4 (master equation), 3.5 (realizations)

Table 3.1: (A) An overview of the models defined and compared throughout the text. (B) A quick reference for the defining equations and sections for the various models.

Chapter 4

Results

... showing by mathematical simulation that a theory leads to plausible results is not evidence that the theory is correct.

Andrew Huxley in (Huxley, 2002)

In this chapter, the various reduced Markov models (1DM, 2DM, ER) are compared to Monte-Carlo simulations of the conductance-based spike-frequency adapting relative refractory integrate-and-fire neuron driven by Poisson spike trains (5DF). The two-dimensional Markov (2DM) model, derived from the 5DF master equation by an adiabatic elimination in chapter 2, is shown to accurately reproduce the dynamic ensemble firing rate statistics and static ISI correlations of 5DF Monte-Carlo. Subsequently, the one-dimensional Markov model is used to analyse mean-adaptation treatments of spike-frequency adaptation (SFA). A mean+variance-adaptation theory is derived and used to clarify the domain of validity of mean-adaptation theories. Further, ISI correlations due to temporal averaging of an inhomogeneous process are treated. Finally, the inhomogeneous gamma renewal process is used to investigate the filtering properties of SFA, the compounding effects of SFA in subsequent populations, and the network response to SFA induced transients at weak changes in stimulation.

4.1 Comparisons of Calibrated Models to Full System

In this section, the ISI distributions, static ISI correlations, and firing rate dynamics of the 1DM, 2DM, and ER models are compared to those of 5DF Monte-Carlo.

4.1.1 Interspike Interval Distributions

The predictions due to the ER and 2DM model are in excellent agreement with the static ISI distribution of 5DF Monte-Carlo (not shown). The prediction due

Model	Corr. coef.
$\alpha = 6.33$ Hz	
5DF	-0.148 ± 0.004
2DM	-0.147 ± 0.003
1DM	-0.160 ± 0.003
ER	0.0042 ± 0.0043
$\alpha = 18.67$ Hz	
5DF	-0.235 ± 0.002
2DM	-0.236 ± 0.002
1DM	-0.283 ± 0.002
ER	0.001 ± 0.002

Table 4.1: Correlation coefficients for Monte-Carlo simulations of the full five-dimensional system (5DF), realizations of the one- and two-dimensional Markov models (1DM, 2DM) as described in section 3.3, and realizations of the effective renewal theory model (ER) as described in section 3.5, for ensemble firing rates $\alpha = 6.33$ Hz and $\alpha = 18.67$ Hz.

to the 1DM model neglects refractory effects and is therefore poor for low ISIs as can be seen in Figure 4.1.

4.1.2 Interspike Interval Correlations

In this section, correlations between subsequent ISIs are investigated, a feature of the proposed 1DM and 2DM models which is absent by definition in renewal theory models of spike statistics.

The correlation coefficient, r , for a finite number of observations is computed by

$$r^2 = \frac{(\sum(x_i - \bar{x})(y_i - \bar{y}))^2}{\sum(x_i - \bar{x})^2 \sum(y_i - \bar{y})^2}, \quad (4.1)$$

and is the standard measure by which to quantify correlations between two random variables x, y , where x_i, y_i denote the individual observations and \bar{x}, \bar{y} denote the means.

The correlation coefficients of subsequent ISIs under static stimulation were calculated for 100 runs of 100s and the mean and deviation in the mean are given in Table 4.1. Indeed, the renewal process shows no ISI correlations. For low and high firing rates, the difference between the correlation coefficients for 5DF Monte-Carlo and realizations of the 2DM model is consistent with zero. Both exhibit negative ISI correlations, implying short ISIs are generally followed by long ISIs and vice versa, as has been observed in previous experimental and theoretical studies (Longtin & Racicot, 1997; Chacron, Longtin, & Maler, 2000; Chacron et al., 2003; Nawrot et al., 2006).

The conditional ISI distribution, $f(\tau_{i+1}|\tau_i)$ can be computed for the 1DM and 2DM models by equation 1.50 and its two-dimensional generalization. Predictions due to the 2DM model are in agreement with 5DF Monte-Carlo for low and high-rates, and both long and short τ_i , as shown in Figure 4.1. Applying equation 1.50, one can compute the quantity

$$\langle \tau_{i+1} | \tau_i \rangle_{\tau_{i+1}} = \int_0^{\infty} \tau_{i+1} f(\tau_{i+1} | \tau_i) d\tau_{i+1}. \quad (4.2)$$

As discussed in (Whittaker & Robinson, 1967, pp. 334-337), this is a linear function of τ_i for normal distributions, the slope of which is the correlation coefficient. As the ISI distributions here are not normal, there are deviations from linearity, as shown in Figure 4.2. Predictions due to equation 4.2 for the 2DM model are consistent with 5DF Monte-Carlo for both low and high rates, as seen in Figure 4.2. Thus when considering static correlations, the 2DM model is indistinguishable from the full system.

4.1.3 Firing Rate Dynamics

In this section, the ensemble firing rates of the 1DM, 2DM and ER models are compared to 5DF Monte-Carlo for small to large step-stimuli, and for random fluctuating stimuli generated by an Ornstein-Uhlenbeck process.

The neural ensemble is subjected to a dynamic stimulus by specifying a time-varying excitatory Poisson input rate, $\lambda_e(t)$. Given the time dependent hazard function determined by the Poisson input rates as described in section 2.3.2, the ensemble firing rate, $\alpha(t)$, of the 1DM and 2DM models can be calculated by solving equations 1.26 and 2.24 respectively for the time dependent state distribution, and subsequently applying equation 1.34 or the 2-D generalization of it. For the ER model, the hazard function was calculated by the methods discussed in section 2.3.3, and the ensemble firing rate was determined by solving equation 1.17.

For weak step-stimuli that do not bring the system too far from equilibrium, all models (ER, 1DM, 2DM) faithfully reproduce the step stimulus response of 5DF Monte-Carlo (not shown, but for GRPs see Figure 4.13). For moderate step-stimuli, only the 2DM model faithfully reproduces the step stimulus response of 5DF Monte-Carlo, shown in Figure 4.3. For large step-stimuli, the 2DM model starts to deviate from 5DF Monte-Carlo as seen in Figure 4.4.

The effective renewal theory (ER) model does a reasonable job of predicting the ensemble firing rate of the system to low-amplitude step-stimuli. This is perhaps surprising, since one does not expect renewal models to faithfully reproduce the dynamical responses of spike-frequency adapting neurons, as renewal models do not account for the dependencies of the firing probability density (hazard function) on spikes prior to the most recent. However, this shows that if the system is not pushed too far from equilibrium, knowledge of just the last spike is sufficient to predict the firing rate of the ensemble.

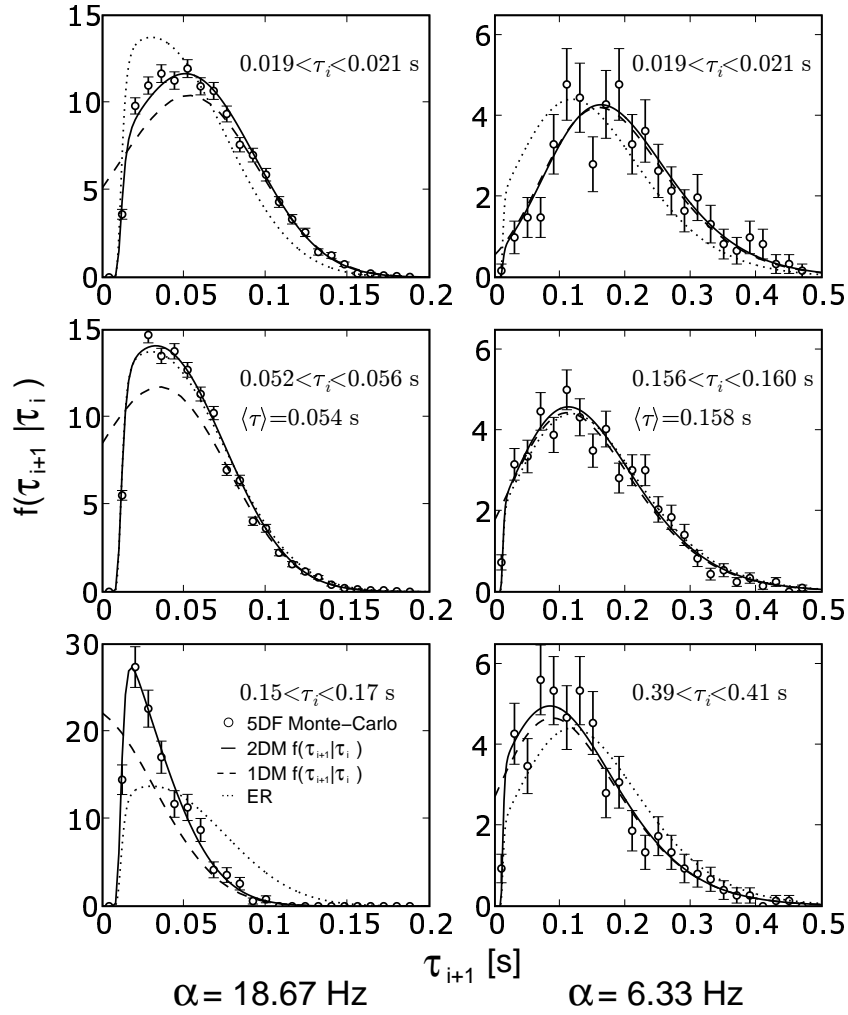


Figure 4.1: A comparison of the conditional ISI distributions due to 5DF Monte-Carlo with predictions due to effective renewal theory (ER, dotted line), the 1DM model (dashed line, determined by equation 1.50), and the 2DM model (solid line, determined by the 2-D generalization of equation 1.50). For the definition of the 1DM, 2DM, 5DF, and ER models, see Table 3.1. The left column shows three representative conditional ISI distributions for an ensemble firing rate of $\alpha = 18.67$ Hz, and the right column shows the same for $\alpha = 6.33$ Hz. The upper, middle, and lower rows of plots show the conditional ISI distribution for τ_i much shorter than, equal to, and much longer than the mean, respectively. The preceding ISI, τ_i , is given on each plot, and a small interval around τ_i is used to compute the distributions from 5DF Monte-Carlo to yield sufficient statistics. The theoretical predictions of the conditional ISI distributions using the 2DM model are in good agreement with 5DF Monte-Carlo for all situations considered. The ISI distribution due to 5DF Monte-Carlo is consistent with the renewal ISI distribution only when the preceding ISI is equal to the mean ISI (middle row). Spike trains of duration 10^4 s were used. Error bars represent the relative error in the histogram bin counts, $1/\sqrt{\text{count}}$.

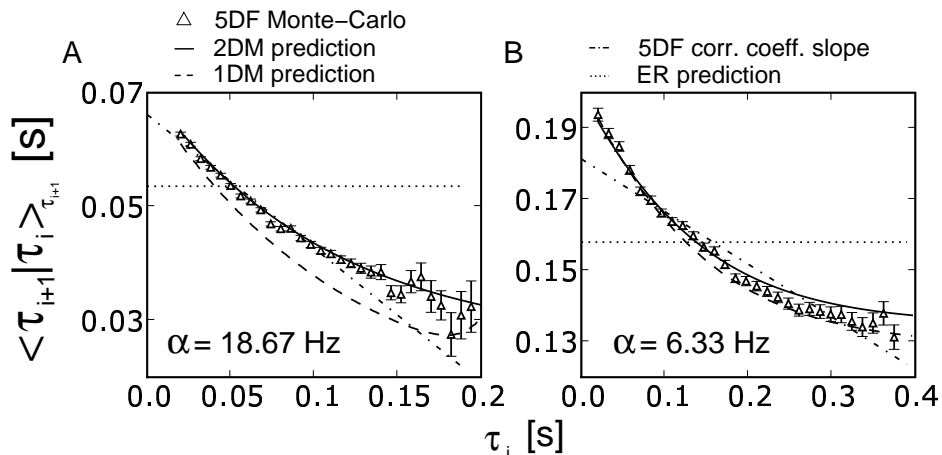


Figure 4.2: The mean of the conditional ISI distribution (defined by equation 4.2) as a function of the preceding ISI, τ_i , for high ensemble firing rates (A, $\alpha = 18.67$ Hz) and low ensemble firing rates (B, $\alpha = 6.33$ Hz). The data points (triangles) shown are for 5DF Monte-Carlo. Theoretical predictions due to the 1DM (dashed line), 2DM (solid line), and ER (dotted line) models are shown. For the definition of the 1DM, 2DM, 5DF, and ER models, see Table 3.1. A linear function with slope equal to the correlation coefficient would be the functional form if the ISI distributions were normal. Thus, these linear functions are plotted for comparison (dashed-dotted line).

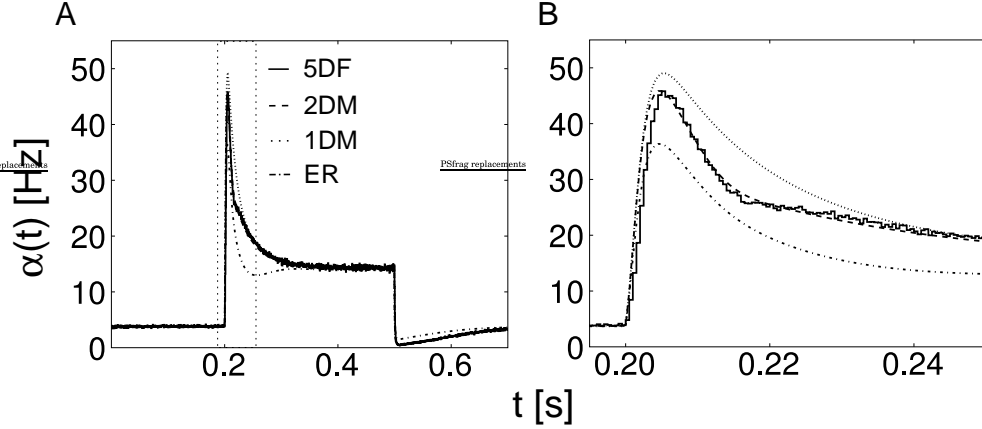


Figure 4.3: (A) The ensemble firing rate, $\alpha(t)$, in response to a moderate step stimulus, determined by 5DF Monte-Carlo ($5 \cdot 10^5$ trials, solid line), and numerical solution of the 1DM (dotted line), 2DM (dashed line), and ER (dashed dotted line) master equations. For the definition of the 5DF, 1DM, 2DM, and ER models, see Table 3.1. The region outlined by the dashed rectangle is enlarged in (B) showing consistency between the two-dimensional Markov (2DM) model and the full system (5DF Monte-Carlo) apart from a 0.5 ms lead of the 2DM solution. This discrepancy is likely due to the neglected membrane potential dynamics.

Further, 5DF Monte-Carlo and predictions of the 2DM model were compared for a stimulus, $\lambda_e(t)$, generated by an Ornstein-Uhlenbeck (OU) process. Let $\zeta(t)$ be an OU process with mean of 10 Hz, standard deviation of 0.6 Hz, and time constant of 0.2 s. Then the excitatory synaptic inputs were supplied with Poisson input rates $\lambda_e(t) = \zeta(t)$.

The ensemble firing rates for the 2DM model, its adiabatic solution, and 5DF Monte-Carlo and are shown in Figure 4.5. The adiabatic solution of the 2DM model is defined as the system which at each instant in time has a distribution of states equal to the instantaneous equilibrium distribution, $P_\infty(t_s, t_r, t)$, the asymptotic state distribution for large time resulting from a $h(t_s, t_r, t)$ fixed at the instantaneous value at time t . The firing rate of the adiabatic 2DM model is then calculated by

$$\alpha_\infty(t) = \int_{-\infty}^{\infty} h(t_s, t_r, t) P_\infty(t_s, t_r, t) dt_s dt_r. \quad (4.3)$$

By comparison of the ensemble firing rates of the 2DM model with its adiabatic solution in Figure 4.5, one can see that the system is being driven from equilibrium by the stimulus. Furthermore, the behavior of the 2DM model far from equilibrium captures the ensemble firing rate dynamics of 5DF Monte-Carlo faithfully. This is a robust result under variation of neuron parameters and stimuli, so long as the ensemble is not pushed too far from equilibrium.

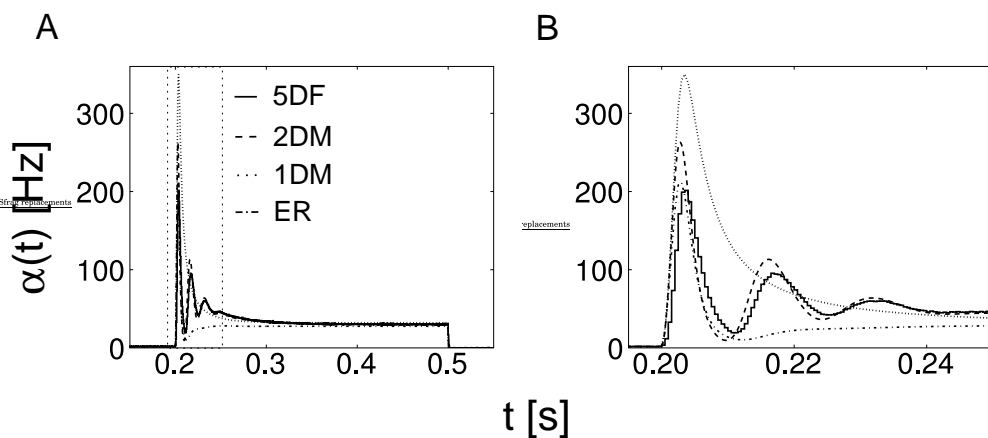


Figure 4.4: (A) The ensemble firing rate, $\alpha(t)$, in response to a large step stimulus, determined by 5DF Monte-Carlo ($5 \cdot 10^5$ trials, solid line), and numerical solution of the 1DM (dotted line), 2DM (dashed line), and ER (dashed dotted line) master equations. For the definition of the 5DF, 1DM, 2DM, and ER models, see Table 3.1. The region outlined by the dashed rectangle is enlarged in (B) showing the two-dimensional Markov (2DM) model does a fairly good job of reproducing the oscillations of the full system (5DF Monte-Carlo). The oscillation amplitude discrepancy is likely due to the poor fitting of the hazard function for g_s near 0 for high rates observed in figure 2.1.

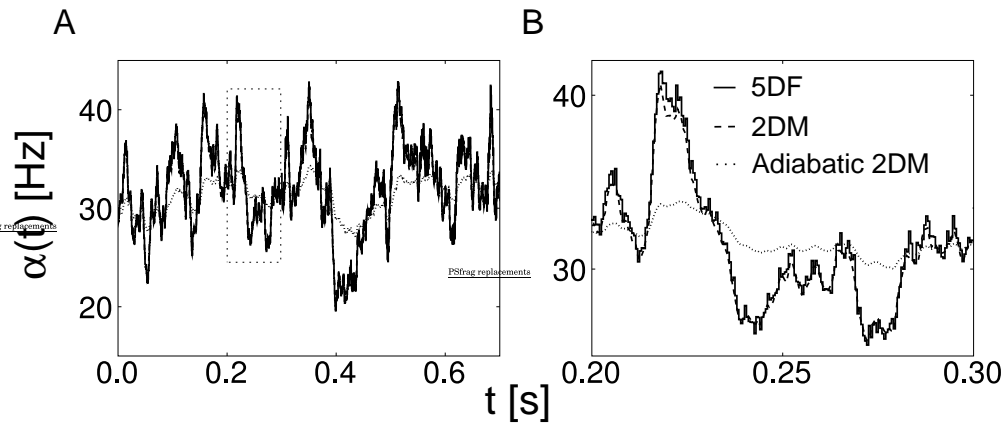


Figure 4.5: (A) The ensemble firing rate, $\alpha(t)$, in response to an Ornstein-Uhlenbeck process stimulus (as described in the text), determined by 5DF Monte-Carlo (solid line), numerical solution of the 2DM master equation (dashed line), and the adiabatic solution (adiabatic 2DM, dotted line) computed by equation 4.3. For the definition of the 5DF, and 2DM models, see Table 3.1. The region outlined by the dashed rectangle is enlarged in (B) showing consistency between the two-dimensional Markov (2DM) model and the full system (5DF Monte-Carlo), even though the system is far from equilibrium, as is evident from the large discrepancy with the adiabatic solution.

4.2 Beyond Mean-Adaptation Approximations

In this section, it is show that statistical moment theory approximations such as the mean-adaptation theories due to (La Camera et al., 2004) can be derived from the 1DM master equation. The approach generalizes, and the next order moment theory approximation, a mean+variance-adaptation theory, is derived and used to clarify the domain of validity of mean-adaptation theories.

Recall the 1DM master equation for a spike-frequency adapting neuron,

$$\begin{aligned} \frac{\partial}{\partial t} P(g_s, t) &= \frac{\partial}{\partial g_s} \left[\frac{g_s}{\tau_s} P(g_s, t) \right] \\ &\quad + h_g(g_s - q_s, t) P(g_s - q_s, t) \\ &\quad - h_g(g_s, t) P(g_s, t), \end{aligned} \quad (4.4)$$

where $P(g_s, t)$ is the probability density of the adaptation state variable, g_s , and $P(g_s < 0, t) = 0$. The ensemble firing rate, $\alpha(t)$, is given by

$$\alpha(t) = \int_{-\infty}^{\infty} h_g(g_s, t) P(g_s, t) dg_s. \quad (4.5)$$

The mean adaptation variable is:

$$\langle g_s(t) \rangle = \int_{-\infty}^{\infty} g_s P(g_s, t) dg_s. \quad (4.6)$$

Multiplying equation 4.4 by g_s and integrating over g_s yields the time evolution of the mean, $\langle g_s(t) \rangle$,

$$\frac{d\langle g_s(t) \rangle}{dt} = -\frac{1}{\tau_s} \langle g_s(t) \rangle + q_s \alpha(t). \quad (4.7)$$

By Taylor expanding $h_g(g_s)$ in equation 4.5 around $\langle g_s(t) \rangle$, and keeping up to linear terms, a mean-adaptation theory as in (La Camera et al., 2004) results. Keeping up to quadratic terms one has

$$\alpha(t) \approx \alpha\left(\langle g_s(t) \rangle, \langle \Delta g_s^2(t) \rangle\right) = h_g\left(\langle g_s(t) \rangle\right) - \frac{1}{2} h_g''\left(\langle g_s(t) \rangle\right) \cdot \langle \Delta g_s^2(t) \rangle, \quad (4.8)$$

where the $h_g'\left(\langle g_s(t) \rangle\right)$ term vanishes by a cancellation of means. A mean+variance-adaptation theory results, but we require the time evolution of the variance. Multiplying equation 4.4 by $\left(g_s - \langle g_s(t) \rangle\right)^2$ and integrating over g_s yields the time evolution of the variance, $\langle \Delta g_s^2(t) \rangle$,

$$\frac{d\langle \Delta g_s^2(t) \rangle}{dt} = -\frac{2}{\tau_s} \langle \Delta g_s^2(t) \rangle + q_s^2 \alpha(t) + 2q_s \int_0^{\infty} \left(g_s - \langle g_s(t) \rangle\right) h_g(g_s, t) P(g_s, t) dg_s. \quad (4.9)$$

Approximating $h_g(g_s) \approx h_g(\langle g_s(t) \rangle) + h'_g(\langle g_s(t) \rangle)(g_s - \langle g_s(t) \rangle)$, equation 4.9 becomes

$$\frac{d\langle \Delta g_s^2(t) \rangle}{dt} \approx -\frac{2}{\tau_s} \langle \Delta g_s^2(t) \rangle + q_s^2 \alpha \left(\langle g_s(t) \rangle, \langle \Delta g_s^2(t) \rangle \right) + 2q_s h'_g \left(\langle g_s(t) \rangle \right) \cdot \langle \Delta g_s^2(t) \rangle, \quad (4.10)$$

which has a steady state

$$\langle \Delta g_s^2 \rangle = \frac{1}{2} \frac{q_s^2 \alpha \left(\langle g_s \rangle, \langle \Delta g_s^2 \rangle \right)}{\frac{1}{\tau} - q_s h'_g \left(\langle g_s \rangle \right)}. \quad (4.11)$$

Thus the mean+variance-adaptation theory consistency relation for the adapted equilibrium firing rate, α^* , reads:

$$\alpha^* = h_g(q_s \tau_s \alpha^*) + \frac{1}{4} h''_g(q_s \tau_s \alpha^*) \left[\frac{q_s^2 \alpha^*}{\frac{1}{\tau} - q_s h'_g(q_s \tau_s \alpha^*)} \right]. \quad (4.12)$$

Higher order moment theories can be derived by keeping higher terms in the expansions in equations 4.8 and 4.10, and computing the necessary equations for the time evolution of higher statistical moments from the master equation 4.4.

4.2.1 Validity of Mean-Adaptation Theories

In this section, a heuristic criterion is given for the validity of mean-adaptation theories in the static case, and the improved accuracy of the mean+variance-adaptation theory is demonstrated by a numerical example. It is illustrative to first investigate the exactly solvable leaky integrate-and-fire neuron driven by white noise for the parameters considered in (La Camera et al., 2004), and subsequently contrast the findings to the 5DF model defined by equations 2.13-2.15.

It can be seen by inspection of equation 4.12 that if $h''_g(g_s) \approx 0$ over the regime where $P(g_s)$ is appreciably non-zero, then the mean-adaptation consistency relation,

$$\alpha^* = h_g(q_s \tau_s \alpha^*), \quad (4.13)$$

as in (La Camera et al., 2004) results.

First, the 1DM master equation is used to verify the ensemble firing rate predictions of the mean-adaptation theory for the leaky integrate-and-fire neuron driven by white noise considered in (La Camera et al., 2004). The hazard function, $h_g(g_s, t)$, is referred to there as the response function in the presence of noise, and has the exact solution,

$$h_g(g_s, t) = \left[\tau \int_{\frac{C V_r - (m - g_s) \tau}{\sigma \sqrt{\tau}}}{\frac{C \theta - (m - g_s) \tau}{\sigma \sqrt{\tau}}} \sqrt{\pi} e^{x^2} (1 + \operatorname{erf}(x)) dx \right]^{-1}, \quad (4.14)$$

due to (Siegert, 1951; Ricciardi, 1977; Amit & Tsodyks, 1991), where V_r is the reset potential, θ is the threshold, τ is the membrane potential, C is the membrane

capacitance and $\text{erf}(x) = (2/\sqrt{\pi}) \int_0^x e^{-t^2} dt$ is the error function. As in (La Camera et al., 2004), m and σ are the mean and standard deviation of the input current. Upon firing, the adaptation current, g_s , makes a jump of q_s and relaxes with a time-constant τ_s . As can be seen in Figure 4.6a, $h_g(g_s)$ is quite near linear over the regime where $P(g_s)$ is appreciably non-zero, and predictions of the adapted firing rate due to a mean-adaptation theory predictions are in excellent agreement with the 1DM master equation as shown in Figure 4.6b. The mean+variance-adaptation theory helps us to understand this: agreement is good because $h_g''(g_s) \approx 0$ over the regime where $P(g_s)$ is appreciably non-zero for all firing rates considered.

For the 5DF models defined by equations 2.13-2.15, one has $h_g(g_s) \approx a_h \cdot \exp(-b_h g_s)$. As can be seen in Figure 4.7a, $h_g(g_s)$ has an appreciable second derivative over $P(g_s)$, and thus one expects mean-adaptation equilibrium ensemble firing rate predictions to deviate from the ensemble firing rate of the 1DM master equation. Indeed, such deviations are observed and are corrected by the mean+variance-adaptation consistency relation, as seen in Figure 4.7b. Thus, a heuristic condition for the validity of mean-adaptation theories is that one must have $h_g''(g_s) \approx 0$ over the regime where $P(g_s)$ is appreciably non-zero. Less heuristically, the contributions due to the second term (and all neglected higher order terms) on the rhs of equation 4.12 must vanish compared to the first. When this condition is violated, higher-order moment theories such as the mean+variance-adaptation theory given here, or the 1DM master equation should be applied to determine the ensemble firing rate.

For the neuron models considered here, the accuracy of the mean+variance-adaptation theory was also verified in the dynamic case for an OU stimulus as in Figure 4.5, as shown in Figure 4.8.

4.3 Correlations due to Temporal Averaging

In section 1.5.2, a general expression for the inhomogeneous joint distribution of subsequent ISIs was derived and subsequently shown to be correlation free for the case of a inhomogeneous renewal process. Interestingly, this result denies the presence of correlations between successive ISIs even for any arbitrary time-varying hazard function. This is due to the fact that the instantaneous or local ISI statistics of the ensemble are being considered. Another common definition of the ISI distribution is to collect events over *time* for a single trial or realization of the process. For the homogeneous case, such an ISI distribution is equivalent to the instantaneous ISI distribution determined by collecting statistics over the ensemble or realizations. In the inhomogeneous case, i.e. the case of a time-varying stimulus, they are not equivalent.

In this section, an expression for the time-averaged joint ISI distribution in terms of the joint distribution, equation 1.50, is given. For the case of an inhomogeneous renewal process, the distribution is not in general ISI correlation free, as shown by considering a Poisson process with sinusoidal hazard rate.

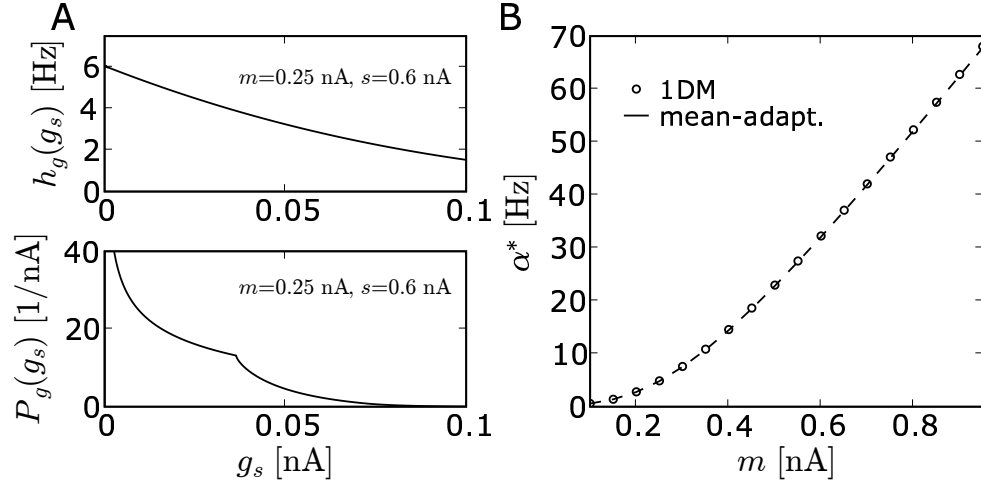


Figure 4.6: (A, top) The hazard function, $h_g(g_s)$, and (A, bottom) the equilibrium distribution of adaptation states, $P(g_s)$, in the low-firing rate regime ($\alpha^* = 4.83$ Hz, mean current input $m = 0.25$ nA and noise $\sigma = \sqrt{0.72}$ nA \cdot ms $^{\frac{1}{2}}$) of the leaky integrate-and-fire neuron (LIF) used in (La Camera et al., 2004). $P(g_s)$ was determined by numerical solution of the 1DM master equation using the hazard function given in equation 4.14. Neuron parameters: $C = 0.5$ nF, $\tau_m = 20$ ms, $V_{th} = 20$ mV, $V_r = 10$ mV. Adaptation parameters: $\tau_s = 110$ ms, $q_s \cdot \tau_s = 4$ pA \cdot s. For comparison, the neuron and adaptation parameters are as for Figure 1a in (La Camera et al., 2004), except $\tau_r = 0$ ms and $\tau_s = 110$ ms. For the definition of the 1DM model, see Table 3.1. The hazard function is nearly linear over the distribution of states, thus terms depending on the variance of $P(g_s)$ in equation 4.12 can be neglected, and mean-adaptation theories will yield good approximations to the adapted ensemble firing rate. (B) The adapted ensemble firing rate, α^* , for a range of mean current inputs, m , determined by numerical solution of the 1DM master equation (circles), and the mean-adaptation theory consistency relation (solid line).

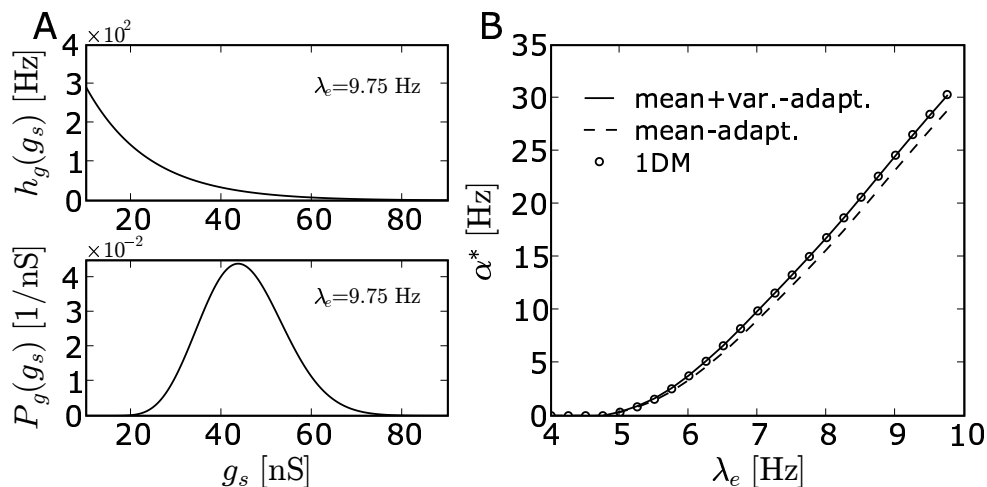


Figure 4.7: (A, top) The hazard function, $h_g(g_s)$, and (A, bottom) the equilibrium distribution of adaptation states, $P(g_s)$, determined by numerical solution of the 1DM master equation. The hazard function, $h_g(g_s)$, was determined by fitting to 5DF Monte-Carlo as in Figure 2.1 with $\lambda_e = 9.75$ Hz, $\lambda_i = 11.4$ Hz. For the definition of the 5DF and 1DM model, see Table 3.1. The hazard function has non-zero curvature ($h_g''(g_s) > 0$) over the distribution of states, thus terms depending on the variance of $P(g_s)$ in equation 4.12 cannot be neglected, and mean-adaptation theory predictions for the adapted ensemble firing rate are expected to be in error. (B) The adapted ensemble firing rate, α^* , for a range of Poisson input rates, λ_e , determined by solution of the 1DM master equation (circles), the mean-adaptation theory consistency relation (dashed line), and the mean+variance-adaptation consistency relation (solid line). As expected, mean-adaptation theory predictions for the adapted firing rate are corrected by the mean+variance-adaptation theory consistency relation given by equation 4.12.

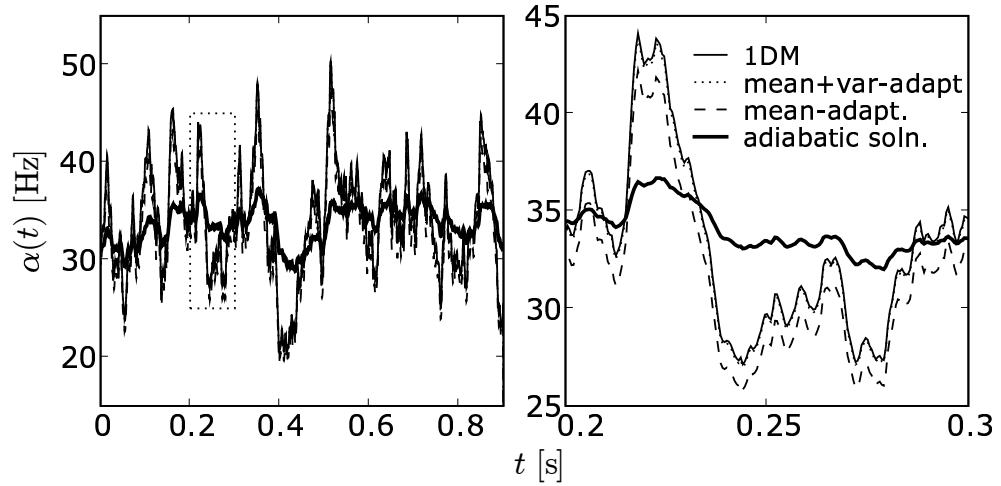


Figure 4.8: (A) The ensemble firing rate, $\alpha(t)$, in response to an Ornstein-Uhlenbeck process stimulus (as for Figure 4.5), determined by the 1DM model (solid line), the adiabatic solution (thick solid line) computed by the mean+variance-adaptation consistency relation equation 4.12, the dynamic mean+variance-adaptation theory equations 4.7-4.9 (dotted line), and the dynamic mean-adaptation theory equations (dashed line). The region outlined by the dashed rectangle is enlarged in (B) showing consistency between the 1DM model and the mean+variance-adaptation theory, while predictions due to the mean-adaptation theory are poor. For the definition of the 1DM model, see Table 3.1.

4.3.1 Time-Averaged Joint ISI Distribution

The joint ISI distribution averaged over some time interval $t \in [t_0, t_1)$, denoted by $f_{[t_0, t_1)}(\tau_{i+1}, \tau_i)$, can be determined by the weighted average over time of equation 1.50, where the weight is $\alpha(t - \tau_i)$:

$$\begin{aligned} f_{[t_0, t_1)}(\tau_{i+1}, \tau_i) &= \left(\int_{t_0}^{t_1} \alpha(s - \tau_i) ds \right)^{-1} \\ &\times \int_{t_0}^{t_1} \alpha(t - \tau_i) \int_{-\infty}^{\infty} h(\psi(t_s) + \tau_{i+1}, t + \tau_{i+1}) \mathcal{W}(\tau_{i+1}, \psi(t_s), t) \\ &\quad \times h(t_s, t) \mathcal{W}(\tau_i, t_s - \tau_i, t - \tau_i) P^\dagger(t_s - \tau_i, t - \tau_i) dt_s dt. \end{aligned} \quad (4.15)$$

For the renewal process, this reduces to

$$\begin{aligned} f_{[t_0, t_1)}(\tau_{i+1}, \tau_i) &= \left(\int_{t_0}^{t_1} \alpha(s - \tau_i) ds \right)^{-1} \\ &\times \int_{t_0}^{t_1} \alpha(t - \tau_i) h(\tau_{i+1}, t + \tau_{i+1}) \mathcal{W}(\tau_{i+1}, 0, t) \cdot h(\tau_i, t) \mathcal{W}(\tau_i, 0, t - \tau_i) dt. \end{aligned} \quad (4.16)$$

4.3.2 Example: Sinusoidal Poisson Process

Now consider the Poisson process with sinusoidal hazard function

$$\alpha(t) = h(t) = \alpha_0 + A \sin(2\pi Ft), \quad (4.17)$$

where $A < \alpha_0$ ensures $\alpha(t) > 0$ for all t . Further, consider the average over a time interval large compared to the period, $1/F$. Then, to a good approximation one can consider the average over one period of $\alpha(t)$ in equation 4.16:

$$\begin{aligned} f_{[0, 1/F)}(\tau_{i+1}, \tau_i) &= \\ \frac{1}{\alpha_0} \int_0^1 \alpha(\xi/F - \tau_i) \alpha(\xi/F) \alpha(\xi/F + \tau_{i+1}) \exp\left(-\int_{\frac{\xi}{F} - \tau_i}^{\frac{\xi}{F} + \tau_{i+1}} \alpha(s) ds\right) d\xi, \end{aligned} \quad (4.18)$$

where the integration variable has been changed to the fractional period variable ξ , the factors of $1/F$ in the numerator and denominator cancel, and the survival functions have been massaged into one term. The integral inside the exponential can be evaluated resulting in

$$\begin{aligned} f_{[0, 1/F)}(\tau_{i+1}, \tau_i) &= \\ \frac{1}{\alpha_0} \int_0^1 \alpha(\xi/F - \tau_i) \alpha(\xi/F) \alpha(\xi/F + \tau_{i+1}) \exp(-\alpha_0(\tau_{i+1} + \tau_i)) \\ &\quad \times \exp(A \cos(\xi/F + \tau_{i+1}) - A \cos(\xi/F - \tau_i)) d\xi. \end{aligned} \quad (4.19)$$

Equation 4.19 is not separable into a form $f(\tau_{i+1})f(\tau_i)$, and thus will exhibit ISI correlations. This fact will now be verified by comparing the predicted joint distribution to those actually obtained from time averaging of realizations of a Poisson process with sinusoidal hazard rate.

Spike-trains of a Poisson process with sinusoidal hazard rate and 1×10^5 s duration were generated by the thinning method given in section 3.5. The hazard rate, $\alpha(t) = h(t) = \rho(t)$, took the form given in equation 4.17, with $A = 5$ Hz and $\alpha_0 = 10$ Hz. The conditional ISI distribution was determined by the distribution of all ISIs with a preceding ISI in the range $[\tau_i - \Delta\tau, \tau_i + \Delta\tau)$ with $\Delta\tau = 0.01$ s to yield sufficient statistics. The conditional mean, given by equation 4.2, and the conditional ISI distribution for high and low mean were compared to predictions due to equation 4.19 for various hazard rate oscillation frequencies. Hazard rate oscillations with a period ten times the mean ISI ($F = 1$ Hz), twice the mean ISI ($F = 5$ Hz), and half the mean ISI ($F = 20$ Hz) in figures 4.9, 4.10, and 4.11 respectively, were considered. Predictions due to equation 4.19 are in excellent agreement with the quantities computed from the Poisson spike-trains.

In figure 4.9 it can be seen that a slow hazard rate introduces significant serial ISI correlations for the time-averaged ISI distribution. However, such modulations are slow compared to the average ISI and could be detected in the firing rate of a single trial and eliminated. For modulations on the order of the mean ISI, significant correlations were still observed, as seen in figure 4.10. Such correlations could not be reliably eliminated without multiple trials to determine the ensemble firing rate. Such ensemble data is usually not possible in *in-vivo* or awake preparations, as the background activity is only poorly controlled. In figure 4.11 it can be seen that the correlations introduced in the time-averaged ISI distribution for hazard rate oscillation frequencies faster than the mean ISI are vanishing.

It would be interesting to further refine the techniques given in this section and apply them to a combination of *in-vitro* and awake data to separate correlation effects due to SFA from correlation effects due to on-going background activity, and determine the statistics of the latter, for the case of oscillations of the background activity on the timescale of the mean ISI.

4.4 Inhomogeneous Gamma Renewal Process Models

In this section, the transient response to step stimuli for the inhomogeneous GRP random number generator and the master equation for an inhomogeneous GRP are calculated and agreement between the two models is verified, as is qualitative agreement with adapting I&F neuron models in a high-conductance state. The filtering properties of an inhomogeneous GRP are investigated using numerical solution of the renewal master equation for sinusoidal stimuli. The compounding effects of SFA are investigated in successive populations of inhomogeneous GRPs. Finally, the response to step stimuli of a network model characterizing a local circuit of cortical layer IV is investigated. Specifically, the network response to the

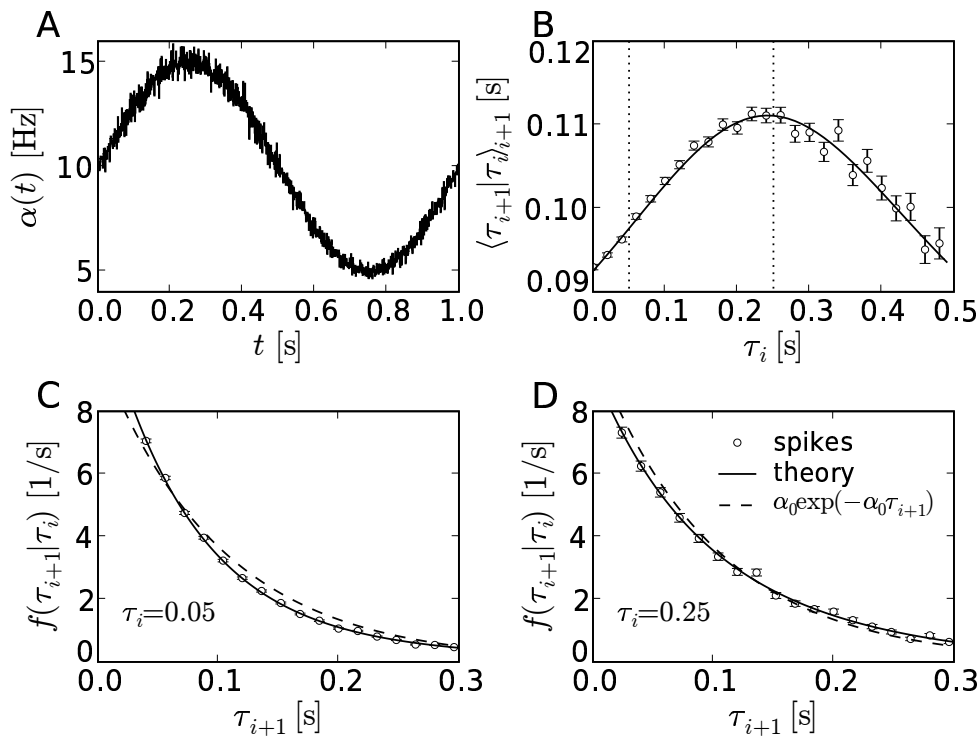


Figure 4.9: The time-averaged statistics of a Poisson process with a sinusoidal hazard rate as given by equation 4.17 with $A = 5.0$ Hz, $\alpha_0 = 10.0$ Hz, $F = 1.0$ Hz. (A) The ensemble firing rate time-histogram for 1×10^5 trials and a bin size of 1 ms. (B) The conditional mean, $\langle \tau_{i+1} | \tau_i \rangle_{\tau_{i+1}}$, as a function of τ_i given by equation 4.2 for the time-averaged joint distribution determined by equation 4.19 (solid line) and from a realization of 1×10^5 s duration (data points) as described in the text. The dashed vertical lines indicate the τ_i for which the conditional time-averaged ISI distributions were determined. The left is shown in (C), and the right in (D). The exponential ISI distribution for a Poisson process with hazard rate α_0 is shown (dashed-line) in (C) and (D) for comparison.

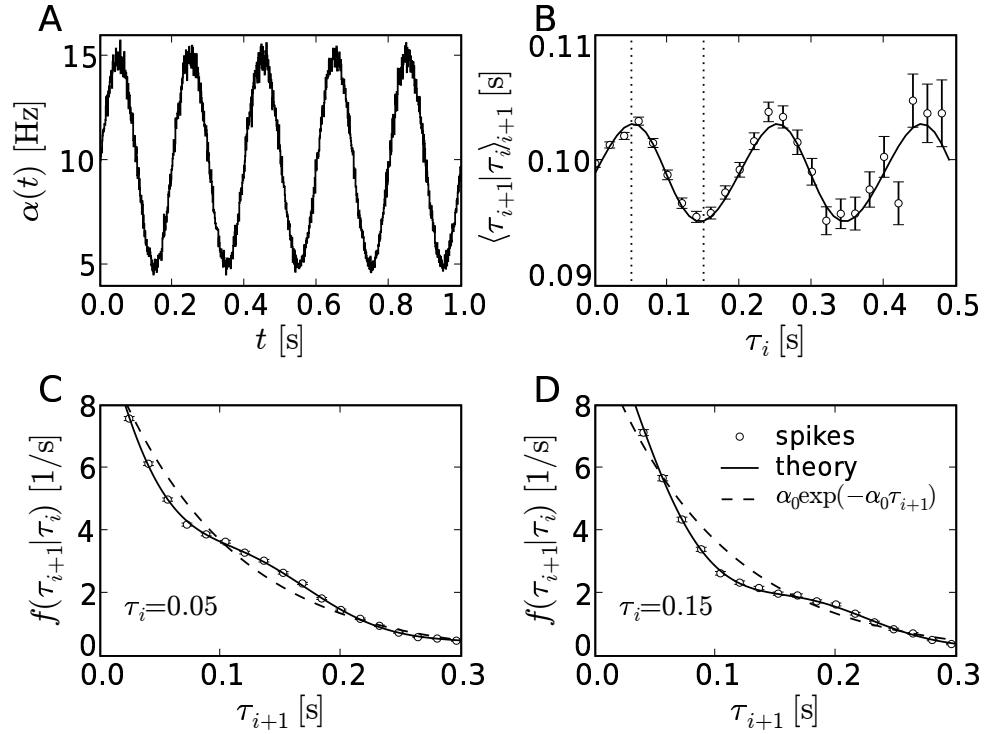


Figure 4.10: The time-averaged statistics of a Poisson process with a sinusoidal hazard rate as given by equation 4.17 with $A = 5.0$ Hz, $\alpha_0 = 10.0$ Hz, $F = 5.0$ Hz. (A) The ensemble firing rate time-histogram for 1×10^5 trials and a bin size of 1 ms. (B) The conditional mean, $\langle \tau_{i+1} | \tau_i \rangle_{\tau_{i+1}}$, as a function of τ_i given by equation 4.2 for the time-averaged joint distribution determined by equation 4.19 (solid line) and from a realization of 1×10^5 s duration (data points) as described in the text. The dashed vertical lines indicate the τ_i for which the conditional time-averaged ISI distributions were determined. The left is shown in (C), and the right in (D). The exponential ISI distribution for a Poisson process with hazard rate α_0 is shown (dashed-line) in (C) and (D) for comparison.

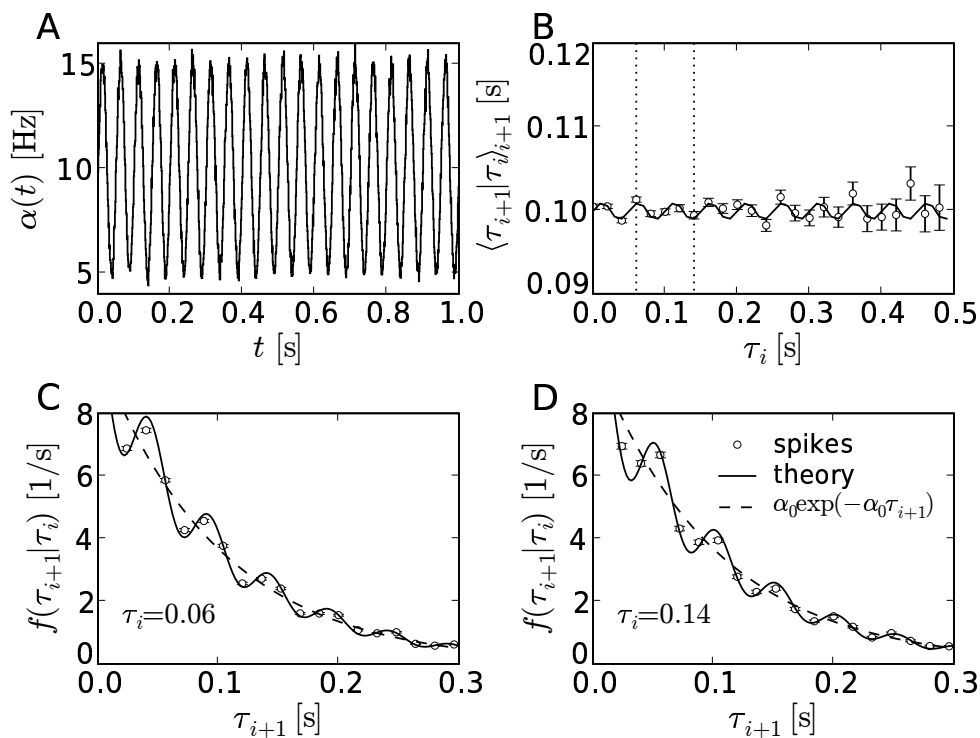


Figure 4.11: The time-averaged statistics of a Poisson process with a sinusoidal hazard rate as given by equation 4.17 with $A = 5.0$ Hz, $\alpha_0 = 10.0$ Hz, $F = 20.0$ Hz. (A) The ensemble firing rate time-histogram for 1×10^5 trials and a bin size of 1 ms. (B) The conditional mean, $\langle \tau_{i+1} | \tau_i \rangle_{\tau_{i+1}}$, as a function of τ_i given by equation 4.2 for the time-averaged joint distribution determined by equation 4.19 (solid line) and from a realization of 1×10^5 s duration (data points) as described in the text. The dashed vertical lines indicate the τ_i for which the conditional time-averaged ISI distributions were determined. The left is shown in (C), and the right in (D). The exponential ISI distribution for a Poisson process with hazard rate α_0 is shown (dashed-line) in (C) and (D) for comparison.

initial transient in the input at step up for an inhomogeneous GRP is contrasted to the inhomogeneous Poisson input case where no such transient exists.

4.4.1 Response to Step Stimuli

Consider a step change in the excitatory Poisson input rate, $\lambda_e(t)$, such that the adiabatic equilibrium firing rate, $\alpha_\infty(t)$, takes the form

$$\alpha_\infty(t) = \begin{cases} \alpha_0, & t < 0.3 \text{ s} \\ \alpha + \Delta\alpha, & 0.3 \text{ s} \leq t < 0.6 \text{ s} \\ \alpha_0, & t \geq 0.6 \text{ s} \end{cases}, \quad (4.20)$$

where α_0 is the initial adiabatic firing rate and $\Delta\alpha$ is the transient increase in the adiabatic firing rate. For the inhomogeneous Poisson process, the integral in (1.10) collapses and $\alpha(t) = \rho(t)$. Thus, the ensemble firing rate is exactly the adiabatic firing rate. This implies that the inhomogeneous Poisson process is immediately and always at equilibrium, a special property of the Poisson process which is not true for a general inhomogeneous renewal process.

For the inhomogeneous GRP, the parameters $a(t)$ and $b(t)$ in 1.3 were determined by fitting the ISI statistics of the 5DF neuron model which exhibits equilibrium ensemble firing rates α_0 and $\alpha_0 + \Delta\alpha$ accordingly.

As seen in Figure 4.12 (top), the Poisson process responds instantaneously and linearly, reproducing, as expected, exactly the adiabatic solution. For the GRP, the deviation from Poisson behavior is striking. The ensemble firing rate exhibits transient behavior following the change in stimulus at $\tau = 0.3 \text{ s}$, whereby it responds promptly to the stimulus change and peaks at more than twice its equilibrium value as shown in Figure 4.12 (bottom). Also shown is the ensemble firing rate estimated from time-histograms for realizations of the respective inhomogeneous processes as discussed in section 3.5. Indeed, numerical solutions of the renewal master equation 1.17 model the ensemble firing rate of the spike train realizations. Conversely, the transients which emerge for the inhomogeneous GRP random number generator at instantaneous changes in parameters are not artifacts but represent the inherent dynamics of the GRP.

The ensemble firing rate response of the GRPs was compared to that of the 5DF neuron (synaptic filtering was not accounted for). Behavior of the 5DF neuron is qualitatively similar to the GRP model, with reasonable quantitative agreement for a moderate step stimulus which does not bring the system too far from equilibrium, as shown in Figure 4.13.

4.4.2 Filtering Properties of an Inhomogeneous Gamma Renewal Process

Following observations of the high-pass filtering properties of SFA due to (Benda, Longtin, & Maler, 2005), the gain as a function of stimulus oscillation frequency

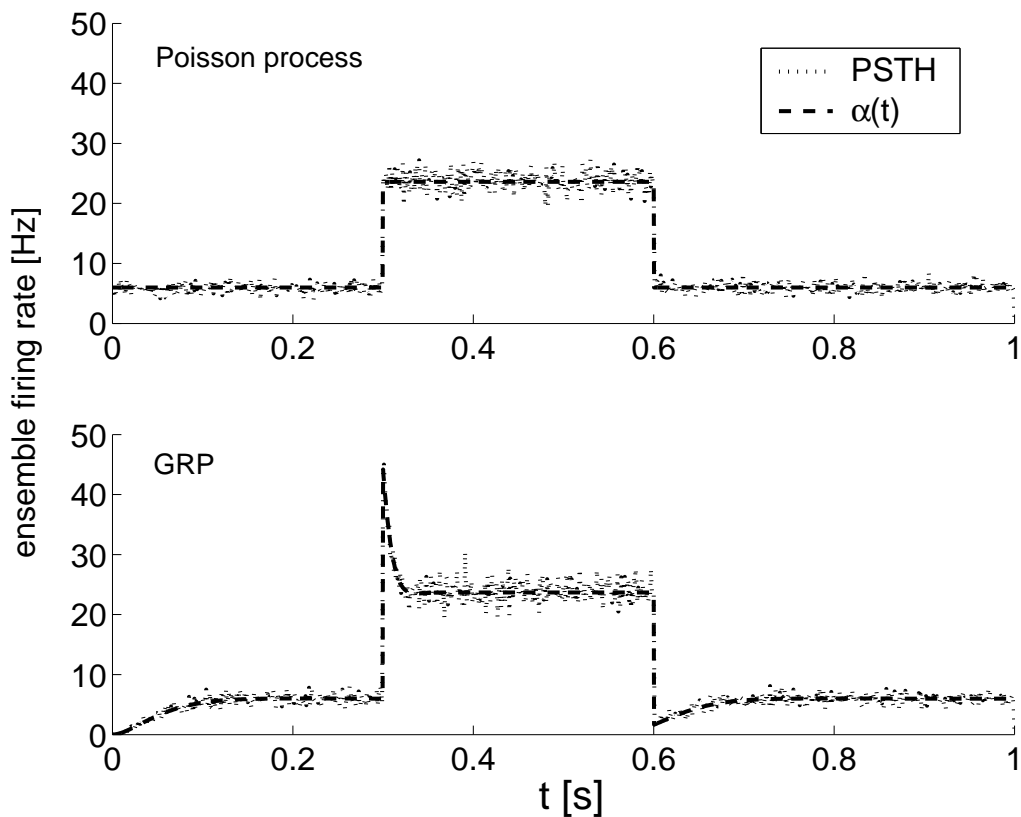


Figure 4.12: The ensemble firing rate given a step-stimulus by numerical solution of the renewal master equation 1.17 ($\alpha(t)$, dashed line) and a time histogram of spike-train realizations (PSTH, dotted line) for a Poisson process (top) and GRP (bottom) undergoing a step in the adiabatic firing rate at $t = 0.3\text{ s} - 0.6\text{ s}$ (50000 trials, bin size $\Delta t = 1\text{ ms}$) from 5.67 Hz to 23.87 Hz.

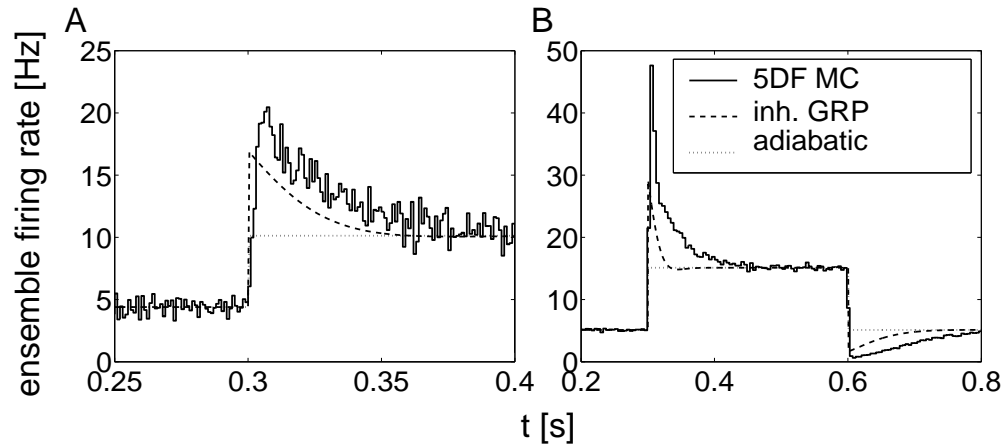


Figure 4.13: The ensemble firing rate for a 5DF neuron undergoing a step increase in excitatory Poisson synaptic bombardment rate at $t = 0.3$ s – 0.6 s determined by Monte-Carlo simulations (solid line, 50000 trials, bin size $\Delta t = 0.2$ ms). The adiabatic firing rate (adiabatic, dotted line) and the inhomogeneous GRP response (dashed line) with parameters determined by fitting to 5DF ISI distributions in the static case are shown for (A): a moderate step increase in stimulus where a reasonable fit to the 5DF ISI distribution with a GRP was possible, and (B): a larger step increase in stimulus where the equilibrium firing rate in the step is ~ 15 Hz and the 5DF hazard function deviates from GRP behavior as was seen in Figure 2.2.

for an inhomogeneous GRP was calculated by numerical solution of the renewal master equation.

Consider a sinusoidal stimulus such that the adiabatic firing rate, $\alpha_\infty(t)$, takes the form,

$$\alpha_\infty(t) = \alpha_0 + A \sin(2\pi Ft).$$

The signal gain as a function of stimulus frequency, F , defined as

$$g(F) := A_{GRP}(F)/A, \quad (4.21)$$

where $A_{GRP}(F)$ is the GRP response amplitude, was investigated for various stimulus means, α_0 , and oscillation amplitudes, A . As can be seen in Figure 4.14B for $\alpha_0 = 10$ Hz, the gain shows a characteristic frequency dependence which is independent of A . The gain was observed to be independent of amplitude for all α_0 and A considered, except for $\alpha_0 = 5$ Hz where large oscillations approached the x-axis, inducing asymmetries in the equilibrium firing rate oscillations about the mean. This explains the reduction in gain for large F and large A seen in Figure 4.14A.

Shown in Figure 4.14D are the $g(F)$ curves for $A = 0.1$ Hz for all α_0 considered. For increasing α_0 , the gain onset occurs at ever increasing frequency. A sigmoidal function in $\log(x) - \log(y)$ space of the form

$$\log(y) = \frac{c_1}{1 + e^{-c_2 \log(\frac{x}{x_0})}},$$

where c_1 , c_2 , and x_0 are fit parameters, was found to fit the observed gain functions well. The filtering behavior in the high-gain regime is indeed that of a high-pass filter, whereby in the low-gain regime there is deviation from high-pass filter behavior: For low frequencies the gain never falls below unity while for a high-pass filter the gain vanishes for small frequencies. The cut-off frequency of a high-pass filter, the frequency at which the gain falls to $1/\sqrt{2}$ its maximum value, can be determined from the sigmoidal fit. Shown in Figure 4.14C is the cut-off frequency as a function of α_0 . The cut-off frequency is found to be proportional to α_0 with a slope of 0.384 ± 0.002 .

4.4.3 Compounding Effects in Successive Adapting Populations

It is interesting to consider the compounding effects of successive GRP populations characterizing the successive adapting populations of, for example, the visual pathway from a cone/rod population to a bipolar population (the cone/rod and bipolar response is also similarly adapted, though not due to SFA as they do not spike) to a ganglion population to a LGN population to a V1 population and then to other populations in other areas of the cortex. The suggestion is that the transient and filtering effects of SFA observed in sections 4.4.1 and 4.4.2 are amplified in successive adapting populations.

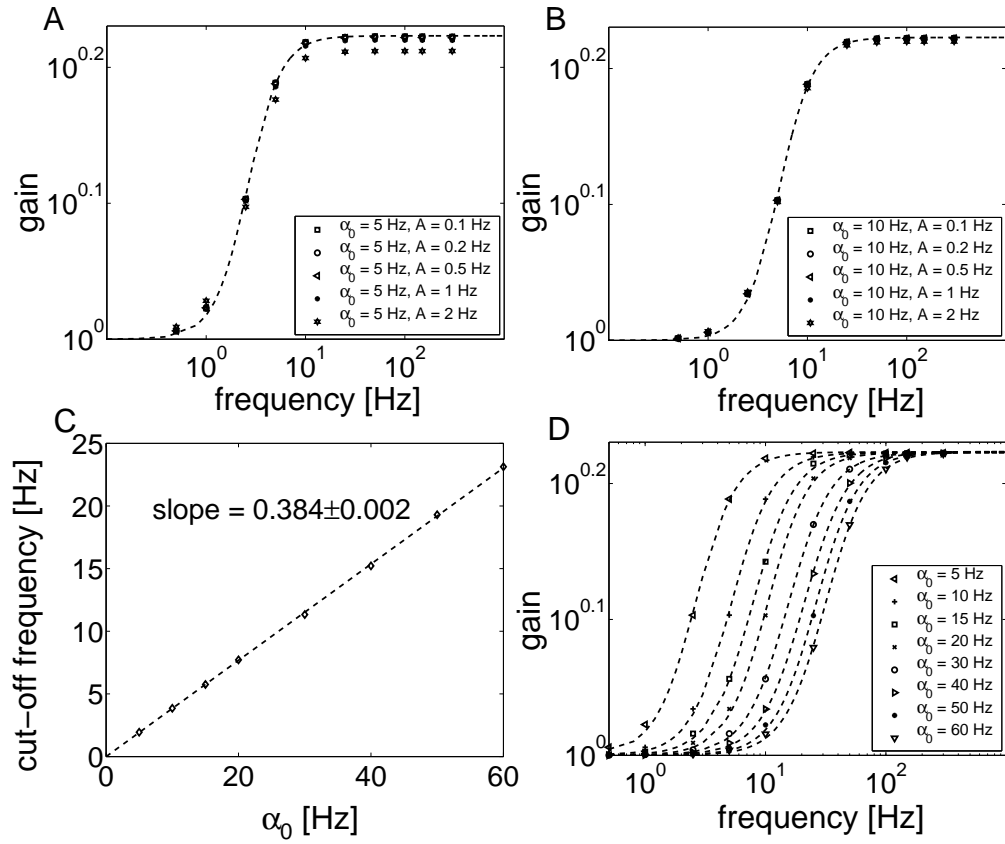


Figure 4.14: The filtering properties of an ensemble of inhomogeneous GRPs. (A–B) show the GRP ensemble gain as a function of stimulus oscillation frequency and oscillation amplitude. The gain is found to be independent of oscillation amplitude for small oscillations. For $\alpha_0 = 5$ Hz, an amplitude dependence in the gain for oscillation amplitudes $A = 2$ Hz and greater is observed, as the stimulus function is approaching zero, introducing asymmetry in the GRP ensemble firing rate. For the high-gain region, the gain exhibits the frequency dependence of a high-pass filter. For the low-gain region, the gain converges to unity, in contrast to vanishing gain for a high-pass filter. The gain-frequency curves are well fit by a sigmoid in log-log space (dashed lines in A, C, and D). (D) shows the gain as a function of frequency for various stimulation function means, α_0 . For increasing α_0 the gain-frequency curves are shifted to ever larger frequencies. (C) The cut-off frequency of the high-pass regime is found to be proportional to α_0 .

Given an arbitrary stimulus, the adiabatic ensemble firing rate, $\alpha_\infty(t)$, is uniquely determined and the parameters $a(t)$ and $b(t)$ of a GRP can be determined by fitting the equilibrium ISI statistics of the 5DF model neuron with the equilibrium ensemble firing rate $\alpha_\infty(t)$. For successive GRP ensembles the adiabatic ensemble firing rate, $\alpha_\infty(t)$, of the $i + 1^{\text{th}}$ population was chosen to be the ensemble firing rate of the i^{th} . Thus, due to this assumption, only the case where a neuron's adiabatic ensemble firing rate follows its input rate unamplified is treated. This is not necessarily the case for real networks of both excitatory and inhibitory neurons with feedback, or even single neurons. However, by considering such non-amplifying successions of neuron populations, the transient and filtering properties of adaptation in successive populations can be isolated.

For a GRP with a step in adiabatic firing rate, as in section 4.4.1, the ensemble firing rate of successive populations computed using the renewal master equation is shown in Figure 4.15. Clearly, sharp peaks are emerging as the transient effects of SFA are compounding down the populations. It should be stressed that such peaks do not emerge for successive populations of Poisson processes because for such systems the amplification is independent of the activity history and therefore unity.

Consider as in the previous section, a GRP with a sinusoidal equilibrium firing rate, $\alpha_\infty(t)$ of the form,

$$\alpha_\infty(t) = \alpha_0 + A \sin(2\pi Ft).$$

For $\alpha_0 = 5$ Hz, $A = 1$ Hz, and $F = 5$ Hz, the stimulus has a period comparable to $1/\alpha_0$, the preferred firing period of the individual neurons. The observed hazard rate of successive populations is shown in Figure 4.16A.

If the stimulus has a period which is long compared to $1/\alpha_0$, the preferred firing period of the individual neurons, multiple peaks emerge for a single stimulus period as shown in Figure 4.16B.

If the stimulus is periodic with a period short compared to $1/\alpha_0$, the GRP population density model predicts responses of successive populations identical to those in Figure 4.16A merely of higher frequency.

4.4.4 Network Response

In this section, a network characterizing a local cortical layer IV circuit is considered, and the network response to step stimuli due to GRP stimulation (transient behavior) is contrasted to that of Poisson process stimulation (no transient behavior).

The response of a balanced network of inhibitory and adapting excitatory model I&F neurons, based on (Muller, 2003) characterizing a local circuit of cortical layer IV, to stimulation by the presented inhomogeneous GRPs or Poisson processes was investigated in simulation.

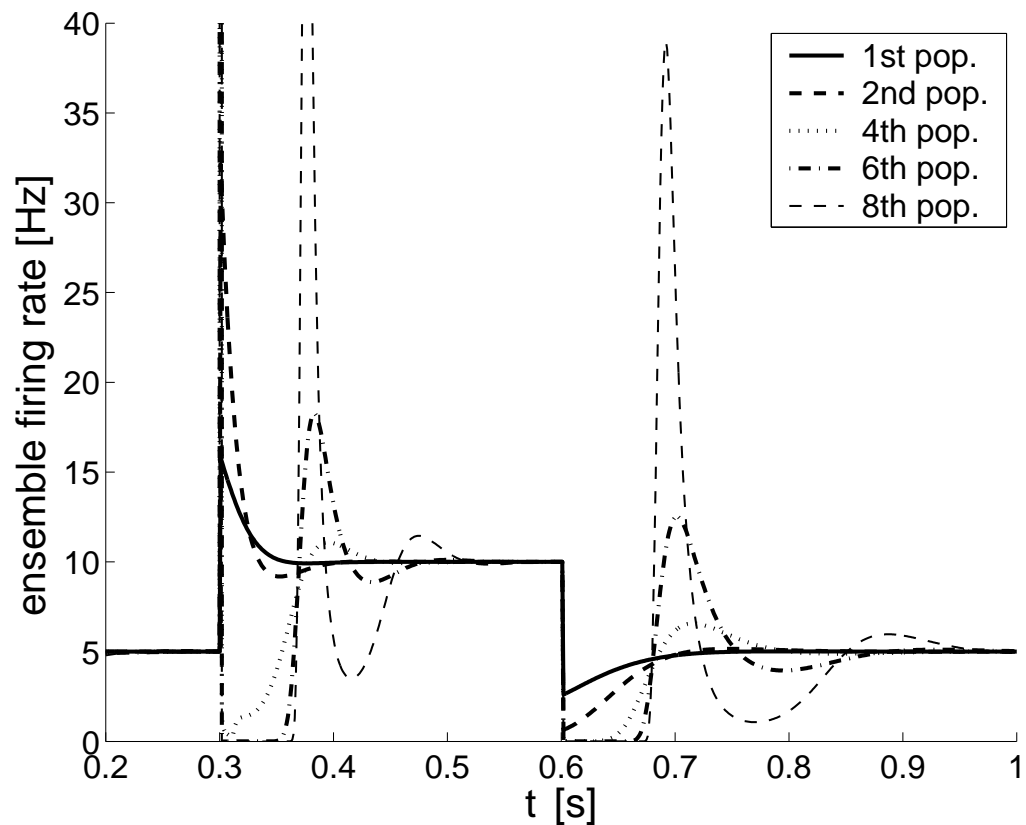


Figure 4.15: The compounding effects of adaptation in successive GRP populations for a step stimulus. Population 1: The response of a GRP population to a step stimulus. Population i : The response of a GRP population to a stimulus equal to the ensemble firing rate of GRP population $i - 1$.

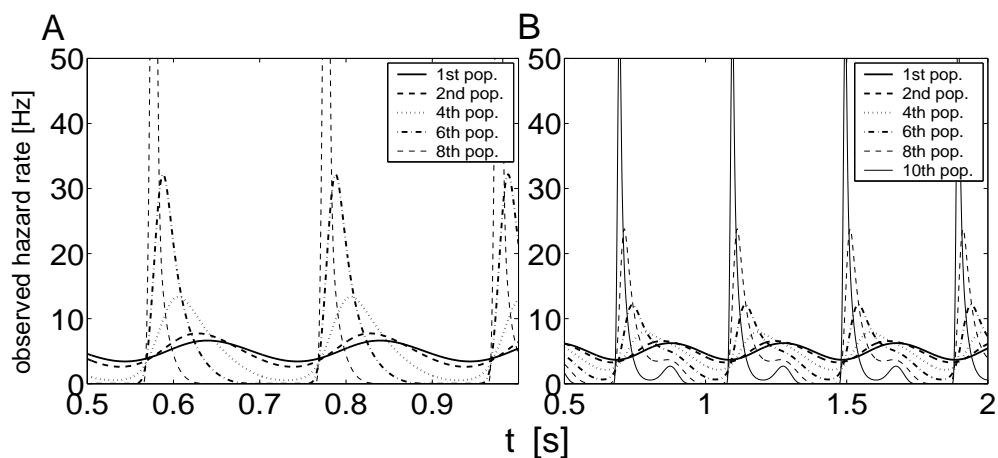


Figure 4.16: The compounding effects of adaptation in successive GRP populations for a sinusoidal stimulus. (A) Population 1 shows the response of a GRP population to a sinusoidal equilibrium firing rate $\alpha_\infty(t) = 5 \text{ Hz} + (1 \text{ Hz}) \cdot \sin(2\pi(5 \text{ Hz})t)$. Population i shows the response of a GRP population to a stimulus identical to the ensemble firing rate of GRP population $i - 1$. (B) As A with stimulus $\alpha_\infty(t) = 5 \text{ Hz} + (1 \text{ Hz}) \cdot \sin(2\pi(2.5 \text{ Hz})t)$. Multiple peaks per stimulus period emerge in successive populations.

The network consisted of 729 neurons (80% excitatory, 20% inhibitory) arranged on a $9 \times 9 \times 9$ lattice, each with 1000 excitatory and 250 inhibitory synapses. The details and parameters of the neuron and synapse models are described in appendix A. A connectivity slightly sparser than in (Muller, 2003) was used as it is known to eliminate the spontaneous oscillations reported there, producing the elusive stable active network state. The connection probabilities used were uniform and as follows: $c_{e \rightarrow e} = 0.14$, $c_{i \rightarrow e} = 0.17$, $c_{e \rightarrow i} = 0.20$, $c_{i \rightarrow i} = 0.20$, where $c_{X \rightarrow Y}$ refers to the proportion (on average) of population Y to which a neuron of population X is presynaptic. The remaining synapses were supplied with GRP activity to maintain the high-conductance state in each neuron. The parameters of the excitatory GRPs were chosen so that their ISI statistics were indistinguishable from the excitatory neurons while the same was true simultaneously for the inhibitory GRPs and neurons, and all had low asynchronous firing rates in the range $\approx 5 - 20$ Hz. Such a consistency between GRP supplied excitatory and inhibitory “background” activity and modeled excitatory and inhibitory neuron activity is possible with plausible I&F neuron model parameters and the resulting average synaptic conductance magnitudes are consistent with observations of the high-conductance state (Destexhe et al., 2003; Muller, 2003). Poisson processes could also have been used to maintain the high-conductance state, with their rate parameter chosen as the equilibrium firing rate of the GRP. For static stimulation, the GRP and Poisson process were observed to be interchangeable. The network activity initialization scheme was the same as in (Muller, 2003). The network was simulated using the CSIM neural simulator (Natschläger & Maass, 2001–).

Compared to an equivalent population of unconnected neurons under static uniform stimulation, the connected network exhibited a larger variability in the ensemble firing rates, and the emergence spontaneous synchronous events or bursts. The frequency of spontaneous bursting was quantified: If one sets an activity threshold of 15 Hz for burst events, one simulation of 7 s in five exhibited a burst event, however weaker burst-like events were more frequent. Shown in Figure 4.17 are three typical simulations of connected networks compared to the unconnected neuron population.

To model time-varying LGN or thalamic input to the network, the static GRPs which remained after the network was connected were replaced so that 20% of the total number of excitatory synaptic inputs of both excitatory and inhibitory neurons were supplied by GRPs or Poisson processes with a time-varying rate, where 20% is based on estimates of thalamocortical synapse densities in layer IV (Braitenberg & Schüz, 1991). A weak step-stimulus was supplied to these synapses specified by an equilibrium ensemble firing rate, α_∞ , of the form

$$\alpha_\infty(t) = \begin{cases} \alpha_0, & t < 2.0 \text{ s} \\ \alpha_0 + \Delta\alpha, & 2.0 \text{ s} \leq t < 4.0 \text{ s} \\ \alpha_0, & t \geq 4.0 \text{ s} \end{cases}, \quad (4.22)$$

where $\alpha_0 = 5.4$ Hz and $\Delta\alpha = 1.5$ Hz. For both the GRP and Poisson process, an absolute refractory period, $\tau_{ref} = 10$ ms, was also modeled so that $a \cdot b =$

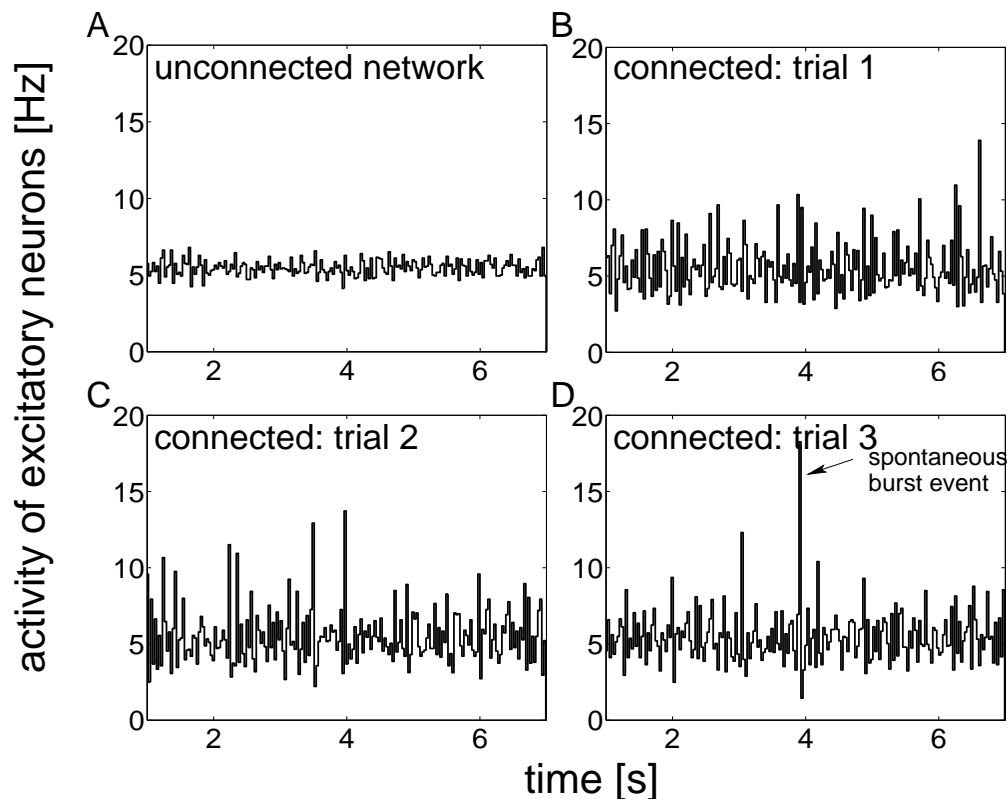


Figure 4.17: (A) shows the activity of the ≈ 580 adapting excitatory I&F neurons unconnected. (B-D) show three trials of the activity of the adapting excitatory I&F neurons participating in the connected network described in the text. The connected network shows largely stable activity but with larger bin-to-bin variation in the activity than for the unconnected neurons in A. Occasionally synchronous bursts occur spontaneously, as indicated in D. The activity is calculated as a PSTH by counting the number of spikes occurring in a small time bin of width $dt = 30$ ms for all m neurons considered, then normalizing by the factor $1/(mdt)$.

$1/\alpha_\infty - \tau_{ref}$ and $1/\rho = 1/\alpha_\infty - \tau_{ref}$ respectively. For the GRP, the parameter a was chosen so that the GRP firing statistics were roughly that of the excitatory I&F neuron class firing at a rate α_∞ ($a \approx 2.0 - 3.0$).

For both GRP and Poisson process input, five simulations of 7 s duration were run. Synchronous events similar to spontaneous synchronous events were observed directly following stimulus step-up, however GRP stimulation was found to evoke stronger network synchronous events more reliably than Poisson process stimulation as seen in Figure 4.18.

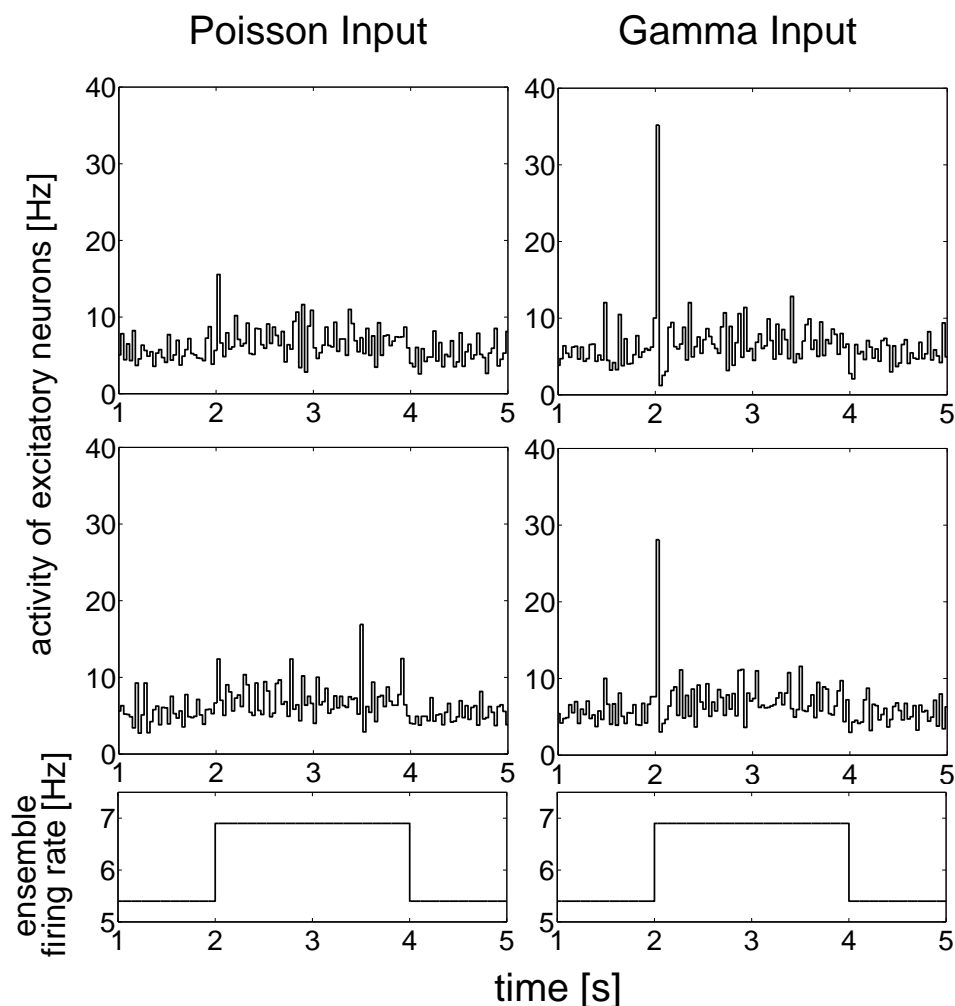


Figure 4.18: A comparison of the activity of the excitatory neurons (≈ 580 neurons) in the connected network (top two rows, one trial per row) for Poisson (left column) and gamma renewal process (right column) input at 20% of excitatory synapses of all neurons with the equilibrium firing rate, $\alpha_\infty(t)$, shown (bottom row). The GRP stimulated network exhibits a synchronous event directly following the step-up in stimulus for all trials, while the Poisson process stimulated network activity directly following the step-up in stimulus is not reliably distinguishable from the activity variations prior to it, except by accumulating extensive statistics in time. A total of five trials per input mode were simulated. The two shown are representative. The activity is calculated as for Figure 4.17.

Chapter 5

Discussion

It would not be paradoxical to say that the person who initiates the solution to a problem is different from the one who solves it.

David Hume, A Treatise of Human Nature

In the present article, a one-dimensional Markov process (the 1DM model) was proposed for modeling neural ensemble activity and spike train statistics which goes beyond renewal theory by accounting for interspike interval (ISI) correlations due to spike-frequency adaptation (SFA) mechanisms without the need to model the high-dimensional space of the microscopic neuronal state variables.

It was demonstrated that the full five-dimensional master equation of a conductance-based integrate-and-fire neuron with SFA and a relative refractory mechanism driven by Poisson spike trains (the 5DF model) can be reduced to a two-dimensional master equation plus filtering differential equations accounting for synaptic dynamics (the 2DM model), under an adiabatic elimination of the fast variables v, g_e, g_i , assuming the neuron has non-zero synaptic time constants and is in the high-conductance state. The resulting 2DM master equation is a two-dimensional generalization of the Markov process proposed at the outset as an extension of renewal theory to account for ISI correlations.

Methods were presented for generating inhomogeneous realizations of the proposed 1DM and 2DM models, and for solving their master equations numerically. The 2DM model was shown to accurately predict firing rate profiles of the full system under dynamic stimulation, and conditional ISI distributions and serial ISI correlations under static stimulation.

It was shown that mean-adaptation theories for spike-frequency adapting neurons with noisy inputs such as in (La Camera et al., 2004), and higher order statistical moment theories can be derived from the 1DM master equation as long as one neglects the refractory period. A heuristic condition for the validity of mean-adaptation theories was derived and found to be violated for the neuron

model (5DF) and parameters considered here. Furthermore, a mean+variance-adaptation theory was derived which corrected the ensemble firing rate predictions of mean-adaptation theories in this case.

5.1 Comparison with Other Studies of Adaptation

Studies of the firing rates of networks and ensembles of spike-frequency adapting neurons due to (Latham et al., 2000; Fuhrmann et al., 2002) augment a Wilson & Cowan equation (Wilson & Cowan, 1972) for the firing rate with a mean adaptation variable.

As is typical of the Wilson & Cowan approach, the ensemble firing rate, α , enters a differential equation of the form

$$\tau_e \frac{d\alpha}{dt} = -\alpha + h_g(\langle g_s(t) \rangle, \dots), \quad (5.1)$$

where $h_g(\langle g_s(t) \rangle, \dots)$ is the static firing rate given input including dependence on the mean adaptation, and τ_e is the timescale for relaxation to a firing rate equilibrium. As is suggested in (Fuhrmann et al., 2002), τ_e is determined mainly by the membrane time constant of the neuron, but is also affected by the mean amplitude of the input, and is treated there as a free parameter.

It has been argued in (Gerstner, 2000; Brunel, Chance, Fourcaud, & Abbott, 2001; Fourcaud & Brunel, 2002; Renart et al., 2004; La Camera et al., 2004) that for current and conductance-based synapses with non-zero time-constants and biological input statistics, the ensemble firing rate responds instantaneously to input currents and filtering due to the synapses dominates. In this case, the Wilson & Cowan equation for α can be replaced by an instantaneous f-I function, and the synaptic currents or conductances modeled by relaxation equations for their means and variances. This is the approach taken in (La Camera et al., 2004). Thus one side-steps the concerns mentioned in (Fuhrmann et al., 2002) that the Wilson & Cowan equation “cannot be rigorously derived from the detailed integrate-and-fire model”, and has been “shown not to accurately describe the firing rate dynamics [by] (Gerstner, 2000).”

The models due to (Latham et al., 2000; Fuhrmann et al., 2002; La Camera et al., 2004) all approximate the evolution of the ensemble of adaptation variables by its mean value, and are therefore mean-adaptation theories. In (La Camera et al., 2004), it is stated that such mean-adaptation theories are a good approximation under the assumption that “adaptation is slow compared to the timescale of the neural dynamics. In such a case, the feedback [adaptation] current ... is a slowly fluctuating variable and does not affect the value of s [the standard deviation of the input current].” They explore an adaptation time constant on the order of 100ms under this assumption that the adaptation dynamics are “typically slower than the average ISI.” They report that “for irregular spike trains the agreement is remarkable also at very low frequencies, where the condition that the average

ISI be smaller than τ_N [the time constant of adaptation] is violated. This may be explained by the fact that although $\langle ISI \rangle > \tau_N$, the ISI distribution is skewed towards smaller values, and [the mean adaptation current proportional to the firing rate] ... is still a good approximation.”

In section 4.2 the 1DM master equation was used to derive a mean+variance-adaptation theory, the next correction to the mean-adaptation theories in (La Camera et al., 2004), yielding another explanation for the success reported there. It was found that the error in the firing rate in (La Camera et al., 2004) remained small because the hazard function used there is a nearly linear function of the adaptation variable in the interesting regime where $P(g_s)$ is appreciably non-zero. Thus perturbing contributions to the average firing rate from deviations of the adaptation variable above and below the mean over the course of one ISI roughly cancel on average, regardless of the timescale of τ_s compared to the mean ISI. For the neuron model (5DF) and parameters considered here, the hazard function has an appreciable non-linearity resulting in erroneous predictions of the firing rate when using a mean-adaptation theory. The mean+variance-adaptation theory derived here corrected the predictions.

It is appropriate to reiterate that both the 1DM master equation and the resulting mean+variance-adaptation theory approximation considered here neglect refractory dynamics. It was demonstrated by the adiabatic reduction of the 5DF model to the 2DM model that the inclusion of a relative refractory period requires a two-dimensional master equation. Indeed, as shown in Figure 4.4, oscillations emerge for large and fast stimulus changes which are qualitatively captured by the 2DM model, but not by the 1DM model. It remains to be seen if a two-dimensional mean- or mean+variance-adaptation theory can be constructed which accounts for this behavior, and under what conditions it can be reduced to a one-dimensional model by simply rescaling the firing rate by $\alpha' = 1/(1/\alpha + \tau_{\text{eff}})$, as in (La Camera et al., 2004) for the absolute refractory period case, where τ_{eff} is some effective absolute refractory period of the relative refractory mechanism.

In (Benda & Herz, 2003), a thorough mathematical analysis of several well known mechanisms for SFA based on biophysical kinetics is undertaken for the case of a supra-threshold current. A universal phenomenological mean-adaptation model for such biophysical mechanisms for SFA is introduced with much the same form as in (La Camera et al., 2004). Methods are given to completely parameterize the model using quantities that can be easily measured by standard recording techniques. Implications for signal processing are considered there and in subsequent publications (Benda et al., 2005).

In (Chacron et al., 2003), a novel approach is taken compared to (Latham et al., 2000; Fuhrmann et al., 2002; Benda & Herz, 2003; La Camera et al., 2004). There, an expression is derived for the serial correlation coefficient of ISIs in the static case by employing a Markov chain. In their analysis, they define a quantity which is analogous to the static distribution $P^\dagger(t_s)$ here. In their framework, they prove that adaptation of the threshold fatigue form used there results in ISI correlations as have been observed experimentally (Longtin & Racicot, 1997;

Chacron et al., 2000; Nawrot et al., 2006). Their expression, however, contains integrals which require “the computation of the FPT [first-passage time] PDF of the Ornstein-Uhlenbeck process through an exponential boundary. Given that no general analytical expression is available for this quantity, derivation of the correlation from the integrals can be computationally more demanding than estimating the same quantities from simulations.” Subsequently, only simulations are performed and the derived expression is never compared to the simulated result. Thus they miss an important benchmark to ensure the calculations are correct. It is possible that the numerical techniques used here could be applied to compute a prediction for the correlation coefficient by the expression they derive, and subsequently compared to the simulated result.

Mean-adaptation theories cannot be used to model the correlation between subsequent ISIs, as they do not preserve the ensemble statistics. Our approach is that one simply not replace the trajectory of the adaptation variable, g_s , by its mean. This resolves the problem in the development in (La Camera et al., 2004) that the mean input current and instantaneous g_s have an equal role in determining the instantaneous firing rate, and g_s cannot be consistently replaced by its mean. What results is the 1DM master equation presented here. Subsequently, an expression for the inhomogeneous conditional ISI distribution was calculated and found to be in good agreement with 5DF Monte-Carlo in the static case. Furthermore, the variation of the mean of the conditional ISI distribution as a function of the preceding ISI, a generalization of the serial correlation coefficient of ISIs, was calculated and compared to 5DF Monte-Carlo. The Markov process master equation avoids the difficulty encountered in (Chacron et al., 2003) of treating the first passage times of an Ornstein-Uhlenbeck process through an exponential boundary, while capturing the full inhomogeneous ensemble dynamics in a framework which is tractable.

5.2 On the Adiabatic Reduction of the Master Equation

Under the assumption that the neuron is in the high-conductance state due to biologically realistic noisy inputs, it is shown that the 5DF master equation for the conductance-based spike-frequency adapting relative refractory integrate-and-fire neuron model used here can be reduced to the 2DM master equation by an adiabatic elimination of fast variables. The variables which remain are those of SFA and the relative refractory mechanism, and the form is analogous to the 1DM master equation proposed to extend renewal theory to a class of Markov processes which account for SFA.

The adiabatic reduction does not solve explicitly the firing rate of the given neuron model (without adaptation or the refractory mechanism) nor does it rely on such a solution. The firing rate dynamics of the given neuron model (without adaptation or the refractory mechanism) is left encapsulated in equation 2.23. The

approach applies to other models of adaptation such as the adapting threshold models in (Chacron et al., 2003) and the current-based adaptation models in (La Camera et al., 2004).

Concerning the generality of the adiabatic elimination for the adaptation variable, it is expected to be applicable to a larger class of formally spiking neuron models with fast intrinsic dynamics compared to adaptation. For those interested in modeling a class of neurons where a solution to equation 2.23 already exists, the framework can be easily and immediately applied. The fitting methods presented allow the connection to be made between models for which an explicit solution for the ensemble firing rate is unknown, and the 1DM and 2DM models presented here. What results is a reduced state space to explore for functional implications.

The generality of treating the relative refractory mechanism as a slow variable in the adiabatic elimination is less clear. There are some issues that need to be clarified before one could specify the class of neurons to which it applies. Specifically, the relationship between the requirement that the neuron be in the high-conductance state (small effective τ_m), and the requirement that the synapses have non-vanishing time-constants ($\tau_e > 0$) resulting in a non-vanishing probability at threshold ($P(v_{th}, \dots) > 0$) remains to be thoroughly investigated. The delta-conductance based approach in (Meffin et al., 2004), for example, does not satisfy the second requirement. The non-vanishing probability at threshold seems to be a necessary condition for the ensemble firing rate to respond on a faster timescale than the refractory mechanism dynamics (Fourcaud & Brunel, 2002; Renart et al., 2004).

An important step in the reduction is the treatment of the synaptic conductances. As their statistics are assumed to instantaneously determine the equilibrium statistics of the membrane potential, they were removed from the Master equation. Then, differential equations were found for their first statistical moments (means) in terms of the rate of the Poisson process input, as in (La Camera et al., 2004). One weakness of the fitting approach used here is that it cannot account for the dynamics of the second central moment (variance), as was done in (La Camera et al., 2004), and modeling both dynamic excitation and inhibition simultaneously requires a laborious fitting of a two dimensional space of synaptic inputs. Further work will apply methods such as those due to (Moreno-Bote & Parga, 2004b) to obtain a solution to equation 2.23 without fitting, thus allowing ensemble studies of adapting network models and analysis as in (Latham et al., 2000) with the rigor of, for example, (Brunel, 2000), and the possibility for quantitative agreement with traditional large-scale network simulations.

5.3 Beyond Renewal Theory

We reviewed standard results of inhomogeneous renewal theory in section 1.4, and uncovered a conceptual error often made in the literature when using the intensity-rescaling transformation to make the transition from homogeneous (static) to in-

homogeneous (dynamic) renewal theory. This problem was clarified and remedied by presenting a correct renewal process generation scheme as discussed in (Devroye, 1986).

By means of a variable transformation, the link between the 1DM model and inhomogeneous renewal theory methods becomes apparent, allowing direct comparison and contrast. The 1DM master equation was found to have an analogous structure to the renewal master equation, however with a state space spanning the whole real line. Furthermore, the 1DM state is not reborn to a universal initial value upon spiking, as in renewal theory (zero age), but reinserted to a state which is a function of the state just prior to spiking. This fact introduces a memory into the system and results in negative ISI correlations as reported in (Chacron et al., 2003).

Due to the detailed adiabatic reduction and fitting, the “nested exponential” form of the hazard function as given by equation 1.27, and the state dependent reinsertion function as given by equation 1.24 were proposed for the conductance-based SFA mechanism considered here. The hazard function (perhaps time-dependent) and the reinsertion function together are a complete specification of the proposed Markov model given an initial distribution of states. A numerical recipe was provided to efficiently generate inhomogeneous realizations of the proposed Markov process.

With an additional dimension for a relative refractory mechanism, the Markov process faithfully reproduces the transient dynamics and ISI correlations of 5DF Monte-Carlo, as expected by the adiabatic reduction. The same comparison between a one-dimensional Markov process and a neuron model without the relative refractory mechanism was not done, as it was found that without a refractory mechanism, the neuron model used exhibited a high probability to spike just after spiking, due to correlations in the synaptic conductance on the timescale of the refractory mechanism. The author feels this is a “bug” rather than a “feature” of neuron models without a refractory mechanism. Thus a Markov process was not built to account for it. Furthermore, the proposed relative refractory mechanism requires only slightly more effort than treating an absolute refractory period as done in (Nykamp & Tranchina, 2001). When the hazard function calibrated for the 2DM model is used directly for the 1DM model, reasonable agreement to refractory neuron models was still observed for the moderate firing rates considered.

5.4 Supra-Threshold Stimuli

For large and rapid changes in stimulus which bring the neurons into the supra-threshold regime, the predictions due to numerical solutions of the 2DM model deviated somewhat from 5DF Monte-Carlo simulations, as seen in Figure 4.4. The reasons for this are twofold. First, the stimulus brings us into a regime where the exponential fitting procedure for $h(t_s, t_r)$ begins to fail, and was poorly populated with data points. This fact likely accounts for the larger amplitude of

the oscillations of the 2DM model compared to 5DF Monte-Carlo. It is likely that a choice of function which improves the fit in this regime, or a proper analytical solution for $h(t_s, t_r)$ would improve the agreement here. Second, following the large stimulus change, a large portion of the population is in the supra-threshold regime where neurons make large migrations from the reset potential directly to the threshold following a spike. The 2DM model completely neglects the dynamics of the membrane potential and thus this migration period, resulting in the phase lead over the full system.

A closer inspection of Figure 4.4, reveals a transition from supra- to sub-threshold firing. Shortly after stimulus onset, a large portion of the population fires almost immediately, and is reinserted with the adaptation conductance increased by q_s , i.e. a mass exodus in phase space. For the 2-D case, the neurons also start a refractory period upon re-insertion, while in the 1-D case they do not. The stimulus is sufficiently strong that, in the 2-D case, it is still supra-threshold following the refractory period. In the 1-D case, there is no refractory period and the neurons can fire immediately following a spike cycle, and no lull is seen in the firing rate following the initial mass exodus. For the 2-D case, and even the renewal case, the system is refractory following the mass exodus, and a lull in the firing rate results, to peak again as the neurons are released from the refractory state. With the accumulation of adaptation, subsequent exodus events are ever diminished as more and more neurons enter the sub-threshold regime where neurons survive for highly variable durations following the refractory period. Thus, for large stimuli which keep the neuron supra-threshold over several spikes, the population is initially synchronized, firing at a rate determined by the refractory mechanism. As adaptation accumulates, spiking becomes more irregular and the neurons desynchronize. A similar effect has been observed experimentally in (Mainen & Sejnowski, 1995).

Thus synchronized supra-threshold preparations are transient in practice, since as adaptation accumulates over several spike cycles, the system relaxes to a sub-threshold stochastic firing mode. This suggests a functional role for adaptation in bringing neurons to and keeping them in the highly variable sub-threshold firing regime given static stimulation, while amplifying and transiently synchronizing the ensemble response to stimulus changes. This is an implementation of novelty detection.

A recent study of the effects of SFA in the context of natural and behaviorally relevant stimuli *in-vivo* suggests that the function of SFA is analogous to that of a high-pass filter on the peri-stimulus time histogram (PSTH) (Benda et al., 2005), i.e. to transmit rapid modulations with a larger gain than slow modulations. At rapid increases in stimulation this results in short transients of high firing probability, which can be interpreted as a population synchronization at stimulus onset. Quantitatively similar transient behavior was observed here at rapid changes in stimulus across all models considered. Using numerical solutions of the renewal master equation, the filtering properties of an inhomogeneous gamma renewal were investigated allowing refinement of the high-pass filter interpretation. A similar

analysis on the 2DM master equation is given in (Büsing, 2006).

5.5 Synchrony

It was shown that adapting I&F model neurons in the high-conductance state exhibit transient behavior in response to step stimuli. Specifically, sharp peaks in the PSTH or observed hazard rate emerged directly following an increase in stimulation. Traditionally, these are thought to be artifact or “garbage” signals sent by a neuron which is reconfiguring its coding scheme to a new realm of sensitivity (Troy & Robson, 1992). Working towards the prospect that it is in fact these transients which are the signal, and not the other way round, in this section the interpretation of these transients as synchrony is discussed.

For discrete time systems, events which occur in the same time step are said to be *synchronous*. For continuous time systems, such as a population of spiking neurons, two or more spikes are said to be synchronous, in the truest sense of the word, if they occur at exactly the same instant. However, such strict definitions of synchrony represent an ideal situation which is experimentally impossible to verify. Innate finite temporal smearing of event times and the ever present limitations in the resolution of observation demand a choice of time scale. Possible time scales might be the time scale of the spike evoked synaptic conductance (~ 10 ms), the pulse length of a spike (~ 1 ms), or the time spread of the first transmitter release event evoked by a spike. At one time scale, two neurons may be said to be firing synchronously, while at another finer scale, the two neurons may not be synchronous at all. Regardless, the standard approach for quantifying the degree of synchrony in continuous-time systems is to discretize time to some arbitrary time scale and count events per time bin. Unfortunately, this approach introduces a phase dependence: two events at the transition between two time bins may not be counted as synchronous. What is needed is a measure of synchrony which accounts for all possible time scales at once, and is compatible with the stochastic nature of neuronal firing.

In the population density formalisms presented here, the exactly synchronous firing of a population of neurons at a time t_0 can be described by an ensemble firing rate delta peaked at t_0 times a scalar between 0 and 1, representing the fraction of the population participating in the synchronous event. However, peaks of the ensemble firing rate of a finite width, Δt , and unit area times a scalar between 0 and 1 would also be said to be synchronous events if the discrete-time approach for quantifying synchrony is employed with a time scale on the order of Δt and the bins are properly aligned so as not to cut the peak in two. Thus the presence of peaks in the ensemble firing rate across a neuron population is an indicator of synchrony on a time scale on the order of the peak width. No extra measure of synchrony is necessary and the duality between dynamic firing rates and synchrony is immediately apparent.

It was shown in section 4.4.1 that inhomogeneous GRP models of adapting

neurons produce a peaked overshoot in the ensemble firing rate with a width on the order of $\sim 10 - 30$ ms when undergoing a step change in stimulus of a realistic magnitude. The width of the overshoot peak is largely determined by the time constant of SFA chosen, $\tau_s = 110$ ms. This indicates that the ensemble firing rate of a population of adapting neurons is a non-linear function of its stimulus history exhibiting synchrony effects for step changes in stimulation on a time scale of $\sim 10 - 30$ ms. Indeed, raster plots of GRPs undergoing step changes in equilibrium firing rates exhibit weak synchrony at the step stimulus increase where sensitivity is initially high but quickly adapts to a lower equilibrium firing rate (not shown). Successive adapting populations, as are involved in the transmission of stimuli to cortex, were found to intensify the effect.

Given that spike-frequency adapting neurons exhibit transients at changes in stimulation, the effect of these transients in the input of simulations of balanced networks of inhibitory and adapting excitatory neurons characterizing cortical layer IV was investigated by comparing the network response to sparse synaptic input consistent with thalamocortical synapse densities from inhomogeneous GRPs and Poisson processes subject to a step stimulus. The transient behavior of the GRP was found to significantly enhance the synchronous response of the network to stimulus step-up over Poisson processes. Thus the simulations here suggest delivering input by spike-frequency adapting neurons enhances local synchrony of the cortex at changes in stimulation.

Due to the observation that weakly synchronous input reliably evokes bursts in networks characterizing cortical layer IV, it is plausible that such bursts would excite waves of synchrony which would stably propagate laterally in the cortex. A distributed version of CSIM or NEST for use on Linux clusters, both currently under development, would allow numerical investigation of this prospect, as would a suitable neural field equation based on the various master equations investigated here.

Finally, given such synchrony coded stimuli, correlation-based learning rules such as STDP are put in a new realm of possibilities for spike correlations whereby their functional relevance for learning may be revealed.

5.6 Implications for Early Visual Coding

In (Uzzell & Chichilnisky, 2004) it is shown that the firing statistics of retinal ganglion cells are well modeled by a Poisson process plus recovery dynamics, due to presumably the same mechanism which results in observations of SFA *in-vitro*. Such models are a special case of the general inhomogeneous renewal process reviewed here. While it is likely that the 2DM process would be a better description of retinal ganglion cell firing, accounting for ISI correlations, for example, one fact is invariant across all such models: Changes in stimulation induce transient responses.

In (Troy & Robson, 1992) it is claimed that if “one wishes to determine the

cell's capacity to signal the difference between two stimuli ... this requires a sample of the cell's discharge following one stimulus to be reliably different from a sample of its discharge following the other." The theoretical framework presented here and recent experimental evidence provide a foundation on which this traditional view of visual coding is to be challenged. Indeed, the authors there observe that "when the sustained discharge rate of a cell was changed by a stationary pattern, an initial transient followed by a monotonic trend in the discharge occurred before the rate reached a steady level." The claim is that it is these transients the authors themselves observed at changes in stimulus which provide a reliable signal of a change in stimulation, not a statistical sample of the steady-state discharge before and after.

It has been demonstrated here that such transients are both amplified in successive populations, and can induce strong synchronous responses in network simulations of I&F neurons characterizing a local circuit of cortical layer IV, even when delivered by sparse connections consistent with thalamocortical synapse densities. Induced by a combination of fixational eye movements and [spike-frequency] adaptation in the attentive animal, salient, high-contrast features are encoded and transmitted to the cortex in the form of these transient peaks in the PSTH, i.e. synchrony in ganglion populations with nearby receptive fields. There is ample experimental support for this view: In primates, it is known that bursts of V1 cells are systematically preceded by microsaccadic fixational eye movements (Martinez-Conde, Macknik, & Hubel, 2000). Moreover, given that visual perception is known to rapidly fade in retinal image stabilization experiments suggests these transients are an important part of the code by which information is transmitted by the retina to the cortex (see (Martinez-Conde, Macknik, & Hubel, 2004) for a review) putting in serious question the notion of the "traditional rate code" of visual stimuli for which the claims of (Troy & Robson, 1992) above are representative.

5.7 Concluding Remarks

The present manuscript has focused on establishing a framework for rigorously treating the dynamic effects of spike-frequency adaptation and refractory mechanisms on neural ensemble spiking. The resulting master equation formalism unifies renewal theory models, and previous studies on adaptation such as (Latham et al., 2000; Fuhrmann et al., 2002; Chacron et al., 2003; Benda & Herz, 2003; La Camera et al., 2004) into an ensemble, or population density framework such as those due to (Knight, 1972, 2000; Brunel, 2000; Omurtag et al., 2000; Nykamp & Tranchina, 2000; Fourcaud & Brunel, 2002; Richardson, 2004; Rudolph & Destexhe, 2005; Meffin et al., 2004; Moreno-Bote & Parga, 2004b). The resulting methods are new and powerful tools for accurately modeling spike-frequency adaptation, an aspect of neuron dynamics ubiquitous in excitatory neurons which has been largely ignored in neural ensemble studies thus far, due to the added difficulties of treating the extra state variable.

By distilling the detailed neuron model down to two essential dimensions, spike-frequency adaptation and a relative refractory period, using an adiabatic elimination, their central role in perturbing neural firing is emphasized. Functional implications for spike-frequency adaptation in visual coding were discussed. Given the variety of intriguing and prominent consequences such as interspike interval correlations, transient synchronization following stimulus changes, amplification of this transient in successive populations, and the sensitivity with which cortical layer IV like networks respond to the transient, it is unlikely that spike-frequency adaptation can be neglected when considering, for example, the dynamic nature of the neural code (Shadlen & Newsome, 1998; Rieke et al., 1997), the propagation of synchrony (Abeles, 1991; Diesmann, Gewaltig, & Aertsen, 1999), or the function of spike-timing based learning rules (Gerstner, Kempter, Leo van Hemmen, & Wagner, 1996; Song, Miller, & Abbott, 2000).

Appendix A

Neuron and Adaptation Model Parameters

The parameters of the 5DF neuron model given in equations 2.13-2.15 were determined by fitting to a single compartment Hodgkin-Huxley (HH) model of a pyramidal neuron under various conditions using NEURON (Hines & Carnevale, 1997) as described in (Muller, 2003). The HH model and parameters are taken from (Destexhe, Contreras, & Steriade, 1998).

The phenomenological mechanism for spike-frequency adaptation (SFA) used here, the counterpart to the M-current and AHP-current mechanisms in the HH model, was inspired by (Dayan & Abbott, 2001, pp. 166), and similar models are proposed in (Koch, 1999, pp. 339), and (Fuhrmann et al., 2002), and more recently generalized in (Brette & Gerstner, 2005).

Additionally, a relative refractory period (RELREF) mechanism identical to the SFA mechanism was added, but with a much shorter time constant and a much larger conductance increase.

For the network simulations, inhibitory neurons were also modeled, as the 5DF neuron model, but without the SFA mechanism. Parameters were determined by fitting to the inhibitory class of HH model neurons in (Destexhe et al., 1998).

Both the SFA and RELREF mechanisms consist of an action potential (AP) activated and exponentially decaying conductance coupled to an inhibiting reversal potential so that the standard membrane equation takes the form:

$$c_m \frac{dv(t)}{dt} = g_l(E_l - v(t)) + g_s(t)(E_s - v(t)) \\ + g_r(t)(E_r - v(t)) + g_e(t)(E_e - v(t)) + g_i(t)(E_i - v(t)).$$

If v exceeds the threshold v_{th} :

- v is reset to v_{reset} .
- $g_s \mapsto g_s + q_s$.

Parameter	Description	Value
v_{th}	threshold voltage	-57 mV (ex) , -54.5 mV (inh)
v_{reset}	reset voltage	-70 mV
c_m	membrane capacitance	289.5 pF (ex) , 141.0 pF (inh)
g_l	membrane leak conductance	28.95 nS (ex) , 21.16 nS (inh)
E_l	membrane reversal potential	-70 mV
q_r	RELREF quantal conductance increase	3214 nS (ex) , 1565 nS (inh)
τ_r	RELREF conductance decay time	1.97 ms
E_r	RELREF reversal potential	-70 mV
q_s	SFA quantal conductance increase	14.48 nS (ex) , 0.0 nS (inh)
τ_s	SFA conductance decay time	110 ms
E_s	SFA reversal potential	-70 mV
$E_{e,i}$	reversal potential of excitatory and inhibitory synapses, respectively	0 mV , -75 mV
$q_{e,i}$	excitatory and inhibitory synaptic quantal conductance increase	2 nS
$\tau_{e,i}$	excitatory and inhibitory synaptic decay time	1.5 ms , 10.0 ms

Table A.1: The neuron and synapse model parameters used for simulations of the full system (5DF) given by equations 2.13-2.15.

- $g_r \mapsto g_r + q_r$.
- The time of threshold crossing is added to the list of spike times.

All conductances, $g_x(t)$, where $x \in \{s, r, e, i\}$, are governed by an equation of the form

$$\frac{dg_x(t)}{dt} = -\frac{1}{\tau_x}g_x(t).$$

The arrival of a spike at a synapse triggers $g_x \mapsto g_x + q_x$ for $x \in \{e, i\}$. GRPs, Poisson processes or other neurons were used to supply spike trains to the 1000 excitatory and 250 inhibitory synapses, where generally firing rates in the range 3 – 20Hz were used as described in the text for each specific simulation. The synaptic model and parameters were directly transferred from the HH models, while the remaining parameters, as determined by fits to the HH model, are given in Table A.1.

Appendix B

Further Details on the Adiabatic Reduction

In this appendix, the mathematical steps that lead from equation 2.16 to 2.20 in a more detailed way are given. The derivation was undertaken by L. Büsing as part of his diploma thesis work (Büsing, 2006) and in contribution the general framework given here and in (Muller, Buesing, Schemmel, & Meier, 2005).

For the sake of notational simplicity the five dimensional state variable $x = (v, g_e, g_i, g_s, g_r)$ is introduced. The indices 1, 2, 3, 4, 5 shall correspond to v, e, i, s, r , as used in the definition of the neuron model in equations 2.13-2.15 (for example $\tau_2 := \tau_e$). The partial derivatives with respect to x_μ are denoted by ∂_μ , and with respect to time by ∂_t . Furthermore, $P(x_1, x_2, x_3, x_4, x_5)$ is defined to be zero if one or more of the conductances x_2, \dots, x_5 is negative.

The master equation governing the evolution of the probability density $P(x, t)$ may be formulated as a conservation equation:

$$\partial_t P(x, t) = -\operatorname{div} J(x, t) + \delta(x_1 - v_{\text{reset}}) J_1(v_{\text{th}}, x_2, x_3, x_4 - q_4, x_5 - q_5, t). \quad (\text{B.1})$$

The second term on the rhs of equation B.1 accounts for neurons that cross the threshold surface $x_1 = v_{\text{th}}$ at time t with the state variables $(v_{\text{th}}, x_2, x_3, x_4 - q_4, x_5 - q_5)$ and are reinserted to $(v_r, x_2, x_3, x_4, x_5)$.

The probability current $J(x, t)$ is determined by the underlying stochastic differential equations 2.13-2.15. The components $J_\mu(x, t)$ for $\mu = 1, \dots, 5$ consist of the current due to the drift terms, $\beta_\mu(x)$, and for $\mu = 2, 3$ of additional currents due to the excitatory and inhibitory input Poisson spike trains, respectively.

The drift term for the membrane potential reads:

$$\beta_1(x) := \frac{1}{c_m} \left(\sum_{\mu=2}^5 x_\mu (E_\mu - x_1) + g_l (E_l - x_1) \right). \quad (\text{B.2})$$

For the conductances x_μ with $\mu = 2, \dots, 5$, the drift terms are:

$$\beta_\mu(x) = \beta_\mu(x_\mu) := -\frac{1}{\tau_\mu} x_\mu. \quad (\text{B.3})$$

The components of the probability current for $\mu = 1, 4, 5$ obey the equation:

$$J_\mu(x, t) = \beta_\mu(x)P(x, t). \quad (\text{B.4})$$

For the excitatory synaptic conductance x_2 the component $J_2(x, t)$ is:

$$\begin{aligned} J_2(x, t) &= \beta_2(x)P(x, t) \\ &+ \int_0^{x_2} \left[\int_0^\infty W_2(y_2, y_1, t)P(x_1, y_1, x_3, \dots, x_5)dy_2 \right] dy_1 \\ &- \int_0^{x_2} \left[\int_0^\infty W_2(y_1, y_2, t)P(x_1, y_2, x_3, \dots, x_5)dy_2 \right] dy_1. \end{aligned} \quad (\text{B.5})$$

The component $J_3(x, t)$ has a similar form with obvious modifications. Since the synaptic input is modeled as a Poisson process, the transition rates $W_\mu(y_1, y_2, t)$ for $\mu = 2, 3$ may be written as

$$W_\mu(y_1, y_2, t) = \nu_\mu(t)\delta(y_1 - (y_2 + q_\mu)), \quad (\text{B.6})$$

given the presynaptic firing rates $\nu_\mu(t)$. The diffusion approximation can be obtained by a Kramers-Moyal expansion of the components J_2 and J_3 (Gardiner, 1985).

Integration

To obtain an equation for the marginal probability distribution, $P(x_4, x_5, t)$, one integrates equation B.1 over x_1, x_2, x_3 . The integral of the terms $\partial_\mu J_\mu(x, t)$ on the rhs in B.1 for $\mu = 2, 3$ vanish due to the boundary condition that the probability current vanishes in the limit $x_\mu \rightarrow 0$ and $x_\mu \rightarrow \infty$ for $\mu = 2, 3$:

$$\int_0^\infty \partial_\mu J_\mu(x, t)dx_\mu = \lim_{x_\mu \rightarrow \infty} J_\mu(x, t) - J_\mu(x, t)\Big|_{x_\mu=0} = 0. \quad (\text{B.7})$$

The component $J_1(x, t)$ yields a nonvanishing contribution:

$$\begin{aligned} \int_0^\infty \int_0^\infty \left(\int_{-\infty}^{v_{\text{th}}} \partial_1 J_1(x, t)dx_1 \right) dx_2 dx_3 = \\ \int_0^\infty \int_0^\infty J_1(v_{\text{th}}, x_2, \dots, x_5, t)dx_2 dx_3. \end{aligned} \quad (\text{B.8})$$

The reinsertion term involves an integration over a delta distribution:

$$\begin{aligned} \int_0^\infty \int_0^\infty \left(\int_{-\infty}^{v_{\text{th}}} \delta(x_1 - v_{\text{reset}})J_1(v_{\text{th}}, x_2, x_3, x_4 - q_4, x_5 - q_5, t)dx_1 \right) dx_2 dx_3 = \\ \int_0^\infty \int_0^\infty J_1(v_{\text{th}}, x_2, x_3, x_4 - q_4, x_5 - q_5, t)dx_2 dx_3. \end{aligned} \quad (\text{B.9})$$

Integration of the lhs in equation B.1 results in:

$$\int_0^\infty \int_0^\infty \int_{-\infty}^{v_{\text{th}}} (\partial_t P(x, t)) dx_1 dx_2 dx_3 = \partial_t P(x_4, x_5, t). \quad (\text{B.10})$$

Plugging these results into equation 2.16 yields:

$$\begin{aligned} \partial_t P(x_4, x_5, t) &= - \sum_{\mu=4,5} \partial_\mu (\beta_\mu(x_\mu) P(x_4, x_5, t)) \\ &\quad + \int_0^\infty \int_0^\infty J_1(v_{\text{th}}, x_2, x_3, x_4 - q_4, x_5 - q_5, t) dx_2 dx_3 \\ &\quad - \int_0^\infty \int_0^\infty J_1(v_{\text{th}}, x_2, \dots, x_5) dx_2 dx_3. \end{aligned} \quad (\text{B.11})$$

Returning to the initial notation and using the definition for $J_1(x, t) = \beta_1(x, t)P(x, t)$ yields equation 2.20.

References

- Abeles, M. (1991). *Corticonics*. Cambridge University Press.
- Amit, D. J., & Tsodyks, M. V. (1991). Quantitative study of attractor neural network retrieving at low spike rates: I. substrate-spikes, rates and neuronal gain. *Network*, *2*, 259-273.
- Barbieri, R., Quirk, M., Frank, L., Wilson, M., & Brown, E. (2001). Construction and analysis of non-poissonian stimulus-response models of neural spiking activity. *Journal of Neuroscience Methods*, *105*, 25-37.
- Benda, J., & Herz, A. (2003). A universal model for spike-frequency adaptation. *Neural Computation*, *15*, 2523-64.
- Benda, J., Longtin, A., & Maler, L. (2005). Spike-frequency adaptation separates transient communication signals from background oscillations. *Journal of Neuroscience*, *25*, 2312-2321.
- Berstein, J. (1902). Untersuchungen zur Thermodynamik der bioelektrischen Ströme. *Pügers Arch*, *92*, 521-562.
- Bialek, W. (2002). Thinking about the brain. In H. Flyvbjerg, F. Jülicher, P. Ormos, & F. David (Eds.), *Physics of biomolecules and cells: Les houches session LXXV* (p. 485-577). EDP Sciences, Les Ulis; Springer-Verlag, Berlin.
- Braitenberg, V., & Schüz, A. (1991). *Anatomy of the cortex: Statistics and geometry*. Berlin: Springer Verlag.
- Brette, R., & Gerstner, W. (2005). Adaptive exponential integrate-and-fire model as an effective description of neuronal activity. *Journal of Neurophysiology*, *94*, 3637-3642.
- Broker, O., Chinellato, O., & Geus, R. (2005). Using Python for large scale linear algebra applications. *Future Generation Computer Systems*, *21*(6), 969-979.
- Brunel, N. (2000). Dynamics of sparsely connected networks of excitatory and inhibitory spiking neurons. *Journal of Computational Neuroscience*, *8*, 183-208.
- Brunel, N., Chance, F. S., Fourcaud, N., & Abbott, L. F. (2001). Effects of synaptic noise and filtering on the frequency response of spiking neurons. *Physical Review Letters*, *86*, 2186-2189.
- Büsing, L. (2006). *Low-dimensional population density equations for integrate-and-fire neurons*. Kirchhoff Institute for Physics, University of Heidelberg, Germany. (MSc Thesis, in press)
- Cannon, R. C., Gewaltig, M.-O., Gleeson, P., Bhalla, U. S., Cornelis, H., Hines,

- M. L., et al. (2006). Interoperability of neuroscience modeling software: current status and future directions. *Neuroinformatics*. (Submitted)
- Chacron, M., Longtin, A., & Maler, L. (2000). Suprathreshold stochastic firing dynamics with memory in p-type electroreceptors. *Physical Review Letter*, *85*, 1576-1579.
- Chacron, M., Pakdaman, K., & Longtin, A. (2003). Interspike interval correlations, memory, adaptation, and refractoriness in a leaky integrate-and-fire model with threshold fatigue. *Neural Computation*, *15*, 253-278.
- Cox, D. R. (1962). *Renewal theory*. London: Methuen.
- Curtis, H., & Cole, K. (1939). Electrical impedance of the squid giant axon during activity. *J. Gen. Physiol.*, *22*, 649-670.
- Dalcin, L., Paz, R., & Storti, M. (2005). MPI for Python. *Journal of Parallel and Distributed Computing*, *65*(9), 1108-1115.
- Dayan, P., & Abbott, L. (2001). *Theoretical neuroscience: Computational and mathematical modeling of neural systems*. Cambridge, Massachusetts: The MIT Press.
- Destexhe, A. (1997). Conductance-based integrate-and-fire models. *Neural Computation*, *9*, 503-514.
- Destexhe, A., Contreras, D., & Steriade, M. (1998). Mechanisms underlying the synchronizing action of corticothalamic feedback through inhibition of thalamic relay cells. *Journal of Neurophysiology*, *79*, 999-1016.
- Destexhe, A., Rudolph, M., Fellous, J., & Sejnowski, T. J. (2001). Fluctuating synaptic conductances recreate in vivo-like activity in neocortical neurons. *Neuroscience*, *107*, 13-24.
- Destexhe, A., Rudolph, M., & Paré, D. (2003). The high-conductance state of neocortical neurons in vivo. *Nature Reviews Neuroscience*, *4*, 739-751.
- Devroye, L. (1986). *Non-uniform random variate generation*. New York: Springer-Verlag.
- Diesmann, M., & Gewaltig, M.-O. (2002). NEST: An environment for neural systems simulations. In T. Plesser & V. Macho (Eds.), *Forschung und wissenschaftliches Rechnen, Beiträge zum Heinz-Billing-Preis 2001* (Vol. 58, pp. 43-70). Göttingen: Ges. für Wiss. Datenverarbeitung.
- Diesmann, M., Gewaltig, M.-O., & Aertsen, A. (1999). Stable propagation of synchronous spiking in cortical neural networks. *Nature*, *402*, 529-533.
- Ermentrout, B., Pascal, M., & Gutkin, B. (2001). The effects of spike frequency adaptation and negative feedback on the synchronization of neural oscillators. *Neural Computation*, *13*, 1285-1310.
- Fourcaud, N., & Brunel, N. (2002). Dynamics of the firing probability of noisy integrate-and-fire neurons. *Neural Computation*, *14*, 2057-2110.
- Fuhrmann, G., Markram, H., & Tsodyks, M. (2002). Spike frequency adaptation and neocortical rhythms. *Journal of Neurophysiology*, *88*, 761-770.
- Gardiner, C. W. (1984). Adiabatic elimination in stochastic systems. i. formulation of methods and application to few-variable systems. *Physical Review A*, *29*, 2814-2823.

- Gardiner, C. W. (1985). *Handbook of stochastic methods*. Berlin: Springer Verlag.
- Gazères, N., Borg-Graham, L. J., & Frégnac, Y. (1998). A phenomenological model of visually evoked spike trains in cat geniculate nonlagged x-cells. *Visual Neuroscience*, *15*, 1157-1174.
- Gerstner, W. (1995). Time structure of the activity in neural network models. *Physical Review E*, *51*, 738-758.
- Gerstner, W. (2000). Population dynamics of spiking neurons: Fast transients, asynchronous states, and locking. *Neural Computation*, *12*, 43-89.
- Gerstner, W. (2001). Coding properties of spiking neurons: Reverse and cross-correlations. *Neural Networks*, *14*, 599-610.
- Gerstner, W., Kempter, R., Leo van Hemmen, J., & Wagner, H. (1996). A neuronal learning rule for sub-millisecond temporal coding. *Nature*, *383*, 76-78.
- Gerstner, W., & Kistler, W. (2002). *Spiking neuron models: Single neurons, populations, plasticity*. Cambridge University Press.
- Haken, H. (1983). *Synergetics* (third ed.). Berlin: Springer-Verlag.
- Hines, M. L., & Carnevale, N. T. (1997). The NEURON simulation environment. *Neural Computation*, *9*, 1179-1209.
- Hodgkin, A., & Huxley, A. (1952). A quantitative description of membrane current and its application to conduction and excitation in nerve. *J. Physiol.*, *117*, 500-544.
- Huxley, A. (2002). From overshoot to voltage clamp. *Trends in Neurosciences*, *25*, 553-558.
- Ihaka, R., & Gentleman, R. (1996). R: A language for data analysis and graphics. *Journal of Computational and Graphical Statistics*, *5*(3), 299-314.
- Jones, E., Oliphant, T., Peterson, P., et al. (2001-). *SciPy and NumPy: Open source scientific tools for Python*. (<http://www.scipy.org/>)
- Knight, B. W. (1972). Dynamics of encoding in a population of neurons. *The Journal Of General Physiology*, *59*.
- Knight, B. W. (2000). Dynamics of encoding in neuron populations: some general mathematical features. *Neural Computation*, *12*, 473-518.
- Knight, B. W., Omurtag, A., & Sirovich, L. (2000). The approach of a neuron population firing rate to a new equilibrium: An exact theoretical result. *Neural Computation*, *12*, 1045-1055.
- Koch, C. (1999). *Biophysics of computation: Information processing in single neurons*. Oxford University Press.
- La Camera, G., Rauch, A., Lüscher, H.-R., Senn, W., & Fusi, S. (2004). Minimal models of adapted neuronal response to *in-vivo*-like input currents. *Neural Computation*, *16*, 2101-2124.
- Lapicque, L. (1907). Recherches quantitatives sur l'excitation électrique des nerfs traitée comme une polarisation. *J. Physiol. (Paris)*, *9*, 620-635.
- Latham, P. E., Richmond, B. J., Nelson, P. G., & Nirenberg, S. (2000). Intrinsic dynamics in neuronal networks. i. theory. *Journal of Neurophysiology*, *83*, 808-827.

- Lindner, B., & Longtin, A. (2003). Nonrenewal spike trains generated by stochastic neuron models. In *SPIE proceedings fluctuations and noise conference*. Sante Fe.
- Longtin, A., & Racicot, D. (1997). Spike train patterning and forecastability. *Biosystems*, *40*, 111-118.
- Mainen, Z., & Sejnowski, T. J. (1995). Reliability of spike timing in neocortical neurons. *Science*, *268*, 1503-1505.
- Martinez-Conde, S., Macknik, S. L., & Hubel, D. H. (2000). Microsaccadic eye movements and firing of single cells in the striate cortex of macaque monkeys. *Nature Neuroscience*, *3*, 251-258.
- Martinez-Conde, S., Macknik, S. L., & Hubel, D. H. (2004). The role of fixational eye movements in visual perception. *Nature Reviews Neuroscience*, *5*, 229-240.
- McCormick, D., Connors, B., Lighthall, J., & Prince, D. (1985). Comparative electrophysiology of pyramidal and sparsely spiny stellate neurons of the neocortex. *Journal of Neurophysiology*, *54*, 782-806.
- Meffin, H., Burkitt, A. N., & Grayden, D. B. (2004). An analytical model for the “large, fluctuating synaptic conductance state” typical of neocortical neurons *in-vivo*. *Journal of Computational Neuroscience*, *16*, 159-175.
- Meunier, C., & Segev, I. (2002). Playing the devil’s advocate: is the Hodgkin-Huxley model useful? *Trends in Neurosciences*, *25*, 558-563.
- Moreno-Bote, R., & Parga, N. (2004a). Membrane potential and response properties of populations of cortical neurons in the high conductance state. *Physical Review Letters*, *94*.
- Moreno-Bote, R., & Parga, N. (2004b). Role of synaptic filtering on the firing response of simple model neurons. *Physical Review Letters*, *92*. (DOI: 10.1103/PhysRevLett.92.028102)
- Muller, E. (2003). *Simulation of high-conductance states in cortical neural networks*. Kirchhoff Institute for Physics, University of Heidelberg, Germany. (MSc Thesis, HD-KIP-03-22)
- Muller, E., Buesing, L., Schemmel, J., & Meier, K. (2005). Spike-frequency adapting neural ensembles: Beyond mean-adaptation and renewal theories. *Neural Computation*. (Submitted)
- Natschläger, T., & Maass, W. (2001-). *CSIM: A neural Circuit SIMulator*. (<http://www.lsm.tugraz.at/csim>)
- Nawrot, M. P., Boucsein, C., Rodriguez-Molina, V., Aertsen, A., Grün, S., & Rotter, S. (2006). Serial interval statistics of spontaneous activity in cortical neurons *in-vivo* and *in-vitro*. *Neurocomputing*. (in press)
- Nykamp, D. Q., & Tranchina, D. (2000). A population density approach that facilitates large-scale modeling of neural networks: Analysis and an application to orientation tuning. *Journal of Computational Neuroscience*, *8*, 51-63.
- Nykamp, D. Q., & Tranchina, D. (2001). A population density approach that facilitates large-scale modeling of neural networks: Extension to slow inhibitory synapses. *Neural Computation*, *13*, 511-546.

- O'Brien, B. J., Isayama, T., Richardson, R., & Berson, D. M. (2002). Intrinsic physiological properties of cat retinal ganglion cells. *Journal of Physiology*, *538*, 787-802.
- Omurtag, A., Knight, B. W., & Sirovich, L. (2000). On the simulation of large populations of neurons. *Journal of Computational Neuroscience*, *8*, 51-63.
- Papoulis, A., & Pillai, S. U. (1991). *Probability, random variables and stochastic processes* (fourth ed.). New York: McGraw-Hill.
- Renart, A., Brunel, N., & Wang, X.-J. (2004). Mean-field theory of irregularly spiking neuronal populations and working memory in recurrent cortical networks. In J. Feng (Ed.), *Computational neuroscience: A comprehensive approach* (p. 431-490). New York: Chapman&Hall/CRC.
- Ricciardi, L. (1977). Diffusion processes and related topics in biology. In *Lecture notes on biomathematics*. Berlin: Springer-Verlag.
- Richardson, M. J. E. (2004). Effects of synaptic conductance on the voltage distribution and firing rate of spiking neurons. *Physical Review E*, *69*(5), 051918.
- Richardson, M. J. E., & Gerstner, W. (2005). Synaptic shot noise and conductance fluctuations affect the membrane voltage with equal significance. *Neural Computation*, *17*, 923-947.
- Rieke, F., Warland, D., de Ruyter van Steveninck, R., & Bialek, W. (1997). *Spikes: Exploring the neural code*. Cambridge, Massachusetts: MIT Press.
- Risken, H. (1996). *The Fokker-Planck equation: Methods of solution and applications* (Second ed.). Berlin: Springer-Verlag.
- Rudolph, M., & Destexhe, A. (2003). Characterization of subthreshold voltage fluctuations in neuronal membranes. *Neural Computation*, *15*, 2577-2618.
- Rudolph, M., & Destexhe, A. (2005). An extended analytic expression for the membrane potential distribution of conductance-based synaptic noise. *Neural Computation*, *17*, 2301-2315.
- Schuetze, S. M. (1983). The discovery of the action potential. *Trends in Neurosciences*, *6*, 164-168.
- Seyfarth, E. (2006). Julius Bernstein (1839-1917): pioneer neurobiologist and biophysicist. *Biological Cybernetics*, *94*, 2-8.
- Shadlen, M., & Newsome, W. (1998). The variable discharge of cortical neurons: Implications for connectivity, computation, and information coding. *Journal of Neuroscience*, *18*, 3870-3896.
- Shea, B. L. (1988). Algorithm AS 239, incomplete gamma function. *Applied Statistics*, *37*, 466-473.
- Shelley, M., McLaughlin, D., Shapley, R., & Wielaard, D. (2002). States of high conductance in a large-scale model of the visual cortex. *Journal of Computational Neuroscience*, *13*, 93-109.
- Siebert, A. J. F. (1951). On the first passage time probability function. *Physical Review*, *81*, 617-623.
- Smith, G. D., Cox, C. L., Sherman, S. M., & Rinzel, J. (2001). A firing-rate

- model of spike-frequency adaptation in sinusoidally-driven thalamocortical relay neurons. *Thalamus & Related Systems*, 1, 135-156.
- Softky, W. R., & Koch, C. (1993). The highly irregular firing of cortical cells is inconsistent with temporal integration of random EPSPs. *Journal of Neuroscience*, 13, 334-350.
- Song, S., Miller, K., & Abbott, L. F. (2000). Competitive hebbian learning through spike-timing-dependent synaptic plasticity. *Nature Neuroscience*, 3, 919-926.
- Troy, J. B., & Robson, J. G. (1992). Steady discharges of X and Y retinal ganglion cells of cat under photopic illuminance. *Visual Neuroscience*, 9, 535-553.
- Uzzell, V. J., & Chichilnisky, E. J. (2004). Precision of spike trains in primate retinal ganglion cells. *Journal of Neurophysiology*, 92, 780-789.
- van Vreeswijk, C. A., & Hansel, D. (2001). Patterns of synchrony in neural networks with spike adaptation. *Neural Computation*, 13, 959-992.
- Whittaker, E. T., & Robinson, G. (1967). *The calculus of observations: A treatise on numerical mathematics* (fourth ed.). New York: Dover.
- Wilson, H. R., & Cowan, J. D. (1972). Excitatory and inhibitory interactions in localized populations of model neurons. *Biophysical Journal*, 12, 1-24.

Acknowledgments

Many thanks to all those who made this work possible. I would especially like to thank:

My family for supporting me in many diverse and generous ways on my present jaunt abroad.

Prof. Dr. Karlheinz Meier who throughout my time at the Kirchhoff Institute generously supported me, both morally and otherwise, in his humorous and friendly way. Between all demanding responsibilities, he always found time to discuss for example the frustrations of publication. I haven't yet figured out if he eats lunch. Thank you for both the roots and the wings.

Prof. Dr. Alain Destexhe for his continued kindness and support throughout my dissertation work. The several extended visits to UNIC-CNRS, offerings of model source code, literature pointers, discussion and feedback even at early stages of the work, and the recommendation to participate in the Arcachon summer school are some of the friendly offerings which have had an invaluable positive impact.

Dr. Johannes Schemmel for his sharp wit and fast rebuttals which kept my two feet planted on firm scientific ground. I can't wait for FACETS stage 2.

The two anonymous reviewers of "Neural Computation" which generously gave of their time to provide careful reviews of each of the several version of the story. For each round, their comments brought about important scientific steps.

Prof. Dr. Bruce Knight and Prof. Dr. Nicolas Brunel, among others, for the neural ensemble framework and the many cool papers. This turtle, I think, goes all the way down. Thanks to Nicolas for the discussion at the Arcachon course which got me finally rolling on the formulation of the master equation.

Dr. Abigail Morrison and Dr. Markus Diesmann for inviting me to talk on my thesis work in Freiburg when it was still an inhomogeneous renewal theory, and for their encouragements and criticisms which in part triggered the search for the Markov process. Also for their support of PyNEST.

Lars Büsing who was a great help setting up the cluster, who quickly understood the master equation framework, with whom discussion of it was invaluable, and

who devised the integration of the 5-D master equation on one fine Thursday morning at an Electronic Vision group meeting! He beat me to it! I can't imagine a worse Diplom student.

Dr. Marc-Oliver Gewaltig for supporting the development of PyNEST.

Dr. Michelle Rudolph for always emailing immediate, extensive and exhaustive answers to my computational neuroscience modeling questions. I knew if Michelle didn't know of a recipe to generate realizations of an general inhomogeneous renewal process, then it was very likely no one in the community did, and thats how the whole thing got started.

Dr. Andrew Davison for relieving me of my guilty conscience for acquiring a python addiction by acquiring one himself, and for the PyNN initiative.

Dr. Steffen Hohmann, the friendly HiWi "Betreuer" that got a young scientist his start, whose lingo, greatly resembling a Douglas Adams novel, kept us all in the Software Zimmer smiling, and whose dissertation is such a great template!

Johannes Fieres for his contributions to maintaining the cool and chillout atmosphere in the "Softies" Zimmer, and for knowledgeable coding help.

Felix Schürmann for the objective coffee talk.

Daniel Brüderle for keeping the Software Zimmer sporty, for initiating the lunchtime initiative, and for representing us "Softies" in the Hardware Zimmer.

Martin Pospischil for lots of friendly discussion at various stages of the work.

Allen Visionären und auch Mitarbeiter des Kirchhoff-Instituts für die Hilfsbereitschaft und stets angenehme und freundschaftliche Arbeitsatmosphäre, in der mein Deutsch sich ständig verbessert.

Ania Szarzynska for your way that makes me smile, for believing in me, for being there for me, and for our dreams. Thanks for your patience, especially during the wonderful month in Warsaw October, 2005 where I was a workaholic and the Markov process formalism all fell into place.

Nurzhas Nurpeissoov and Slavomir Hnatic for the comradery in a foreign land.